

**PRODUCTION OF BIOJET FUEL FROM PALM FATTY ACID  
DISTILLATE OVER Ni/HZSM-12 CATALYST**

Chayanee Hiranyasiri

A Thesis Submitted in Partial Fulfilment of the Requirements  
for the Degree of Master of Science  
The Petroleum and Petrochemical College, Chulalongkorn University  
in Academic Partnership with  
The University of Michigan, The University of Oklahoma,  
Case Western Reserve University, and Institut Français du Pétrole  
2018

บทคัดย่อและแฟ้มข้อมูลฉบับเต็มของวิทยานิพนธ์ตั้งแต่ปีการศึกษา 2554 ที่ให้บริการในคลังปัญญาจุฬาฯ (CUIR)  
เป็นแฟ้มข้อมูลของนิสิตเจ้าของวิทยานิพนธ์ที่ส่งผ่านทางบัณฑิตวิทยาลัย

The abstract and full text of theses from the academic year 2011 in Chulalongkorn University Intellectual Repository (CUIR)  
are the thesis authors' files submitted through the Graduate School.

**Thesis Title:** Production of Biojet Fuel from Palm Fatty Acid Distillate  
over Ni/HZSM-12 Catalyst  
**By:** Chayanee Hiranyasiri  
**Program:** Petrochemical Technology  
**Thesis Advisor:** Assoc. Prof. Siriporn Jongpatiwut

---

Accepted by The Petroleum and Petrochemical College, Chulalongkorn University, in partial fulfilment of the requirements for the Degree of Master of Science.

..... College Dean  
(Prof. Suwabun Chirachanchai)

**Thesis Committee:**

.....  
(Assoc. Prof. Siriporn Jongpatiwut)

.....  
(Prof. Apanee Luengnaruemitchai)

.....  
(Assoc. Prof. Tawan Suknoi)

## ABSTRACT

5971003063: Petrochemical Technology Program  
Chayanee Hiranyasiri: Production of Biojet Fuel from Palm Fatty Acid Distillate over Ni/HZSM-12 Catalyst  
Thesis Advisor: Assoc. Prof. Siriporn Jongpatiwut 89 pp.  
Keywords: Biojet fuel/ PFAD/ Deoxygenation/ Hydrocracking/  
Hydroisomerization

Generally, jet fuels are mainly derived from the refining of petroleum feedstock which exhaust greenhouse gases. Therefore, biojet fuel is introduced as an alternative way to solve the problem. Moreover, jet fuel must have a freezing point about  $-47\text{ }^{\circ}\text{C}$  or below so *iso*-paraffins which have low freezing point are required. In this study, the hydroprocessing of palm fatty acid distillate (PFAD) over synthesized Ni/HZSM-12 and conventional Ni/HY catalysts which have different morphology and pore size for producing biojet fuel (hydrocarbon in a range of C9-C14) was studied in a continuous flow fixed-bed reactor under conditions of 350-400  $^{\circ}\text{C}$ , 10-30 bar, LHSV of 1.5-2.5  $\text{h}^{-1}$ , and  $\text{H}_2$ /feed molar ratio of 10. The main reactions are hydrodeoxygenation in order to remove oxygens in the fatty acid molecules then followed by hydroisomerization and hydrocracking reaction. The fresh catalysts were characterized by XRD, XRF, TEM, BET, TPR and TPD. For Ni/HZSM-12 catalyst, the optimal reaction condition was found at 375  $^{\circ}\text{C}$ , 30 bar, LHSV of 1.5  $\text{h}^{-1}$  and  $\text{H}_2$ /feed molar ratio of 10 over 10 wt.% Ni/HZSM-12 catalyst. The results show that Ni/HZSM-12 catalyst exhibited higher biojet yield as compared to Ni/HY catalyst (53 and 21%, respectively) and provided higher selectivity to produce *iso*-paraffin products at optimal condition because HZSM-12 had had narrower pore size so it predominately produced the lighter cracked products and provided *iso*-products. Moreover, Ni/HZSM-12 had low coke formation which is characterized by TPO, corresponding to the high stability of HZSM-12 catalyst.

## บทคัดย่อ

ชญาณี หิรัญญะสิริ : การผลิตน้ำมันไบโอเจ็ทจากกรดไขมันปาล์มโดยใช้ตัวเร่งปฏิกิริยานิกเกิลบนเอซซีเอสเอ็มทเวลฟ์ซีโอไลต์ (Ni/HZSM-12) (Production of Biojet Fuel from Palm Fatty Acid Distillate over Ni/HZSM-12 Catalyst) อ. ที่ปรึกษา : รศ.ดร. ศิริพร จงผาดิวุฒิ 89 หน้า

โดยทั่วไปน้ำมันเจ็ทสามารถผลิตได้จากกระบวนการกลั่นน้ำมันจากแหล่งเชื้อเพลิงฟอสซิล ซึ่งเป็นสาเหตุหนึ่งของการปล่อยแก๊สเรือนกระจก ดังนั้นการผลิตน้ำมันไบโอเจ็ทจึงเป็นอีกทางเลือกหนึ่งที่จะสามารถช่วยแก้ปัญหานี้ได้ นอกจากนี้ ข้อกำหนดคุณภาพของน้ำมันเจ็ทจะต้องมีจุดเยือกแข็งที่ต่ำ ที่ประมาณ -47 องศาเซลเซียสหรือต่ำกว่า สารประกอบไฮโดรคาร์บอนสายโซ่กิ่งในน้ำมันเจ็ทจึงมีความจำเป็น เนื่องจากมีคุณสมบัติจุดเยือกแข็งที่ต่ำเมื่อเทียบกับไฮโดรคาร์บอนสายโซ่ตรง ในงานวิจัยนี้จึงมุ่งเน้นในการพัฒนากระบวนการผลิตน้ำมันไบโอเจ็ทที่มีไฮโดรคาร์บอนสายโซ่กิ่งปริมาณมากจากกรดไขมันปาล์ม ซึ่งเป็นผลิตภัณฑ์พลอยได้จากกระบวนการกลั่นน้ำมันปาล์ม โดยผ่านกระบวนการไฮโดรต็อกซิฟิเคชัน, ไฮโดรดีคาร์บอนิเลชัน/ไฮโดรดีคาร์บอกซิเลชัน เพื่อขจัดออกซิเจนในโมเลกุลกรดไขมัน ตามด้วยกระบวนการไฮโดรไอโซเมอไรเซชัน และไฮโดรแครกกิง เพื่อทำให้เกิดสายโซ่กิ่งและทำให้โมเลกุลของสายโซ่แตกตัวเล็กลงในช่วงไบโอเจ็ท โดยใช้เครื่องปฏิกรณ์ระบบเบดคงที่ชนิดไหลต่อเนื่อง ภายใต้บรรยากาศแก๊สไฮโดรเจนความดันสูง ที่อุณหภูมิ 350-400 องศาเซลเซียส ความดัน 10-20 บาร์ สัดส่วนสารป้อนต่อปริมาณตัวเร่งปฏิกิริยา 1.5-2.5 ต่อชั่วโมง และสัดส่วนโดยโมลของไฮโดรเจนต่อสารป้อนเท่ากับ 10 โดยใช้ตัวเร่งปฏิกิริยาแบบบิวริคพัพนิกเกิลบนซีโอไลต์เอซซีเอสเอ็มทเวลฟ์ (Ni/HZSM-12) และนิกเกิลบนซีโอไลต์เอชวาย (Ni/HY) โดยเติมโลหะนิกเกิลลงบนตัวรองรับด้วยวิธีการเคลือบฝังด้วยเทคนิคแบบเปียกพอดกับพื้นผิว จากผลการทดลองพบว่า สภาวะที่เหมาะสมสำหรับการใช้ตัวเร่งปฏิกิริยานิกเกิลบนซีโอไลต์เอซซีเอสเอ็มทเวลฟ์ 10 เปอร์เซ็นต์โดยน้ำหนัก อุณหภูมิ 375 องศาเซลเซียส ความดัน 30 บาร์ และ สัดส่วนสารป้อนต่อปริมาณตัวเร่งปฏิกิริยา 1.5 ต่อชั่วโมง สามารถผลิตน้ำมันไบโอเจ็ทได้ถึง 53 เปอร์เซ็นต์ และนอกจากนี้ยังให้ผลิตภัณฑ์ไฮโดรคาร์บอนสายโซ่กิ่งปริมาณมากกว่าการใช้ตัวเร่งปฏิกิริยานิกเกิลบนซีโอไลต์เอชวายที่สภาวะเดียวกัน เนื่องจากตัวเร่งปฏิกิริยา Ni/HZSM-12 มีขนาดรูพรุนเล็กกว่าตัวเร่งปฏิกิริยา HY ส่งผลให้สามารถผลิตผลิตภัณฑ์ไฮโดรคาร์บอนที่มีโมเลกุลเล็กได้มากกว่าการใช้ตัวเร่งปฏิกิริยา HY และมีขนาดเหมาะสมในการเกิดผลิตภัณฑ์สายโซ่กิ่งอีกด้วย

## ACKNOWLEDGEMENTS

For the success of this thesis, I would like to take this chance to thank many people and organization who have contributed to my thesis work.

First of all, I would like to express my sincere gratitude to thank the most important people for my Master degree, Assoc. Prof. Siriporn Jongpatiwut for the supervisions, suggestions, guidance and insight throughout this research project.

I would also like to thank my thesis committees, Prof. Apanee Luengnaruemitchai and Assoc. Prof. Tawan Sooknoi for their suggestions which are certainly important and helpful for completion of this thesis.

I am grateful for the partial scholarship and partial funding of the thesis work provided by the Petroleum and Petrochemical College.

This thesis work is funded by the Petroleum and Petrochemical College and Center of Excellence on Petrochemical and Materials Technology.

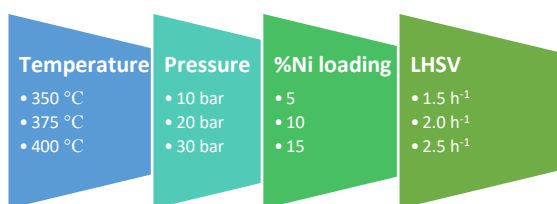
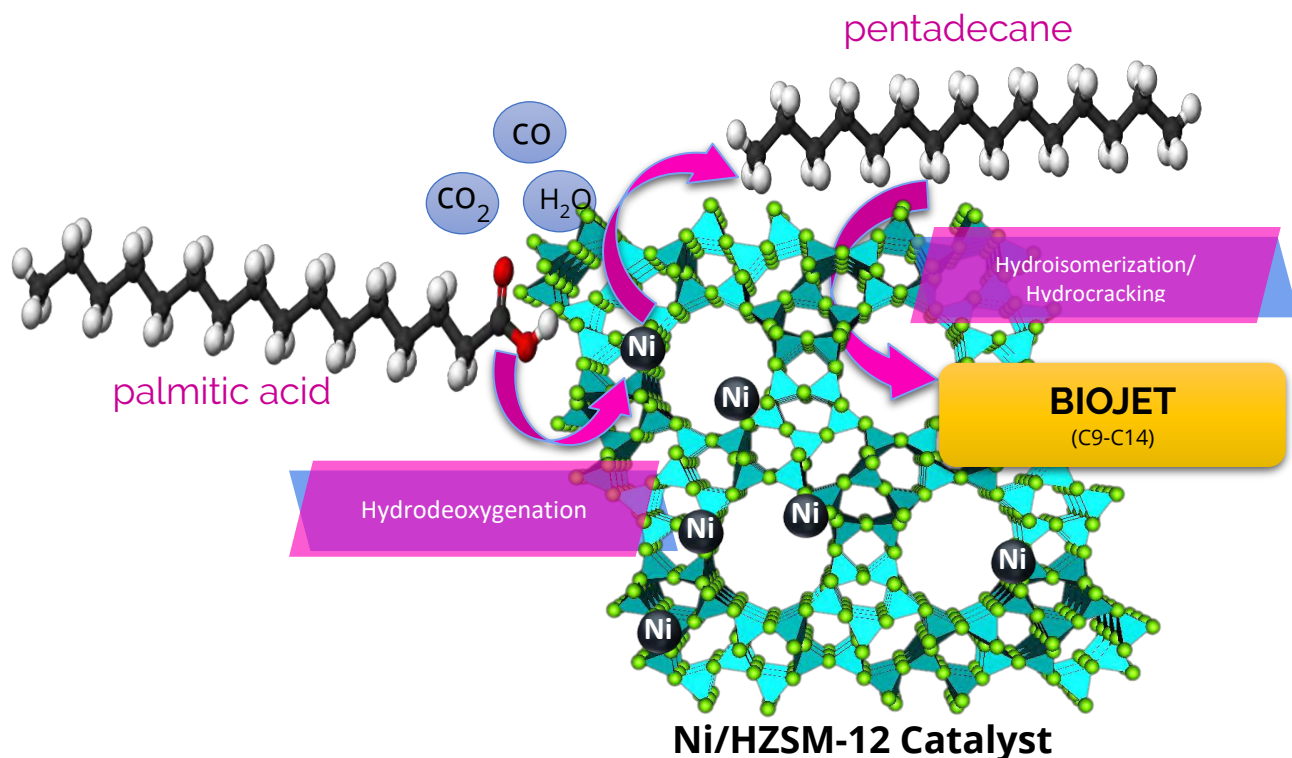
I would like to thank Ms. Chanakarn Homla-or, Ms. Yanika Sangasang and Mr. Katipot Inkong for all suggestions and all laboratory members for their kindly supports and encouragements.

I would like to acknowledge all faculty and staff at The Petroleum and Petrochemical College, Chulalongkorn University for their kind assistance and co-operation.

Moreover, I would like to thank my PPC friends for all support and encouragement in my hard time.

Finally, I would like to express my deepest thanks to my parents for their supporting, encouragement and believe in me since I was young until completing this project.

## Graphical Abstract



The optimum condition was found at 350 °C, 30 bar, LHSV of 1.5 h<sup>-1</sup> and H<sub>2</sub>/feed molar ratio of 10 over 10 wt.% Ni/HZSM-12 catalyst.

- ✓ Ni/HZSM-12 provided higher selectivity to biojet fuel and *iso*-alkane selectivity than Ni/HY.
- ✓ Ni/HZSM-12 had low tendency for coke formation corresponding to the high stability of HZSM-12 catalyst.

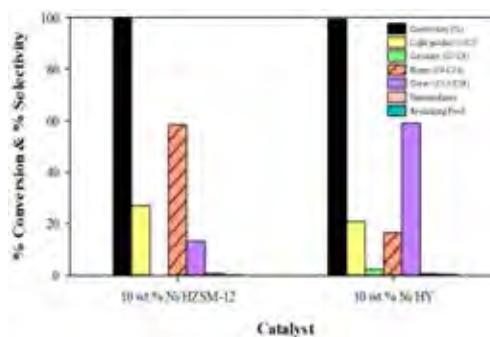


## TABLE OF CONTENTS

	<b>PAGE</b>
Title Page	i
Abstract (in English)	iii
Abstract (in Thai)	iv
Graphical Abstract	v
Acknowledgements	vi
Table of Contents	vii
List of Tables	xi
List of Figures	xiii
 <b>CHAPTER</b>	
<b>I INTRODUCTION</b>	<b>1</b>
 <b>II LITERATURE REVIEW</b>	
2.1 Biojet Fuel	3
2.2 Bio-based Fuel Feedstock	5
2.2.1 Vegetable Oil	5
2.2.2 Fatty Acid	8
2.3 Palm Fatty Acid Distillate Feedstock	9
2.4 The Overall Reaction for Biojet Fuel Production	14
2.4.1 Hydrodeoxygenation	16
2.4.2 Hydrocracking	19
2.4.3 Hydroisomerization	20
2.4.4 Hydrogenation and Dehydrogenation	23
2.4.5 Hydrogenolysis	24
2.5 Catalyst for Biojet Production	25
2.5.1 Zeolites as A Catalyst for Biojet Fuel Production	25
2.5.2 Zeolite ZSM-12	28
2.5.3 Supported Metal Catalyst Type	30

<b>CHAPTER</b>		<b>PAGE</b>
<b>III</b>	<b>EXPERIMENTAL</b>	32
	3.1 Materials and Equipment	32
	3.1.1 Materials	32
	3.1.2 Equipment	33
	3.2 Experimental Procedures	33
	3.2.1 Catalyst Preparation	33
	3.2.2 Ni Loading on HZSM-12	34
	3.3 Catalyst Characterization	34
	3.3.1 X-ray Diffractometer (XRD)	34
	3.3.2 Brunauer-Emmett-Teller (BET)	35
	3.3.3 Temperature Programmed Reduction (TPR)	35
	3.3.4 Temperature Programmed Desorption (TPD) of Isopropylamine	35
	3.3.5 Temperature Programmed Oxidation (TPO)	36
	3.3.6 Transmission Electron Microscopy (TEM)	36
	3.4 Catalytic Activity Testing	36
	3.5 Product Analysis	39
	3.5.1 Liquid Product Analysis	39
	3.5.2 Gas Product Analysis	40
<b>IV</b>	<b>RESULTS AND DISCUSSION</b>	42
	4.1 Characterization of Fresh Catalysts	42
	4.1.1 X-ray Diffraction (XRD)	42
	4.1.2 X-ray Fluorescence (XRF)	43
	4.1.3 Transmission Electron Microscope (TEM)	44
	4.1.4 Brunauer-Emmett-Teller (BET)	47
	4.1.5 Temperature Programmed Reduction (TPR)	48
	4.1.6 Temperature Programmed Desorption of Isopropylamine (IPA-TPD)	49



<b>CHAPTER</b>	<b>PAGE</b>
4.2 Gas Chromatography of Feed and Standard Analysis	50
4.2.1 Feed Analysis	50
4.2.2 Standard Analysis	52
4.3 Catalytic Activity Testing	53
4.3.1 Effect of Reaction Temperature	54
4.3.2 Effect of Reaction Pressure	56
4.3.3 Effect of Percent Ni Loading	57
4.3.4 Effect of LHSVs	58
4.3.5 Effect of Supported Catalyst (Ni/HZSM-12 and Ni/HY)	60
4.4 Proposed Reaction Pathway	67
4.5 Characterization of Spent Catalysts	69
4.5.1 Temperature-Programmed Oxidation (TPO)	69
<b>V CONCLUSIONS AND RECOMMENDATIONS</b>	<b>71</b>
<b>REFERENCES</b>	<b>73</b>
<b>APPENDIX</b>	<b>79</b>
<b>Appendix A1</b> Overall Mass Balance of Deoxygenation- hydroprocessing at Different in Temperature	79
<b>Appendix A2</b> Overall Mass Balance of Deoxygenation- hydroprocessing at Different in Pressure	81
<b>Appendix A3</b> Overall Mass Balance of Deoxygenation- hydroprocessing at Different in Percent Ni Loading	83
<b>Appendix A4</b> Overall Mass Balance of Deoxygenation- hydroprocessing at Different in Liquid Hourly Space Velocity	85

<b>CHAPTER</b>	<b>PAGE</b>
<b>Appendix A5</b> Overall Mass Balance of Deoxygenation- hydroprocessing over Different Catalyst	87
<b>CURRICULUM VITAE</b>	89

## LIST OF TABLES

<b>TABLE</b>	<b>PAGE</b>
2.1 The chemical structure of common fatty acids in vegetable oils	6
2.2 The selected properties of variety vegetable oils and diesel	6
2.3 The compositions and properties of PFAD	12
3.1 Description of system in flow diagram of the continuous flow fixed-bed reactor	37
3.2 The reaction conditions for hydroprocessing of palm fatty acid distillate in continuous flow fixed-bed reactor	38
3.3 The chromatographic temperature program for liquid product analysis	39
3.4 The chromatographic temperature program for gas-phase product analysis	40
4.1 Chemical composition of the synthesized HZSM-12 and 5, 10 and 15 wt.% Ni/HZSM-12 catalysts	44
4.2 Physical characteristics of the prepared catalysts	47
4.3 Brønsted acidity of the parent HZSM-12 and 5,10, 15 wt.% Ni/HZSM-12, 10 wt.% Ni/HY and the parent HY catalysts from IPA-TPD	50
4.4 Composition of PFAD feedstock	51
4.5 Amount of carbon deposits on prepared catalyst after reaction	69
A1 Overall mass balance of deoxygenation-hydroprocessing one-pot reaction over 10 wt.% Ni/HZSM-12 catalyst at different in temperature. (Reaction condition: 30 bar, H <sub>2</sub> /feed molar ratio of 10, LHSV of 1.5 h <sup>-1</sup> and TOS at 5 h)	79

<b>TABLE</b>		<b>PAGE</b>
A2	Overall mass balance of deoxygenation-hydroprocessing one-pot reaction over 10 wt.% Ni/HZSM-12 catalyst at different in pressure. (Reaction condition: 375 °C, H <sub>2</sub> /feed molar ratio of 10, LHSV of 1.5 h <sup>-1</sup> and TOS at 5 h)	81
A3	Overall mass balance of deoxygenation-hydroprocessing one-pot reaction over Ni/HZSM-12 catalyst at different in percent Ni loading. (Reaction condition: 375 °C, 30 bar, H <sub>2</sub> /feed molar ratio of 10, LHSV of 1.5 h <sup>-1</sup> and TOS at 5 h)	83
A4	Overall mass balance of deoxygenation-hydroprocessing one-pot reaction over 10 wt.% Ni/HZSM-12 catalyst at different in LHSV. (Reaction condition: 375 °C, 30 bar, H <sub>2</sub> /feed molar ratio of 10 and TOS at 5 h)	85
A5	Overall mass balance of deoxygenation-hydroprocessing one-pot reaction over different catalyst. (Reaction condition: 375 °C, 30 bar, H <sub>2</sub> /feed molar ratio of 10, LHSV of 1.5 h <sup>-1</sup> and TOS at 5 h)	87

## LIST OF FIGURES

FIGURE	PAGE	
2.1	Life-cycle greenhouse gas emissions for conventional and alternative jet fuels (The unit of 'g CO <sub>2</sub> /eMJ' represent the CO <sub>2</sub> equivalent emissions per unit of energy).	4
2.2	World oils and fats production in 2009 (Oil World & MPOC estimates).	10
2.3	World palm oil exports by country in 2014 (Oil World & MPOC estimates).	10
2.4	Physical refining process of crude palm oil.	11
2.5	Prices of PFAD, CPO, and RBD palm oil.	13
2.6	The four catalytic pathways proposed for deoxygenation of palmitic acid on 40NiPZ. (a) Decarbonylation, (b) Decarboxylation, (c) Initial isomerization and (d) Initial isomerization and cracking.	16
2.7	Various deoxygenation reaction schemes with other possible reactions including thermodynamic data ( $\Delta G_{573}$ in kJ/mol at 0.1 MPa).	17
2.8	The schematic of hydrocracking reaction.	19
2.9	Mechanism of n-paraffins/n-alkanes hydroisomerization over bifunctional catalysts (e.g. zeolites loaded with metals) using n-decane as a model compound.	21
2.10	Effect of reaction temperature on iso-to-normal paraffin ratio in products obtained from hydrocracking of n-decane over strongly acidic catalyst.	22
2.11	Schematic of hydrogenolysis reaction.	24
2.12	Formation of three common zeolites from primary unit.	26
2.13	Three commercial zeolites of difference dimensionalitie.	27

<b>FIGURE</b>		<b>PAGE</b>
2.14	The NMR-refined crystal structure of silica-ZSM-12 (framework type code MTW) with Si sites labeled and unit cell indicated.	29
3.1	The schematic diagram of the reactor system.	37
4.1	XRD patterns of synthesized parent ZSM-12, HZSM-12 and 5, 10 and 15 wt.% Ni/HZSM-12 catalysts.	43
4.2	TEM images of calcined parent HZSM-12 zeolite.	45
4.3	TEM images of calcined 5 wt.% Ni/HZSM-12 catalyst.	45
4.4	TEM images of calcined 10 wt.% Ni/HZSM-12 catalyst.	46
4.5	TEM images of calcined 15 wt.% Ni/HZSM-12 catalyst.	46
4.6	Temperature programmed reduction (TPR) profiles of the 5, 10 and 15 wt.% Ni/HZSM-12 catalysts.	48
4.7	Temperature programmed desorption of isopropylamine (IPA-TPD) profiles of the parent HZSM-12 and 5, 10, 15 wt.% Ni/HZSM-12, 10 wt.% Ni/HY and the parent HY catalysts.	49
4.8	The chromatogram of various components in PFAD range analyzed by a GC/FID.	51
4.9	Chromatograms of standard oxygenated compounds.	52
4.10	Chromatograms of standard n-alkanes.	53
4.11	The conversion and selectivity of products that obtained over 10 wt.% Ni/HZSM-12 catalyst at different temperatures (Reaction condition: 30 bar, H <sub>2</sub> /feed molar ratio of 10, LHSV of 1.5 h <sup>-1</sup> , and TOS at 5 h).	55
4.12	The product distribution over 10 wt.% Ni/HZSM-12 catalyst at different temperatures (Reaction condition: 30 bar, H <sub>2</sub> /feed molar ratio of 10, LHSV of 1.5 h <sup>-1</sup> , and TOS at 5 h).	55

<b>FIGURE</b>		<b>PAGE</b>
4.13	The conversion and selectivity of products that obtained over 10 wt.% Ni/HZSM-12 catalyst at different pressures (Reaction condition: 375 °C, H <sub>2</sub> /feed molar ratio of 10, LHSV of 1.5 h <sup>-1</sup> , and TOS at 5 h).	56
4.14	The conversion and selectivity of products that obtained over different percent nickel loading over parent HZSM-12 support (Reaction condition: 375 °C, 30 bar, H <sub>2</sub> /feed molar ratio of 10, LHSV of 1.5 h <sup>-1</sup> , and TOS at 5 h).	57
4.15	The conversion and selectivity of products that obtained over 10 wt.% Ni/HZSM-12 catalyst at different LHSV (Reaction condition: 375 °C, 30 bar, H <sub>2</sub> /feed molar ratio of 10, and TOS at 5 h).	58
4.16	Product distribution of products obtained over 10 wt.% Ni/HZSM12 catalyst at different LHSV (a) LHSV 1.5 h <sup>-1</sup> (b) LHSV 2.0 h <sup>-1</sup> (c) LHSV 2.5 h <sup>-1</sup> (Reaction condition: 375 °C, 30 bar, H <sub>2</sub> /feed molar ratio of 10, and TOS at 5 h).	59
4.17	Liquid products that obtained over (a) 10 wt.% Ni/HZSM-12 and (b) 10 wt.% Ni/HY catalysts (Reaction condition: 375 °C, 30 bar, LHSV 1.5 h <sup>-1</sup> , H <sub>2</sub> /feed molar ratio of 10).	60
4.18	The conversion and selectivity of products that obtained over (a) 10 wt.% Ni/HZSM-12 and (b) 10 wt.% Ni/HY catalysts (Reaction condition: 375 °C, 30 bar, LHSV 1.5 h <sup>-1</sup> , H <sub>2</sub> /feed molar ratio of 10).	61
4.19	The conversion and selectivity of products that obtained over 10 wt.% Ni/HZSM-12 and 10 wt.% Ni/HY catalysts (Reaction condition: 375 °C, 30 bar, LHSV 1.5 h <sup>-1</sup> , H <sub>2</sub> /feed molar ratio of 10 and TOS at 5 h).	62

<b>FIGURE</b>		<b>PAGE</b>
4.20	Product distribution of products that obtained over (a) 10 wt.% Ni/HZSM-12 and (b) 10 wt.% Ni/HY catalysts (Reaction condition: 375 °C, 30 bar, LHSV 1.5 h <sup>-1</sup> , H <sub>2</sub> /feed molar ratio of 10, and TOS at 5 h).	63
4.21	(a) liquid products chromatogram, and (b) gas products chromatogram over Ni/HZSM-12 catalyst operated at operating conditions: 375 °C, 30 bar, LHSV of 1.5 h <sup>-1</sup> , H <sub>2</sub> /feed molar ratio of 10, and TOS of 5 h.	65
4.22	(a) liquid products chromatogram, and (b) gas products chromatogram over Ni/HY catalyst operated at operating conditions: 375 °C, 30 bar, LHSV of 1.5 h <sup>-1</sup> , H <sub>2</sub> /feed molar ratio of 10, and TOS of 5 h.	66
4.23	Proposed reaction pathway of biojet fuel production from palmitic acid.	68
4.24	Temperature programmed oxidation (TPO) profiles of 10 wt.% Ni/HZSM-12 and 10 wt.% Ni/HY catalysts.	70



## CHAPTER I

### INTRODUCTION

In recent decades, there has been increasing in the air transportation demand because of increased industrialization and motorization. The jet fuel, otherwise referred to as aviation fuels, is mainly derived from the refining of petroleum feedstock called as “conventional jet fuels”. The combustion of fossil fuels has elicited concern with regard to its impact on environmental, mainly through the greenhouse gases (GHG), and public health. Furthermore, the world is confronting a problem with increasing air pollution emission. Hence, it is necessary to find the alternative jet fuels like biojet fuel from bio-based feedstock which saving the environmental and reducing GHG emission, sustainable, as well as the economic advantages associated with increased availability and lower fuel cost.

Vegetable oils are normally used for alternative diesel and biojet fuel production because they contain fatty acids in the proper carbon range (in most oils from C14 to C20) and low oxygen content that can be easily removed by hydrotreating. Palm is one of alternative resources used in biofuel production. In refining process of the crude palm oil, palm fatty acid distillate also known as PFAD, is a by-product which is generally generated in the deodorization step. PFAD mainly contains of free fatty acids approximately 90% normally used in soap industries, oleochemical industries, and biofuel production. Because the price of PFAD is much lower than palm oil feedstock and less critical as compared to the use of edible oil in term of ‘food for fuel’ sentiment, thus it is much preferred feedstock for alternative diesel and biojet fuel production.

The main reactions for biojet fuel production are hydrodeoxygenation, hydrodecarboxylation/ hydrodecarbonylation in order to remove oxygenated compounds, carboxylic and carbonyl groups in the fatty acid molecules then followed by hydroprocessing which involves hydrogenation, hydrocracking and hydroisomerization reaction. The heterogeneous catalyst is used to convert PFAD into saturated paraffins in the range of jet fuels (C9-C14). The Ni/HZSM-12 catalyst should be considered for biojet fuel production by the active metals (Ni) exhibited high efficiency in deoxygenation process to produce long chain hydrocarbons and also used to de-

velop the efficiency of biojet fuel production and HZSM-12 as a support is considered for hydroisomerization/hydrocracking process because of its suitable structure and acidity properties. The conventional HY catalyst was used to compare with HZSM-12 to observe the effect of pore size and morphology that suitable for biojet fuel production.

In this study, the production of biojet fuels from PFAD was investigated in a continuous flow fixed-bed reactor. The Ni/HZSM-12 and Ni/HY catalysts were prepared by incipient wetness impregnation method and used to indicate the conversion, selectivity, and stability during the catalytic activity testing. The fresh catalysts were characterized by XRD, XRF, TEM, BET, TPR and TPD. In addition, the spent catalysts were characterized by TPO. Moreover, the effect of temperature, pressure, % Ni loading and space velocity are also optimized to satisfy the yield of biojet fuels.

## **CHAPTER II**

### **LITERATURE REVIEW**

Jet fuel is a type of aviation fuels used to power the aircrafts by gas turbine power unit, mainly derived from distillate crude oil in refinery. Jet fuel is mainly composed of liquid hydrocarbon mixtures in a range of C9-C14 with a straw-coloured. The components in jet fuel which are normal, isomer and aromatic hydrocarbons effect to the properties that should meet the specifications of conventional jet fuel such as fluidity at low temperature, combustion characteristics, density, energy content, compatibility with construction materials, especially seals and sealants (Rabaev *et al.*, 2015). There are two main standard international specification of aviation in market which are Jet A/Jet A-1 and Jet B. Jet A and Jet A-1 are kerosene-type fuels that can be distinguished by the difference of the freezing point. Jet A must have a freezing point of -40 °C or below and normally not contain any additive for using in the United States while Jet A-1 must have a freeze point of -47 °C or below and normally contains static dissipator additive for using in locations outside the United States. The another type of jet fuel, Jet B, is naphtha-kerosene which has a very low freezing point of -60 °C for using to perform in cold weather (Zhang *et al.*, 2016).

Recently, the instable price of crude oil and environmental issue are the reasons for developing alternative sustainable energy which friendly with environment, inexpensive and meet the specification with the market.

#### **2.1 Biojet Fuel**

In the present, the used of aviation transport is rapidly increasing because of increased industrialization and motorization. It has been reported that the air transport is growing faster than other transport mode in transportation sector and consume energy much to 40% of primary energy consumed in the world. Jet fuel, a type of aviation fuel, is mainly come from petroleum-based fuel which have a negative impact on the environmental, mainly through the greenhouse gases (GHG) due to the carbon emission (Liu *et al.*, 2015). Furthermore, the price of petroleum-based

jet fuel correlated with the price of crude oil. The uncertainty of crude oil prices make it difficult to plan and budget long-term operating expenses (Wang and Tao, 2016). Hence, it is necessary to find the alternative fuels which saving the environmental and reducing GHG emission, sustainable, as well as the economic advantages associated with increased availability and lower fuel cost. The biojet fuel is a potential alternative to petroleum-based jet fuel by offer a solution to these issues. Figure 2.1 displayed life-cycle greenhouse gas emissions for conventional and alternative jet fuels. Based on crude to conventional jet fuel, the bio-based materials can reduce life-cycle greenhouse gas emissions for producing alternative jet fuels.

Biojet fuel can be produced from several processes are hydrotreatment of plant oil, Fischer-Tropsch synthesis of biomass and pyrolysis. However, hydrotreatment of plant oil offers a simpler approach to the production of jet fuel than others.

According to American Society for Testing and Materials (ASTM) D7566, biojet fuel are used as mixing component in aviation fuels with the largest portion being less than 50% (Wang and Tao, 2016). Therefore, the key points for meeting the mixing standard are high C9-C14 selectivity and the degree of isomerization.

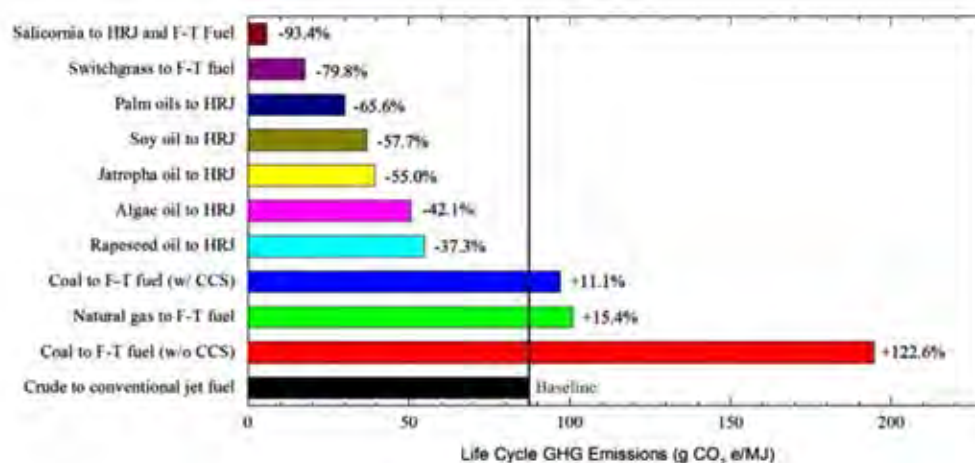


**Figure 2.1** Life-cycle greenhouse gas emissions for conventional and alternative jet fuels (The unit of 'g CO<sub>2</sub>/eMJ' represent the CO<sub>2</sub> equivalent emissions per unit of energy) (Zhang *et al.*, 2016).

## 2.2 Bio-based Fuel Feedstock

Nowadays, vegetable oils and fatty acids have been used as resources for biofuel production instead of jet fuel derived from petroleum distillation.

### 2.2.1 Vegetable Oil

Vegetable oils normally be used for renewable diesel and jet fuel production because they contain fatty acids in the proper carbon range (in most oils from C14 to C20) and little oxygen about 11 wt.% that can be easily removed by hydrotreating (Rabaev *et al.*, 2015). Vegetable oils contain triglyceride as the main component which is ester derived from glycerol and three fatty acids. By the most common fatty acids in vegetable oils such as stearic, oleic, linolenic and palmitic acids are shown in Table 2.1. Furthermore, using vegetable oils can give advantages for agricultural economy, environmental and stable material to provide.

There are many choices of vegetable oil that suitable for using to produce biofuels. Then, choosing type of feedstocks depends on agriculture in local land and transportation cost in each country. The feedstock choices for the diesel and jet fuel production have been studied using various vegetable oils including jatropha oil, palm oil, soy bean oil, rapeseed oil, algae oil, canola oil, and oil-extract from coffee ground. Furthermore, waste-cooking oil, animal fat, and bio-oil have become potential feedstock candidates.

The vegetable oil is divided into edible and non-edible oil. Table 2.2 shows fatty acid compositions and properties found in the different vegetable oils both edible oil and non-edible oil that many research use to investigate the reaction of alternative fuel production. The use of non-edible oil is more preferable than edible oil because of the food versus fuel dilemma (Liu *et al.*, 2015). Furthermore, the heating values of vegetable oils are around 39–40 MJ/kg which higher than FAME (Fatty Acid Methyl Ester) required of European Union standard EN 14214 for bio-diesel fuel minimum high heating value at 35 MJ/kg.

**Table 2.1** The chemical structure of common fatty acids in vegetable oils (Ong *et al.*, 2011)

Name	Chemical name	Structure (xx:y) <sup>a</sup>	Formula
Lauric	Dodecanoic	12:0	C <sub>12</sub> H <sub>24</sub> O <sub>2</sub>
Myristic	Tetradecanoic	14:0	C <sub>14</sub> H <sub>28</sub> O <sub>2</sub>
Palmitic	Hexadecanoic	16:0	C <sub>16</sub> H <sub>32</sub> O <sub>2</sub>
Stearic	Octadecanoic	18:0	C <sub>18</sub> H <sub>36</sub> O <sub>2</sub>
Oleic	cis-9-Octadecenoic	18:1	C <sub>18</sub> H <sub>34</sub> O <sub>2</sub>
Linoleic	cis-9,cis-12-Octadecadienoic	18:2	C <sub>18</sub> H <sub>32</sub> O <sub>2</sub>
	cis-9,cis-12,cis-15-		
Linolenic	Octadecatrienoic	18:3	C <sub>18</sub> H <sub>30</sub> O <sub>2</sub>
Arachidic	Eicosanoic	20:0	C <sub>20</sub> H <sub>40</sub> O <sub>2</sub>
Gadoleic	11-eicosenoic	20:1	C <sub>20</sub> H <sub>38</sub> O <sub>2</sub>
Behenic	Docosanoic	22:0	C <sub>22</sub> H <sub>44</sub> O <sub>2</sub>
Erucle	cis-13-Docosenoic	22:1	C <sub>22</sub> H <sub>42</sub> O <sub>2</sub>
Lignoceric	Tetracosanoic	24:0	C <sub>24</sub> H <sub>48</sub> O <sub>2</sub>

<sup>a</sup> xx = total number of carbon atoms and y = number of double bonds.

**Table 2.2** The selected properties of variety vegetable oils and diesel (Talebian-Kiakalaieh *et al.*, 2013)

Type of oil	Species	Fatty acid composition (wt.%)	Viscosity (at 40 °C)	Density (g/cm <sup>3</sup> )	Flash point (°C)	Heating value (MJ/kg)
Edible oil	Soybean	C16:0, C18:1, C18:2, C18:3	32.9	0.91	254	39.6
	Rapeseed	C16:0, C18:0, C18:1, C18:2	35.1	0.91	246	39.7
	Sunflower	C16:0, C18:0, C18:1, C18:2	32.6	0.92	274	39.6

**Table 2.2 (Cont.)** The selected properties of variety vegetable oils and diesel  
(Talebian-Kiakalaieh *et al.*, 2013)

Type of Oil	Species	Fatty acid composition (wt.%)	Viscosity (at 40 °C)	Density (g/cm <sup>3</sup> )	Flash point (°C)	Heating value (MJ/kg)
Edible oil	Palm	C16:0, C18:0, C18:1, C18:2	39.6	0.92	267	-
	Peanut	C16:0, C18:0, C18:1, C18:2, C20:0, C22:0	22.72	0.90	271	39.8
	Corn	C16:0, C18:0, C18:1, C18:2, C18:3	34.9	0.91	277	39.5
	Camelina	C16:0, C18:0, C18:1, C18:2, C18:3, C20:0, C20:1, C20:3	-	0.91	-	42.2
	Canola	C16:0, C18:0, C18:1, C18:2, C18:3	38.2			
	Cotton	C16:0, C18:0, C18:1, C18:2	18.2	0.91	234	39.5
	Pumpkin	C16:0, C18:0, C18:1, C18:2	35.6	0.92	>230	39
Non-edible oil	Jatropha urcas	C16:0, C16:1, C18:0, C18:1, C18:2	29.4	0.92	225	38.5
	Pongamina-innata	C16:0, C18:0, C18:1, C18:2, C18:3	27.8	0.91	205	34
	Sea mango	C16:0, C18:0, C18:1, C18:2	29.6	0.92	-	40.86
	Palanga	C16:0, C18:0, C18:1, C18:2	72.0	0.90	221	39.25
	Tallow	C14:0, C16:0, C16:1, C17:0, C18:0, C18:1, C18:2	-	0.92	-	40.05
	Nile tilapia	C16:0, C18:1, C20:5, C22:6, other acids	32.1	0.91	-	-
	Poultry	C16:0, C16:1, C18:0, C18:1, C18:2, C18:3	-	0.90	-	39.4
Others	WCO	Depends on fresh cooking oil	44.7	0.90	-	-
-	Diesel	-	3.06	0.855	76	43.8

Honeywell's UOP also has successfully commercialized the deoxygenating process to convert vegetable oils and wastes to green jet fuels by Ecofining<sup>TM</sup> SPK process. UOP has produced renewable jet fuel from a variety of feedstocks, including first generation oils such as palm and soybean oils, as well as second generation oils like camelina, jatropha and algal oils. (Liu *et al.*, 2013)

There are a lot of prior studied about converting vegetable oils to renewable jet fuel. Verma *et al.* (2015) investigated the hydrocracking of non-edible jatropha oil over sulfided NiMo and NiW supported on SAPO-11 catalysts in fixed bed reactor under conditions of 375-450 °C, 60-80 bar and LHSV 1h<sup>-1</sup>. This process was obtained high yield about 84 wt.% of liquid hydrocarbon products was obtained over all the catalysts, with about 40% diesel and about 40% biojet fuel, remaining 20% being lighter gasoline range hydrocarbon. Moreover, this studied found removing oxygen content pathways of triglyceride has specific on each catalyst. By decarboxylation and decarbonylation are more selective over NiW than NiMo catalysts.

Cheng *et al.* (2014) produced quality jet fuel with high amount of alkanes and low amount of aromatic hydrocarbons by hydrocracking of soybean oil in batch reactor using two zeolites of HY and HZSM-5 supporting Ni (8 wt.%) and Mo (12 wt.%) as catalysts under conditions of 330-410 °C, 10-50 bar hydrogen pressure for 8 h. Zeolite HY exhibited higher jet range alkane selectivity (40.3%) and lower jet range aromatic hydrocarbon selectivity (23.8%) than zeolite HZSM-5 (13.8% and 58.9%, respectively). The results indicated that jet fuel converted from soybean oil over zeolite HY exhibited higher energy density than that over zeolite HZSM-5, which can be attributed to the smaller pore size of zeolite HZSM-5 (0.54 nm) than zeolite HY (0.74 nm), so alkanes were not able to diffuse until they were further cracked into aromatic hydrocarbons with shorter carbon chains higher selectivity to light hydrocarbons.

de Sousa *et al.* (2016) used Pd supported on carbon to quantitatively convert the palm kernel oil by hydrodeoxygenation in fixed bed reactor under mild conditions (300 °C, 5 bar hydrogen pressure, 5 h of reaction) to produce approximately 82% of the hydrocarbons in the jet fuel range.

### 2.2.2 Fatty Acid

Fatty acids are found in vegetable or animal oil and fat. The structure of fatty acid is similar to vegetable oil which is carboxylic acid with long aliphatic chains (either saturated or unsaturated). Saturated fatty acid is fatty acid with no carbon-carbon double bond such as palmitic acid, stearic acid and lauric acid. Meanwhile, unsaturated fatty acid is fatty acid with one or more carbon-carbon double



bonds for example: oleic acid, myristoleic acid and linoleic acid. Fatty acids are formed during enzymatic hydrolysis of triglyceride especially when the oils are kept in humid atmosphere and also be formed during purification of vegetable oil and fat (Hermida *et al.*, 2015).

Most deoxygenation studies are performed on model compounds by stearic acid is the most widely investigated model compounds for the deoxygenation reaction of feedstock. For instance, Siswati Lestari and co-workers (Siswati Lestari, 2009) studied about catalytic deoxygenation of neat stearic acid at 360 °C under 10 bar argon or 5 vol.% hydrogen in argon in a fixed-bed reactor by using mesoporous-supported Pd/C beads as a catalyst. The results showed stable catalyst performance, giving about 15% conversion level of stearic acid. The main liquid-phase product was heptadecane, while the main gaseous products were CO and CO<sub>2</sub>.

Furthermore, palmitic acid is the main composition of palm oil so there are many studies about upgrading palmitic acid to biofuel. Cao *et al.* (2017) studied the high *iso*-alkanes production from palmitic acid over bi-functional Ni/HZSM-22 catalyst under conditions of 150-260 °C, 40 bar for 4 h in batch reactor. The catalyst preparation was varied in three methods are melt infiltration, incipient wetness impregnation and wetness impregnation method. The results indicated that Ni/HZSM-22 performed excellent catalytic performance and stability. Especially, the catalyst prepared by melt infiltration was more inclined to hydrodeoxygenation (HDO) routes and produced more *iso*-alkanes (0.8 mol ratio of *iso*-/*n*- alkanes) than other catalysts prepared by conventional impregnation methods.

### 2.3 Palm Fatty Acid Distillate Feedstock

Palm is a tropical plant represented as one of edible oil which can be grows in pasture land together with humid. In 2014, world production of oils and fats stood at 200.24 million tonnes by palm oil and palm kernel oil provide the largest proportion approximately at 66.15 million tonnes (33%) of this followed by soybean oil provide 45.14 million tonnes (23%) and rapeseed oil at 26.92 million tonnes (13%) as shown in Figure 2.2. In Figure 2.3 showed that South East Asia is the highest palm oil exporter in 2014 with total average around 92%. Due to Indonesia and Ma-

Indonesia and Malaysia are the world's top-two largest crude palm oil (CPO) exporters which export around 22.33 million and 17.31 million tonnes, respectively in 2014. According to palm oil is the most efficient oil in terms of land advantage, efficiency and profitability thus palm oil becomes the choice for biodiesel.

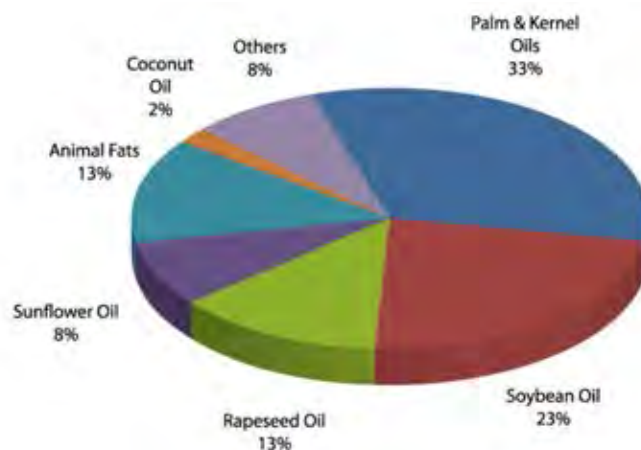


**Figure 2.2** World oils and fats production in 2014 (Oil World & MPOC estimates).

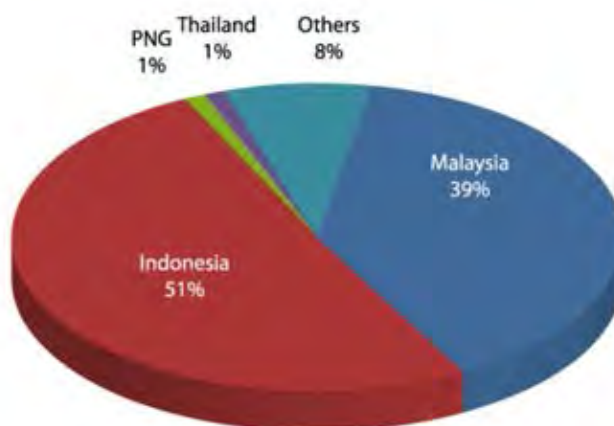


**Figure 2.3** World palm oil exports by country in 2014 (Oil World & MPOC estimates).

In refining process of the crude palm oil, low valuable product called “Palm fatty acid distillate also known as PFAD” is the by-product which is generally generated in the deodorization step.

The crude palm oil is physically refined by removing impurities in order to accept specifications. Figure 2.4 showed the refinery process of palm oil. Firstly, gum (phospholipids and phosphotides) in crude palm oil is removed by precipitation process which occurs at 90-130 °C and uses phosphoric acid as a precipitant. Secondly, degummed palm oil (DPO) from first state is bleached to eliminate undesirable impurities such as trace metals and pigments. Then, the bleached palm oil (BPO) from second state is deodorized to remove free fatty acid content, giving palm fatty acid distillate (PFAD) as a by-product from this step and also refined, bleached, deodorized palm oil (RBDPO) as a product. Finally, RBDPO is fractionated to yield refined palm olein (RPO) and refined palm stearin (RPS) (Kiatkittipong *et al.*, 2013).

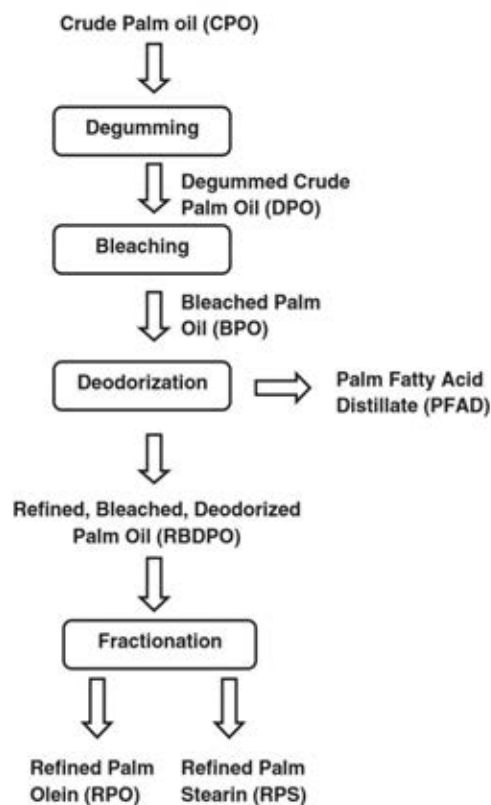


**Figure 2.4** Physical refining process of crude palm oil (Kiatkittipong *et al.*, 2013).

Palm fatty acid distillate (PFAD) is light brown semisolid at room temperature and can be melted to brown liquid at higher temperature. PFAD is a potential low cost palm biofuel second generation feedstock. Generally, PFAD was used as a

source of free fatty acid for non-food applications in industry such as soap production, industry boiler fuel, animal feed industries, and also oleochemical industries (candle factory).

PFAD is mainly contains of free fatty acids by approximate 90% are palmitic acid and oleic acid, the remaining are triglyceride, partial glyceride and unsaponifiable component such as vitamin E, squalene, sterols and volatile components. Table 2.3 showed components and properties of PFAD that is strongly recommended for biodiesel industries.

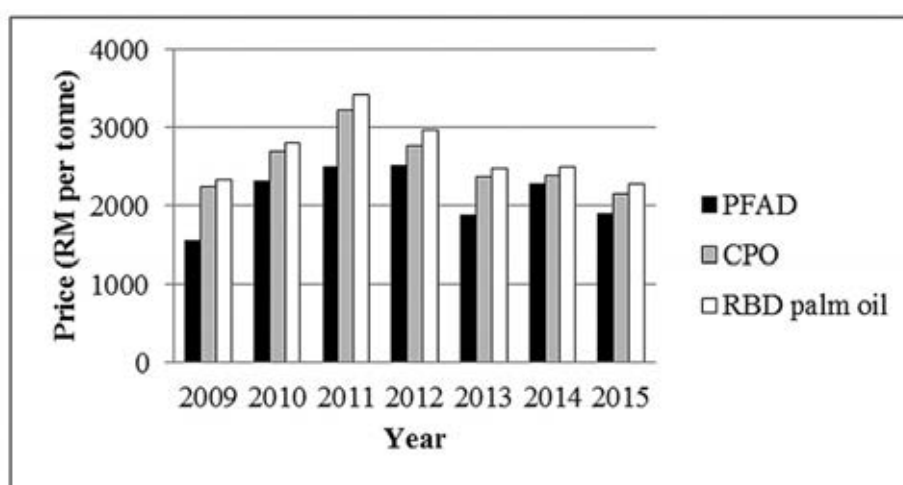
The price of PFAD is much lower compared to other refined oil that being used currently as feedstock in biodiesel plant. Figure 2.5 showed the price of PFAD comparison with crude palm oil (CPO) and RBD palm oil. From the data, the price and its utilization in biodiesel production is seen less critical as compared to the use of edible oil in term of ‘food for fuel’ sentiment so it can be confirmed that PFAD is much preferred feedstock than others.

**Table 2.3** The compositions and properties of PFAD (Kapor *et al.*, 2017)

Properties	(Ping and Yusof, 2009)	(Lokman <i>et al.</i> , 2015)
FFA content (as palmitic, %)	72.7-92.6	86.3 ± 1.75
Iodine value, (g I <sub>2</sub> /100 g)	46.3-57.6	
Saponification value (mg KOH/g)	200.3-251.4	149.74 ± 4.72
Unsaponifiable matter (%)	1.0-2.5	
Moisture content (%)	0.03-0.24	0.089 ± 0.004
Titre (°C)	46.0-48.3	
Fatty acid composition (wt.%)		
C14:0	0.9-1.6	1.9 ± 0.05
C16:0	43.0-49.1	45.7 ± 1.32

**Table 2.3 (Cont.)** The compositions and properties of PFAD (Kapor *et al.*, 2017)

Properties	(Ping and Yusof, 2009)	(Lokman <i>et al.</i> , 2015)
C18:0	4.0-4.5	4.3 ± 0.09
C18:1	34.7-37.2	40.2 ± 1.21
C18:2	8.5-9.7	7.9 ± 0.21

**Figure 2.5** Prices of PFAD, CPO, and RBD palm oil (May, 2016).

Kiatkittipong *et al.* (2013) produced diesel-like hydrocarbon from hydro-processing of crude palm oil (CPO), degummed palm oil (DPO) and palm fatty acid distillate (PFAD) over Pd/C and NiMo/ $\gamma$ -Al<sub>2</sub>O<sub>3</sub> catalysts under conditions of 350-450 °C, 20-60 bar hydrogen pressure and reaction time of 0.25-3 h in batch reactor. The study was examined in order to determine suitable operating condition for each feedstock and compare the suitability between both catalyst for each catalyst. The results showed that Pd/C catalyst showed good catalytic activity for fatty acid feedstocks but became less promising for triglyceride feedstocks when compared to Ni-Mo/ $\gamma$ -Al<sub>2</sub>O<sub>3</sub>.

Choi *et al.* (2015) studied the catalytic conversion of non-edible oil PFAD and soybean oil compared with model compound stearic acid over Pd on beta-zeolite

catalyst in single-step process (SSP) in batch reactor with no added hydrogen to examine the possibility of the direct production of hydrocarbon in the range of jet fuel. The results showed that stearic acid was converted to products 100% and converted in range of jet fuel 69.3% at 270 °C while soybean oil and PFAD have deoxygenation rates of 95.5% and 94.25% respectively with a yield of approximately 31% and 24.58%, respectively of hydrocarbon in the jet fuel range under conditions of 300 °C, 15 bar and reaction time of 6 h. From the results, they indicate that the Pd catalyst is essential for deoxygenation reaction in a single step process (SSP). However, the results suggested that obtained drop-in jet fuel is required mixing step with petroleum-based aromatic hydrocarbons.

Tamiyakul *et al.* (2016) investigated the effect of Ga and Zn over H-ZSM-5 for aromatic production from palm fatty acid distillate (PFAD). They studied over H-ZSM-5, Ga/H-ZSM-5, and Zn/H-ZSM-5 catalysts at 500 °C, atmospheric pressure for 3 h. The purpose of these reaction pathways were the deoxygenation of fatty acid via decarboxylation, decarbonylation, or directly cracking of fatty acid molecules, to produce long chain hydrocarbons (C11–C17) at first step. They demonstrated that the introduction of both Ga and Zn promoted the aromatization of PFAD due to increasing dehydrogenation function. The higher aromatics yield of Zn/H-ZSM-5 was obtained by the presence of two zinc species; exchanged  $Zn^{2+}$  which promotes the dehydrogenation of paraffins and ZnO which promotes the decarboxylation of oxygenates. The shifting from decarbonylation to decarboxylation means shifting from the Brønsted acid site of the parent H-ZSM-5 to ZnO preserved the Brønsted acid site for aromatization, hence increasing the aromatics yield.

## 2.4 The Overall Reaction for Biojet Fuel Production

From UOP's green jet fuel process technology (Ecofining™ SPK process) consists of two main sections, deoxygenation section and isomerization/cracking (or hydrocracking) section. Both of them are based on hydroprocessing technology commonly used in today's refineries to produce transportation fuels.

However, there are many process technologies that convert bio-based materials into jet fuel by some are available at commercial or pre-commercial scale, and others are still in the research development stage.

In this study, the main reaction for biojet fuel production are hydrodeoxygenation and hydroisomerization/hydrocracking and hydrogenation. The similar prior study was obtained by Liu *et al.* (2015). They studied the deoxygenation reactions of palmitic acid in a fixed-bed reactor over HZSM-22, Ni<sub>x</sub>P/HZSM-22, Ni<sub>2</sub>P/HZSM-22, the unsupported Ni<sub>x</sub>P and the unsupported Ni<sub>12</sub>P<sub>5</sub> catalysts. From the results, they reported a new decarbonylation and decarboxylation mechanism of palmitic acid based on in situ DRIFT spectroscopy. The plausible deoxygenation pathways over 40NiPZ are shown in Figure 2.6.

(a) The first step was H<sub>2</sub> dissociation on Ni<sub>x</sub>P (Ni<sub>12</sub>P<sub>5</sub> and Ni<sub>2</sub>P) and then combination of H with OH (in palmitic acid) to form H<sub>2</sub>O, generating the C<sub>14</sub>H<sub>29</sub>-CH<sub>2</sub>-CHO as an intermediate.

(b) Palmitic acid could be converted into a Simultaneously, palmitic acid could be directly converted into pentadecane via decarboxylation.

(c), (d) Finally, isomerization and cracking can occur when palmitic acid directly interacts with Bronsted acid and Lewis acid sites on HZSM-22, respectively. The OH (in palmitic acid) combines with H (in HZSM-22) and the C-C bands (in palmitic acid) are broken by the carbonium ion mechanism. Then H<sub>2</sub>O and ketones are formed. The ketones can be converted into hydrocarbon by decarbonylation in (a). Simultaneously, palmitic acid can be converted to aromatic hydrocarbons (or short chain hydrocarbons) and C<sub>c</sub>H<sub>d</sub>-COOH via cracking and isomerization. Finally, C<sub>c</sub>H<sub>d</sub>-COOH could be further converted into hydrocarbons by decarbonylation and decarboxylation.

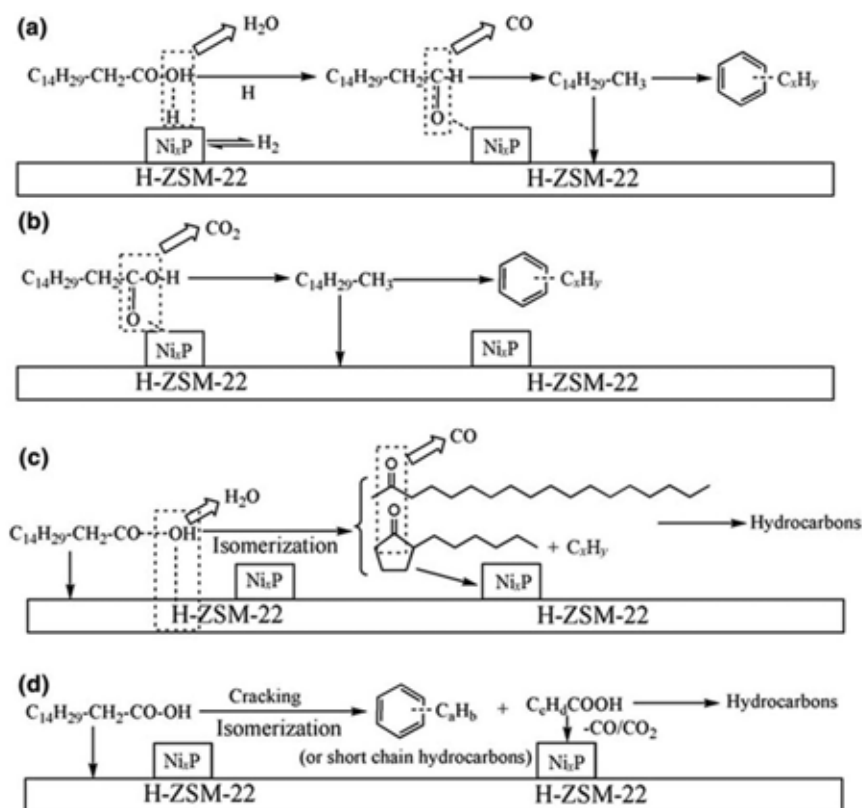


**Figure 2.6** The four catalytic pathways proposed for deoxygenation of palmitic acid on 40NiPZ. (a) Decarbonylation, (b) Decarboxylation, (c) Initial isomerization and (d) Initial isomerization and cracking (Liu *et al.*, 2015).

#### 2.4.1 Hydrodeoxygenation

The high oxygen content of fatty acids and vegetable oils play a key role in fuel properties effects in term of low heating value, thermal and chemical instabilities and corrosive. Therefore, hydrodeoxygenation is a process that important for removing oxygen contents in those feedstocks.

Hydrodeoxygenation is a chemical process which incorporates the transformation of the unsaturated fatty acids into saturated fatty acids and removing oxygenated compounds from the fatty acid structure. The objectives of this process are to reduce the O/C ratio and to increase H/C ratio at the same time. This process occur at moderate or high temperature and higher hydrogen pressure in the presence



of a heterogeneous catalyst. During hydrodeoxygenation process, the major by-product is water which may reduce the catalyst activity (Pattanaik and Misra, 2017).

There are many catalysts used in hydrodeoxygenation process. The most popular catalysts of this process are sulfide cobalt-molybdenum and nickel-molybdenum bimetallic catalysts support on alumina. However, the use of sulfide metal catalysts results in sulfur contaminated hydrocarbon products which are toxic to environment. Furthermore, the cost of noble metals is very high so they are less favorable as hydrodeoxygenation catalysts. Therefore, it becomes essential to develop non-sulfidated transition metal catalysts for the hydrodeoxygenation of fatty acids to produce sulfur-free hydrocarbon fuels (Pattanaik and Misra, 2017).

There are three main reaction pathways: decarbonylation, decarboxylation which is the most desired route (no water product), and direct hydrodeoxygenation (HDO) for deoxygenation process to produce straight chain hydrocarbons and other possible reactions occurring in the process like the water-gas-shift reaction and hydrogenation as shown in Figure 2.7.

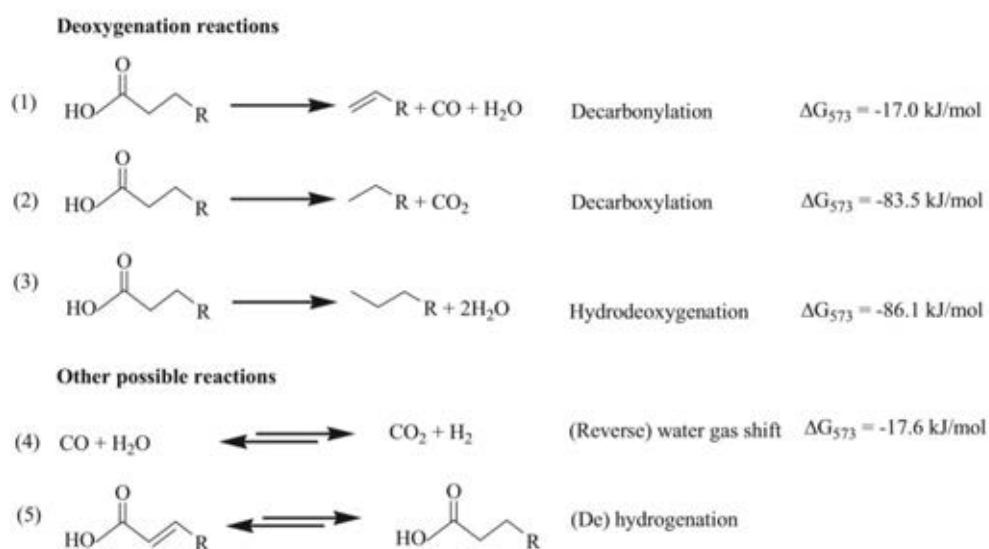


**Figure 2.7** Various deoxygenation reaction schemes with other possible reactions including thermodynamic data ( $\Delta G_{573}$  in kJ/mol at 0.1 MPa) (Pattanaik and Misra, 2017).

(1) Decarbonylation (DCN) pathway which consumed  $H_2$  for forming aldehyde as an intermediate and producing  $H_2O$  and  $CO$  (carbon monoxide) by C–O bond cleavage and C–C bond rupture, respectively,

(2) Decarboxylation (DCX) pathway, occur by elimination  $-COOH$  as  $CO_2$  which consumed no  $H_2$  and favor increasing reaction temperature, oxygen in fatty acid is removed in the form of  $CO_2$  (carbon dioxide) by the direct attack at C–C bond

(3) Hydrodeoxygenation (HDO) pathway which consumed large quantity of  $H_2$  and consequence produced  $H_2O$ , separation of oxygen in fatty acid takes place via C=O bond hydrogenation, C–O bond rupture and further C–C bond cleavage by aldehyde and alcohol as intermediates. (Hermida *et al.*, 2015; Pattanaik and Misra, 2017)

The reaction factor such as the hydrodeoxygenation process, optimization of reaction temperature and hydrogen pressure, species of catalyst and catalyst loading is also essential have to design properly to achieve objective. Catalyst should be designed to avoid side reactions as most as possible and have higher selectivity towards to meet specific products.

There are many catalysts used in hydrodeoxygenation process. The most popular catalysts of this process are sulfide cobalt-molybdenum and nickel-molybdenum bimetallic catalysts support on alumina. However, the use of sulfide metal catalysts results in sulfur contaminated hydrocarbon products which are toxic to environment. Furthermore, the cost of noble metals is very high so they are less favorable as hydrodeoxygenation catalysts. Therefore, it becomes essential to develop non-sulfidated transition metal catalysts for the hydrodeoxygenation of fatty acids to produce sulfur-free hydrocarbon fuels (Pattanaik and Misra, 2017).

Snåre *et al.* (2006) studied the deoxygenation in a semi-batch reactor of stearic acid in the presence of dodecane as solvent by using active components are noble metals (Pd, Pt, Ru, Ir, Os and Rh) and non-noble metal (Ni). The catalyst supports were  $Al_2O_3$ ,  $SiO_2$  and activated carbon. The results showed that the most efficient catalyst for deoxygenation of stearic acid through decarboxylation to produce *n*-heptadecane is Pd supported on mesoporous carbon (5 wt.% Pd/C) was. The 5

wt.% Pd/C catalyst provided successfully completely converting stearic acid with over 98% selectivity toward deoxygenated C<sub>17</sub> products. Furthermore, it was also reported that activities for the deoxygenation of metals incorporated on the same support increased in the order of Os<Ru<Ir<Rh<Ni<Pt<Pd.

#### 2.4.2 Hydrocracking

Hydrocracking is an essential catalytic chemical process used in petroleum refineries for the conversion of the middle and heavy distillates and residuals that have a high-boiling range into more valuable lower-boiling products such as gasoline, kerosene, jet fuel, and diesel oil in the presence of hydrogen and a catalyst. The process takes place in a hydrogen-rich atmosphere at elevated temperatures (260–425 °C) and pressures (35–200 bar) that leads to higher gas production and lower liquid yield. Figure 2.8 represents a hydrocracking reaction:



**Figure 2.8** The schematic of hydrocracking reaction.

There are two main chemical reactions occurring in the hydrocracker: catalytic cracking of heavy hydrocarbon into lighter unsaturated hydrocarbons and the saturation of these newly formed hydrocarbons with hydrogen (Eia, 2013). In fact, there are many steps of hydrocracking over catalyst.

For example, the hydrocracking of *n*-paraffins over a bifunctional catalyst goes through the following steps:

1. Adsorption of *n*-paraffins on metal sites
2. Dehydrogenation with formation of *n*-olefins
3. Desorption from metal sites and diffusion to acid sites
4. Skeletal isomerization and/or cracking of olefins on the acid sites through carbenium ion intermediates
5. Desorption of formed olefins from acid sites and diffusion to metal sites
6. Hydrogenation of these olefins (*n*- and *iso*-) in metal sites

## 7. Desorption of resulting paraffins

Li *et al.* (2016) studied developing zeolite catalysts to produce jet bio-fuel from palm oil by hydrocracking. They used five different Ni-loaded zeolites as catalysts are Ni/SAPO-34, Ni/MCM-41, Ni/HY, Ni/SAPO-11 and Ni/Hbeta under conditions of 370-410 °C, 30 bar and 8 h. They indicate that Ni/SAPO-34 is an excellent catalyst for giving the highest alkane/arene selectivity ratio and Ni/HY gave the highest biojet fuel yield. The reason of these results are structure selectivity of catalysts and acid intensity by Ni/SAPO-34 catalyst has LTA structure and weak acid intensity so zeolite SAPO-34 gave the highest alkane/arene selectivity ratio. For Ni/HY catalyst has FAU structure and high acid density so it gave high arene activity.

### 2.4.3 Hydroisomerization

Hydroisomerization is a conventional method for converting of *n*-paraffins to isoparaffins. Moreover, hydroisomerization is an industrial process employed by petroleum refineries for the transformation of linear paraffins into their corresponding isomers at usually high hydrogen pressure (at least 20 bar), although recent studies indicated that the reaction can be achieved at 1 atm. The process normally proceeds over a supported catalyst with bifunctionality which containing both the metal and acid sites. Normal paraffin to be converted undergo initial dehydrogenation over the metal sites to produce a corresponding *n*-alkene with the same number of carbon chains. The interaction of the latter with Brønsted acid sites generates carbenium ion, which undergo subsequent isomerization into iso-carbenium ion and consequently desorbs as iso-alkene. The final stage of the reaction involved the hydrogenation of the latter over metallic sites to produce the desired branched paraffin as seen in Figure 2.9 (Galadima and Muraza, 2015).

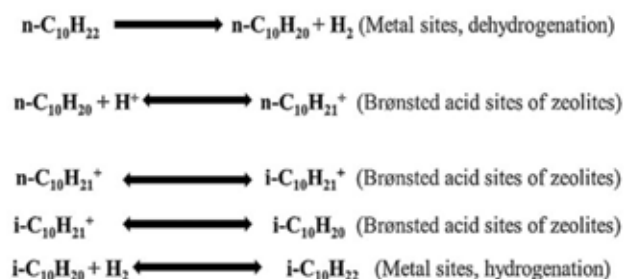


**Figure 2.9** Mechanism of *n*-paraffins/*n*-alkanes hydroisomerization over bifunctional catalysts (e.g. zeolites loaded with metals) using *n*-decane as a model compound (Galadima *et al.*, 2015).

Because of the non-compatible cold flow characteristics of the normal paraffinic hydrocarbons produced from the hydrodeoxygenation of vegetable oils so it can only be blended in low ratios with jet fuels. Therefore, the *n*-paraffins must be converted or upgraded into the corresponding *iso*-paraffins by the process of hydroisomerization to appropriately improve these properties. However, when the chain length of the *n*-alkane produced exceeds *n*-C<sub>15</sub>, a further hydrocracking to lighter alkanes in the range of jet fuel (*n*-C<sub>5</sub> to *n*-C<sub>15</sub>) is necessary before the hydroisomerization reaction for production of jet fuel.

The hydrogenation-to-acidity ratio is significantly effect on the hydrocracking of paraffin. The *iso*-to-normal ratio in product paraffin increased with decreasing reaction temperature because the cracking rate of *iso*-paraffins increases faster than that of *n*-paraffins at higher temperature. This is illustrated by the hydrocracking of *n*-decane in Figure 2.10. The *iso*-to-normal ratio also increases when the catalyst contains a weak hydrogenation component and strong acid component. The higher *iso*-to-normal ratio is attributed to a higher rate of isomerization of olefinic intermediates at the strong acidic sites (Scherzer and Gruia, 1996).

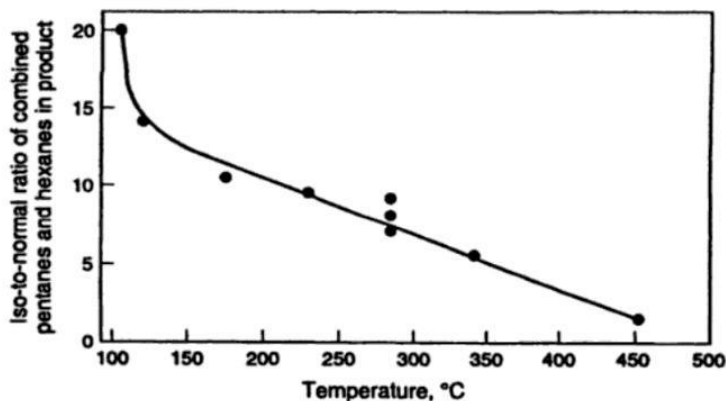


**Figure 2.10** Effect of reaction temperature on *iso*-to-normal paraffin ratio in products obtained from hydrocracking of *n*-decane over strongly acidic catalyst (Scherzer and Gruia, 1996).

Generally acidic supports of bi-functional catalysts in order to promote the hydroisomerization reaction are different oxides such as alumina, zirconia, and sulfides were applied to the reaction. Also, the zeolites such as MOR, BEA, ZSM-5, MAZ, OFF, USY, ZSM-22, MCM-22 and zeolite-like solid acids such as SAPO-11, AlPO-5, SAPO-41 have been used as acidic supports together with a metal such as Pt, Ni, Pd, Co, Mo, Ir, Ru, Rh and Re. There are two processes over zeolites proceed through consecutive branching reactions (i.e., isomerization of *n*-paraffins), while cracking reactions occur in parallel with isomerization (Santos *et al.*, 2011).

In 2013, Lee *et al.* studied hydroisomerization of *n*-dodecane over Pt/Y zeolites with different acid characteristics which *n*-dodecane is a model reactant for producing jet-fuel from FT-wax. They compared different range of acid which are NaY ( $\text{SiO}_2/\text{Al}_2\text{O}_3 = 5.1$ ), HY ( $\text{SiO}_2/\text{Al}_2\text{O}_3 = 80$ ) and HY ( $\text{SiO}_2/\text{Al}_2\text{O}_3 = 200$ ). The results showed that the conversion of *n*-dodecane decreased with increasing  $\text{SiO}_2/\text{Al}_2\text{O}_3$  ratio, whereas the selectivity of isomerization increased with increasing  $\text{SiO}_2/\text{Al}_2\text{O}_3$  ratio. In addition, HY ( $\text{SiO}_2/\text{Al}_2\text{O}_3 = 80$ ) exhibited the highest hydroisomerization activity. In a result of varied temperature in the range of 280–360 °C under a constant pressure of 40 bar, the conversion increased and the selectivity decreased with increasing temperature. However, with increasing pressure were

dropped down the isomerization efficiency due to when increased pressure, the adsorption of *n*-dodecane on the active sites of the catalyst was prevented by hydrogen molecules that compete with *n*-dodecane. When they improved the catalyst by impregnated metal with the range of 0.1–1.0%, they obtained that yield of *iso*-dodecane slightly increased with increasing metal concentration but the effect was not large. They were suggests that the effect of the acid sites is greater than that of the impregnated metal.

In 2016, Ju *et al.* found that Pt/ZSM-12 catalyst is an effective catalyst for the conversion of *n*-C<sub>15</sub> paraffin into multi-branched isomers and mono-branched isomers which satisfied the jet fuel specification. The objective of this study is to produce high yield jet fuel from lipid through the following steps: 1) selecting the lipid oil which is rich in C<sub>16</sub> fatty acid either from algae or oil-bearing crops; 2) all lipids was converted into fatty acid by hydrolysis; 3) the fatty acid was decarboxylated into C<sub>15</sub> rich *n*-paraffin, and finally the *n*-paraffin was further hydroisomerized into multi-branched C<sub>15</sub> molecules which can be used as jet fuel blend. The standard reaction conditions were 30 bar hydrogen pressure and a temperature in a range of 200-340 °C, *n*-pentadecane WHSV is 2.5 h<sup>-1</sup>. They compared the activity of Pt/ZSM-12 with Pt/ZSM-22 and Pt/USY. It was found that the Pt/ZSM-12 catalyst has the highest value on multi/mono-isomers ratio on which the ratio achieves 2.0 so it is a very suitable hydro-isomerization catalyst for jet fuel production from suitable lipid oil.

#### 2.4.4 Hydrogenation and Dehydrogenation

Hydrogenation is a chemical reaction between molecular hydrogen (H<sub>2</sub>) and another compound or element. Generally, hydrogenation is used in reducing process with the presence of a catalyst such as platinum, palladium and nickel or saturating organic compound process by reducing double and triple bonds in hydrocarbons. Whether, catalysts are required for the reaction to be usable, non-catalytic hydrogenation takes place only at very high temperatures.

The industrial importance of the hydrogenation process dates from 1897, when Sabatier encountered that the introduction of a trace of nickel as a catalyst facilitated the addition of hydrogen to molecules of carbon compounds.

The successful performance of a catalytic hydrogenation depends on a suitable choice of catalyst and its amount and the reaction conditions which are temperature, hydrogen pressure, and solvent. Hydrogenation catalysts are also subject to deactivation or promotion by various substances that are referred to as inhibitory (or poisons) or promoters, respectively. In some case, the impurities of the substrate to be hydrogenated or the product may become a factor that retards the hydrogenation, usually in a later stage of the reaction.

The dehydrogenation of hydrocarbons is the breaking of two carbon-hydrogen bonds with the simultaneous formation of a hydrogen molecule and a molecule containing a double carbon-carbon bond, which usually represents the desired product. The double bond is a highly reactive point that permits the use of molecules which contain it as intermediates for the production of typical petrochemical products such as polymers.

#### 2.4.5 Hydrogenolysis

Hydrogenolysis is a chemical reaction which use hydrogen for cleavage or lysis (breakdown) the carbon–carbon or carbon–heteroatom single bond. There are various heteroatom, but it usually is oxygen, nitrogen or sulfur. Generally, hydrogenolysis is used in catalytic reaction by using hydrogen gas. Furthermore, a related reaction is hydrogenation, where hydrogen is added to the molecule, without cleaving bonds. (Connor *et al.*, 1932). The hydrogenolysis reaction as shown in Figure 2.11:

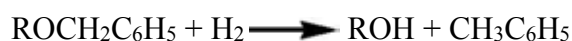


**Figure 2.11** Schematic of hydrogenolysis reaction.



## 2.5 Catalyst For Biojet Production

The material with acid properties is very important for hydrocarbon reaction such as paraffin cracking and isomerization. The required level of the acid site strength is depend on each reaction. Some reactions require sites of stronger acidity than others, for example, in paraffin cracking required stronger strength of the acid sites than that required for isomerization. Moreover, the bifunctional catalyst is obtained by introducing metallic function into the acid supports. This catalyst presents in a more beneficial behavior than the catalyst having only the acid function. The bifunctional metal-acid catalysts are generally small amount of a metal support on porous oxides with acid properties. The acid function of support and the metal function was used to promote the desired reaction selectivity by the addition of promoters (Borghet, 2010).

### 2.5.1 Zeolites as A Catalyst for Biojet Fuel Production

Zeolite is a complex molecule which contains different ratio of silica to alumina. Generally, zeolites consist of the tetrahedral form of  $\text{SiO}_4^{4-}$  and  $\text{AlO}_4^{5-}$ , in three dimensional frameworks which are bonded by oxygen atoms. The general formula of zeolite is  $\text{M}_x/n[(\text{AlO}_2)_x(\text{SiO}_2)_y] \cdot z\text{H}_2\text{O}$ , where M is an extra-framework cation that balances the anionic charge of the framework. The composition of zeolites are identified by the Si/Al atomic ratio or by molar ratio M ( $\text{M} = \text{SiO}_2/\text{Al}_2\text{O}_3$ ). Zeolite can be built by nature or synthesis. Inside of zeolites pore have metals or other cations, which balance negative charge from the anionic framework resulting from the containing aluminium. Zeolite catalysts have various catalysis abilities because of its chemical composition, pore size distribution and ion-exchange abilities. Furthermore, zeolite catalysts have both acidic and basic characteristics.

Because zeolites are inexpensive and environmentally friendly so they are widely used as heterogeneous catalyst in industry. Moreover, zeolites exhibit a potent catalytic activity by the cracking and dehydration reactions for biofuel production. The oxy-compounds adsorb on acid site of zeolite and followed by either decomposition or bimolecular monomer dehydration by its different pore size. Generally, there are three types of zeolites, depending on their pore volume. There are small-

pore zeolites which have diameter between 2.8-4 Å and containing rings with 6–8 members such as Sodalite and zeolite A, medium-pore zeolites which have diameter 5-6 Å and containing 10-membered rings (ZSM-type zeolites) and large-pore zeolites which have diameter more than 7 Å and constructed with 12-membered rings such as zeolites X and Y and faujasite-type zeolites (Shahinuzzaman *et al.*, 2017).

The zeolites growth can be shown in Figure 2.12. The  $\text{SiO}_4$  and  $\text{AlO}_4$ -tetrahedral, which is defined as primary units are polymerized to planar secondary units, then evolve to complex three-dimension unit called polyhedral e.g. cube, hexagonal and octahedral. These polyhedral are ultimately arranged in many connection modes to form porous structure (cages and channels) of zeolites such as sodalite cage and supercage.

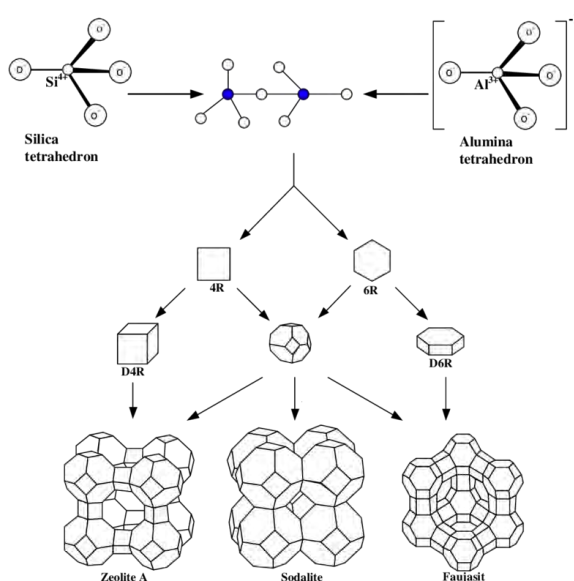


**Figure 2.12** Formation of three common zeolites from primary units.

The pore of zeolites can be oriented in one, two or three dimension (Figure 2.13) and aperture of pore depend on number of T-atom composition (Si, Al, or other metals). The pore size can be changed by exchanging the cation in zeolites: for example, the aperture size of zeolites A can be modified to be 3, 3.8 and 4.3 Å when use  $\text{K}^+$ ,  $\text{Na}^+$ , and  $\text{Ca}^{2+}$  as balancing cation, respectively (Bartholomew and Farrauto, 2005; Hagen, 2015).

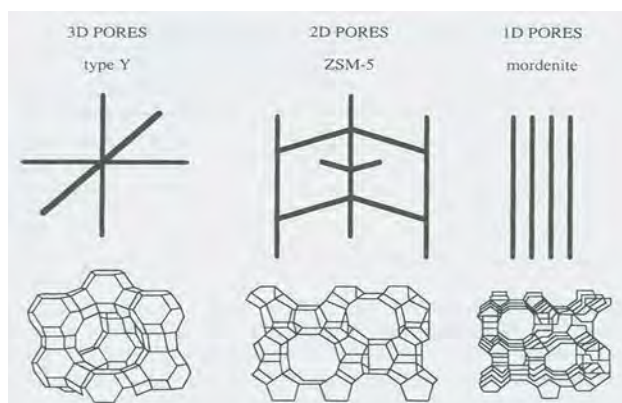


**Figure 2.13** Three commercial zeolites of difference dimensionalities.

For the catalytic cracking of vegetable oil, the most used zeolites are ZSM-5, Zeolite HY, SAPO-11, SBA-15, MCM-41, Ultrastable-Y zeolite (USYZ), beta zeolite, etc. Zeolite Y contains spherical cages 1.3 nm in diameter which are connected tetrahedrally with four neighbouring cages through 0.74 nm diameter so the pore system of zeolite Y is relatively outspread and being the most important heterogeneous catalyst which is the active component for catalytic fluid cracking. Zeolite ZSM-12 consists of 12-membered rings with 0.57–0.61 nm in pore dimension while ZSM-5 which has 10-membered ring pores also has more importance as a heterogeneous catalyst in intersecting system.

Twaiq *et al.* (1999) reported that the ZSM-5 catalyst gave the best performance in terms of conversion, gasoline yield, higher selectivity for aromatics and lower coke formation among three catalysts which are ZSM-5, beta and USY zeolites, whereas USY and zeolite beta catalysts gave higher selectivity for hydrocarbons in the diesel range and lower production of gaseous products. Different studies have shown that zeolite-Y and ZSM-5 are good for the vegetable oil cracking, however, the ZSM-5 provides better performance than zeolite Y because of its smaller pore size about 5.5 Å has limited coking tendencies while the zeolite Y has larger pore size about 7.4 Å (Mante *et al.*, 2012).

In 1998, Souverijins *et al.* studied the hydrocracking of isoheptadecane on Pt/HZSM-22 and Pt/HY catalysts in fixed-bed, vapor-phase reactor. The *n*-C<sub>17</sub> and hydrogen partial pressures at the entrance of reactor were 0.009 bar and 3.5

bar, respectively. The constant space time,  $W/F_0$  equal to 0.5 h kg mol<sup>-1</sup>. The results showed that Pt/HZSM-22 gave products predominate in the light cracked products more than Pt/HY because of the limited penetration of branched molecules into ZSM-22 pores (Souverijins *et al.*, 1998).

### 2.5.2 Zeolite ZSM-12

Generally, medium pore one dimensional zeolites such as ZSM-22, ZSM-23, ZSM-48 and ZSM-12 have been reported to be used as acidic support (Deldari, 2005) because of their favorite pore mouth/key-lock mechanism which are reported to control degree of branching (Martensa *et al.*, 2001) and also their Brønsted acidity level which is suitable for improvement in the isomer selectivity and yields with minimal cracking. As a consequence, the hydroisomerization and hydrocracking reactions appear to occur consecutively, with the sequence of products being monobranched isomers, dibranched isomers and then cracked products (Mehla *et al.*, 2013).

In 1974, the first synthesis of ZSM-12 zeolite (MTW) was described by Ronsinski *et al.* ZSM-12 zeolite is a MTW molecular sieve which has one-dimensional pore system with 12-membered rings (MR). The pore size of ZSM-12 is between 0.56-0.61 nm which is slightly larger than MFI and ZSM-5 zeolites. Therefore, ZSM-12 is important for the shape selective conversion of long hydrocarbon molecules and also showed excellent resistance to deactivation by carbonaceous deposits in hydrocarbon conversion reactions (Gopal and Smirniotis, 2002). Moreover, morphology control of one-dimensional pore zeolites are important to improve mass-transfer and catalytic properties.

In zeolite synthesis, the template is one of the most cost-bearing factors. Several tetraalkylammonium cations can be used as a templating agent in the synthesis of ZSM-12 by the most common being are tetraethylammonium (TEA<sup>+</sup>), methyltriethylammonium (MTEA<sup>+</sup>) and benzyltrimethylammonium (BTMA<sup>+</sup>) which are added during the synthesis in the form of hydroxides, chlorides and bromides (Ronsinski *et al.*, 1974; Rubin, 1986 and Chu and Kuehl, 1984). ZSM-12 synthesis using MTEABr would be relatively expensive, while use of TEAOH or TEABr as the template would prove much more economical (Gopal and Smirniotis,

2001). With TEABr as the cheapest OSDA for MTW. In 2003, Yoo *et al.* reported that the synthesis window of ZSM-12 by using TEABr was narrower than the one with TEAOH.

In 2003, Gopal and Smirniotis have studied about Pt-supported ZSM-12 based catalyst has been investigated for light naphtha isomerization and simultaneous benzene saturation wherein better yields are reported compared to Zeolite Y and  $\beta$  with good resistance to deactivation due to coking. Like-wise, hydroisomerization of  $n$ -C<sub>8</sub>/C<sub>7</sub>/C<sub>6</sub> has been carried out over Pt/Pd-ZSM-12 based catalyst which is reported to favor multi-branched isomers (Deldari *et al.*, 2005). The function of zeolite framework, acidity and its textural properties are often reported to affect to the hydroisomerization of long chain hydrocarbons. Moreover, this is mainly due to the reaction pathways and pore-mouth catalysis wherein external surface area is reported to play vital role in determining the product selectivity (Martensa *et al.*, 2001). From these results, morphology of zeolite in determining the external surface area is anticipated to be crucial. Therefore, it is important to investigate the influence of zeolite morphology and crystal size on hydroisomerization of long chain  $n$ -paraffins especially in terms of product selectivity (Mehla *et al.*, 2013).

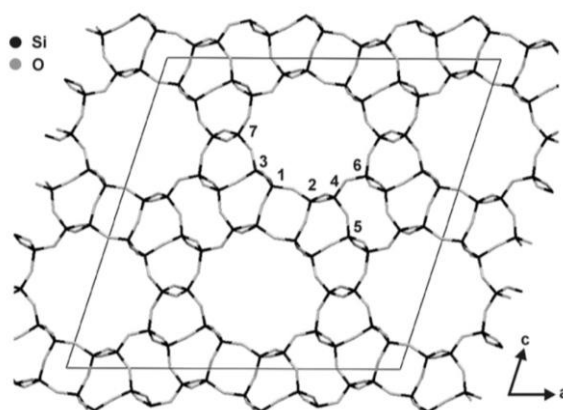


**Figure 2.14** The NMR-refined crystal structure of silica-ZSM-12 (framework type MTW) with Si sites labeled and unit cell indicated (Brouwer, 2008).

### 2.5.3 Supported Metal Catalyst Type

Bifunctional catalysts, with both hydrogenating/dehydrogenating and isomerization function have shown high efficiency in alkane hydroisomerization. Even if, the noble metal are very active but they are not recommended to use because of its high price and the rarity of noble metal catalysts that is not properly used in industry. Furthermore, the poisons and impurities in the feedstock such as sulfur, heavy metals and oxygenated compounds can result in a significant deactivation of noble metal catalysts because the noble metal are very sensitive to catalyst poisons and impurities.

For several industrial zeolites is basically used as hydroisomerization catalysts, which provide the acid function. As the hydrogenating-dehydrogenating function, various species of metals have been tested including Pt, Pd, Rh, Ir, Ru, Re and Ni, mostly associated with mordenite or CaY. Bifunctional catalysts, with both hydrogenating/dehydrogenating and isomerization function have shown high efficiency in alkane hydroisomerization. Noble metal-zeolite catalysts especially Pt or Pd loaded Y, mordenite, and beta leads a high activity and selectivity for hydroisomerization of *n*-alkanes (De Lucas *et al.*, 2006).

Nickel is a very active metal in hydrogenation catalysis. It is also a cheap element thus allowing its use as a bulk metal (e.g. as Raney nickel) as well as in the form of highly loaded supported catalysts. This also gives rise to some sulfur resistance, just because much sulfur is needed to fully poison highly loaded catalysts. On the other hand, the carcinogenic toxicity of nickel compounds is a big concern in the preparation and disposal of catalysts. Many investigators have recognized that nickel oxide when supported on kieselguhr gives much more active catalysts than an unsupported one, although the reduction temperature required for the supported oxide (350–500 °C).

Selective deoxygenation of stearic acid and Microalgae oil over nickel catalysts supported on two types of zeolites (H-ZSM-5 and H-Beta) of varying Si/Al ratio using a batch reactor was studied by Peng *et al.* (2011). Full conversion of stearic acid was obtained over 10% Ni/H-ZSM-5 (Si/Al = 45) catalyst, but severe cracking of the produced alkanes (43% selectivity to C17 and C18) was observed own to its high acidity. However, using 10% Ni/H-ZSM-5 with higher Si/Al ratios

(120 or 200), thus lower acidity, the cracking was gradually suppressed and the selectivity to C17 and C18 alkanes increased to 84 and 93%. For Ni/Beta catalysts with a higher Ni content (10 wt.%, Si/Al=75) displayed a similar activity as the former catalyst, but showed a lower selectivity to isomerized alkanes, indicating that its lower acid site concentration causes a lower isomerization rate. The hydrotreated microalgae oil converted over a 10% Ni/H-Beta catalyst (Si/Al = 180), the yield of saturated fatty acids were the primary products for microalgae oil conversion, that is stearic acid exceeded 70 wt.% within 1 hr. After that, the yield of saturated fatty acids slightly decreased accompanied with an increase in alkane yields (mainly including C17 and C18 alkanes) as a function of time.

## CHAPTER III EXPERIMENTAL

### 3.1 Materials and Equipment

#### 3.1.1 Materials

##### 3.1.1.1 *Feedstock*

- Palm fatty acid distillate (obtained from OPG Tech Co., Ltd.)

##### 3.1.1.2 *Chemical Reagents*

- LUDOX HS-40 colloidal silica (40 wt.%, Dupont)
- Sodium aluminum oxide (Alfa Aesar, Technical grade)
- Tetraethylammonium hydroxide solution (TEAOH, 40 wt.% in water, Fluka)
- HY zeolite (SiO<sub>2</sub>/Al<sub>2</sub>O<sub>3</sub> ratio of 100, Tosoh Company)
- Nickle nitrate hexahydrate (NiNO<sub>3</sub>.6H<sub>2</sub>O)
- Dichloromethane (CH<sub>2</sub>Cl<sub>2</sub>)
- Pyridine (C<sub>5</sub>H<sub>5</sub>N, 98 % purity, Carlo Erba)
- N,O-bis(trimethylsilyl)-trifluoro acetamide (BSTFA, C<sub>8</sub>H<sub>18</sub>F<sub>3</sub>NOSi<sub>2</sub>, 99 % purity, ACROS) or POMA (99.9 % purity)

##### 3.1.1.3 *Standard Chemicals and Others*

- Acetone (CH<sub>3</sub>COCH<sub>3</sub>, 98 % purity, Labscan)
- Methanol (CH<sub>3</sub>OH, 99.9 % purity, Labscan)
- Hexane (C<sub>6</sub>H<sub>14</sub>, 99.9 % purity, Labscan)
- Deionized water

##### 3.1.1.4 *Gases*

- Hydrogen (99.99 % purity, BIG)
- Nitrogen (99.99 % purity, Linde)
- Helium (99.99 % purity, Linde)
- Air zero (99.99 % purity, Linde)



### 3.1.2 Equipment

- High pressure packed-bed continuous flow reactor system;
- Mass flow controller (Brooks instrument 5850E)
- Teledyne ISCO syringe pumps 1000D
- Back pressure regulator (SIEMENS)
- $\frac{3}{4}$ " O.D.x16" long stainless steel reactor
- Three-zone tubular furnace with a temperature controller (Cabolite)
- Gas chromatograph (Agilent GC 7890 equipped with injector, DB-5HT column and FID)
- Chamber Furnace (Cabolite)
- X-ray diffractometer (XRD, Rigaku/ Smartlab)
- X-ray fluorescence (XRF)
- Transmission electron microscopy (TEM)
- Surface area analyzer (SAA, Quantachrome/Autosorb-1)
- Temperature programmed reduction (TPR) apparatus
- Temperature programmed desorption (TPD) apparatus
- Temperature programmed oxidation (TPO) apparatus
- Hot & stirrer plate (Cole Parmer)
- Oven

## 3.2 Experimental Procedures

### 3.2.1 Catalyst Preparation

#### 3.2.1.1 *Synthesis of ZSM-12 Catalyst*

The parent ZSM-12 ( $\text{SiO}_2/\text{Al}_2\text{O}_3$  ratio of 100) was synthesized from hydrogel solutions with the following molar composition  $100\text{SiO}_2:1\text{Al}_2\text{O}_3:1\text{Na}_2\text{O}:25\text{TEAOH}:1500\text{H}_2\text{O}$  according to the study in situ assembly of zeolite nanocrystals into mesoporous aggregate by Yunming Fang *et al.* (2008).

Firstly, TEAOH solution was mixed with deionized water and sodium aluminum oxide and stirred till the solid dissolved. Ludox and the

distilled water were then added to the above solution and stirred at 250 rpm for 24 h till the gel became uniform.

The resultant gel was then transferred to a Teflon-lined stainless-steel autoclaves and crystallized by thermal treatment under autogenous pressure and static conditions at 160 °C for 120 h. After the hydrothermal synthesis, the autoclave is cooled down to room temperature. The product was recovered by filtration, washed thoroughly with deionized water and dried at 120 °C overnight and the organic template was removed by calcination in at 550 °C for 5 h with a heating rate of 10 °C/min.

#### *3.2.1.2 Catalyst Treatment with Ammonium Nitrate*

After the first calcination, the as-synthesized ZSM-12 is ion-exchanged with 1 Molar of  $\text{NH}_4\text{NO}_3$  solution for three times at 80 °C, and then washed with distilled water to remove the nitrate ions. The resultant zeolite is dried overnight at 120 °C and calcined in flowing dry air at 550 °C for 5 h with a heating rate of 10 °C/min to obtain the acidic form of the zeolite (HZSM-12).

#### 3.2.2 Ni Loading on HZSM-12

The zeolite was loaded with Ni by incipient wetness impregnation method. After that, the mixture was gradually dried in an oven at 120 °C to remove excess water for 12 h. Then the dried nickel supported was calcined at 500 °C for 5 h (heating rate of 10 °C/min).

### **3.3 Catalyst Characterization**

#### 3.3.1 X-ray Diffractometer (XRD)

X-ray diffraction was used to determine the information about crystalline phase of synthesized catalyst by a Rigaku X-Ray diffractometer, RINT-2200 with Cu tube for generating  $\text{CuK}\alpha$  radiation (1.5406 Å) and operating condition of 40 kV. The sample was measured in the  $2\theta$  range of 5–50° with a scanning rate of 5 °/s.

### 3.3.2 Brunauer-Emmett-Teller (BET)

The surface areas of the fresh and spent catalysts were measured by BET surface area analyzer (Quantachrome/Autosorb-1). The sample was first outgassed to remove the humidity and volatile adsorbents adsorbed on surface under vacuum at 250 °C for 10 h prior to the analysis. Then, N<sub>2</sub> was purged to adsorb on surface, measuring the quantity of gas adsorbed onto or desorbed from their solid surface at some equilibrium vapor pressure by static volumetric method. The solid sample was maintained at a constant temperature of the sample cell until the equilibrium is established. This volume-pressure data will be used to calculate the BET surface area.

### 3.3.3 Temperature Programmed Reduction (TPR)

Temperature programmed reduction was employed for evaluating the quantity of the reducible species present in the prepared catalyst and the temperature, at which the reduction itself takes place as a function of temperature. In each test 0.1 g of catalyst was placed in a ¼" O.D. quartz tubular reactor, and heated (10 °C/min) under a He flow up to 400 °C, and held at the temperature for 1 h in order to remove moisture from the catalyst surface. The sample was cooled down to 30 °C. Then, the sample would be exposed to a stream of 5% H<sub>2</sub>/Ar with a flow rate of 30 ml/min. After that, the sample was heated to 800 °C with a heating rate of 10 °C/min. The amount of hydrogen consumed was monitored on-line by an SRI model 110 TCD detector as a function of temperature.

### 3.3.4 Temperature Programmed Desorption (TPD) of Isopropylamine

The acidity of prepared catalysts was determined by the amine TPD technique. First, 50 mg of sample was reduced at 600 °C in a flow of H<sub>2</sub> for 1 h. After reduction, the sample was cooled in H<sub>2</sub> to room temperature and then isopropylamine was injected in to sample. After removing the excess isopropylamine, the sample was linearly heated in He to 800 °C at a heating rate of 10 °C/min. Masses 44, 41, and 17 were monitored to determine the evolution of isopropylamine, propylene, and ammonia, respectively.

### 3.3.5 Temperature Programmed Oxidation (TPO)

This technique was employed to analyze the amount and characteristics of the coke deposited on the catalysts during reaction. TPO of the spent catalysts was performed in a continuous flow of 2% O<sub>2</sub> in He while the temperature was linearly increased with a heating rate of 10 °C/min. The oxidation was conducted in a 1/4" quartz fixed-bed reactor after the spent catalyst was dried at 120 °C overnight, weighed (50 mg), and placed between two layers of quartz wool. The sample was further purged at room temperature by flowing 2% O<sub>2</sub> in He for 30 min to stabilize the signal before starting a run. Then, the sample was linearly heated in He to 800 °C at a heating rate of 10 °C/min. The CO<sub>2</sub> produced by the oxidation of the coke species was observed by monitoring mass 44.

### 3.3.6 Transmission Electron Microscopy (TEM)

The morphology of prepared catalyst was observed by a transmission electron microscopy (JEM-1400). For TEM analysis, the catalyst was dilute in the appropriate solvent, sonicated, and dry in the copper grid at room temperature.

## 3.4 **Catalytic Activity Testing**

The schematic of the reactor system and the description of flow-diagram are shown in Figure 3.1 and Table 3.1, respectively. The hydrodeoxygenation, hydrocracking, and hydroisomerization reaction of palm fatty acid distillate (PFAD) were carried through 3/4" O.D., continuous flow fixed-bed reactor under high hydrogen pressure conditions. Firstly, the catalyst was reduced under flowing H<sub>2</sub> for 3 h at the reduction temperature of catalyst. After that, the temperature and pressure of the reactor were set to the desired value in a flowing H<sub>2</sub>. Then, the stream of PFAD was fed into the reactor by teledyne isco syringe pumps 1000D. The flow of carrier gas and the reaction pressure were controlled by a mass flow controller and a back pressure regulator, respectively.

The liquid product was trapped and collected in a condenser while the gas product was analyzed online by using a Shimadzu GC-17A gas chromatograph equipped with a capillary HP-PLOT/Al<sub>2</sub>O<sub>3</sub> "S" deactivated column and FID detector.

Amount of gas product was corrected by using wet test gas meter (Ritter TG 05/2). Finally, the liquid product was analyzed by another gas chromatograph, Agilent 7890 equipped with a DB-5HT column and FID detector. Both gas product and liquid product were collected and analyzed hourly.

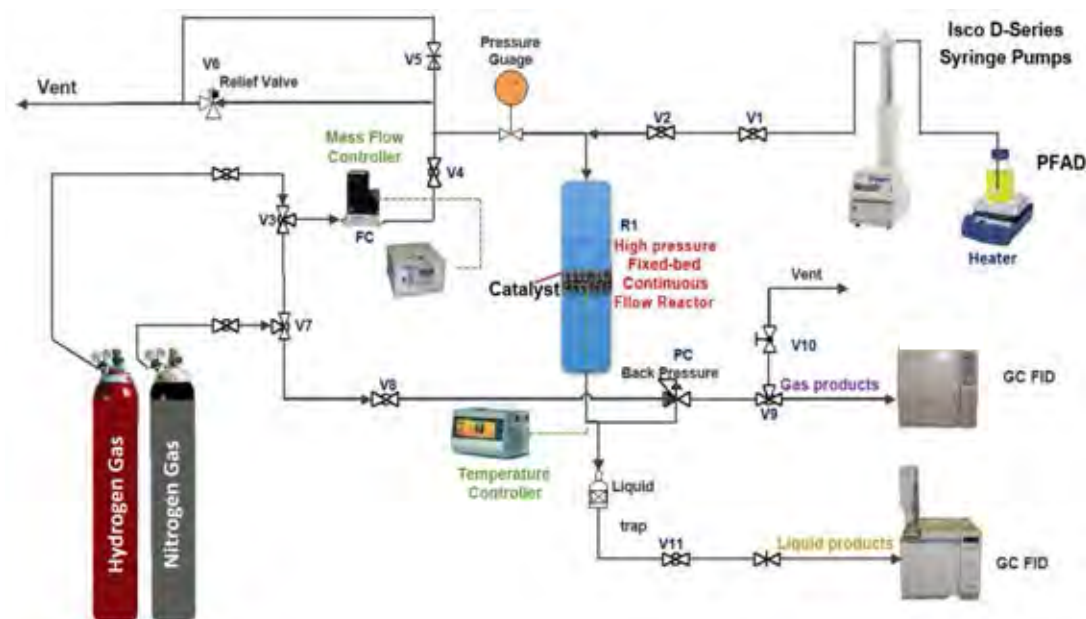


**Figure 3.1** The schematic diagram of the reactor system.

**Table 3.1** Description of system in flow diagram of the continuous flow fixed-bed reactor

No.	Part	Description
1	V1	On-off valve for feedstock from ISCO syringe pumps
2	V2	Checking valve for avoiding the backward flow of the feedstock
3	V3	Three ways valve for switching between nitrogen gas and hydrogen gas flow
4	V4	Checking valve for avoiding the backward flow of hydrogen or nitrogen gas
5	V5	Needle valve for releasing gas from the system
6	V6	Relief valve for releasing pressure overload in the system

No.	Part	Description
7	V7	Three ways valve for switching the direction of nitrogen gas flow
8	V8	Needle valve for controlling pressure in back pressure regulator
9	V9	Three ways valve for switching between vent gas and gas to GC lines
10	V10	On-off valve for releasing pressure from back pressure regulator
11	V11	Metering valve for gathering the liquid product from condenser
12	R1	Continuous flow fixed-bed reactor where hydroprocessing reaction take place
13	FC	Flow controller to set flow rate for the desired H <sub>2</sub> /feed molar ratio
14	PG	Pressure gauge for indicating pressure in packed bed reactor
15	PC	Back pressure regulator for controlling the pressure in reactor

The hydroprocessing reaction of PFAD is performed at temperature, pressure, liquid hourly space velocity (LHSV), and H<sub>2</sub>/Feed ratio as shown in Table 3.2.

**Table 3.2** The reaction conditions for hydroprocessing of palm fatty acid distillate in continuous flow fixed-bed reactor

Parameter	Value
Percent Ni loading (wt.%)	5 - 15
Reaction Temperature (°C)	350 - 400
Reaction pressure (bar)	10 - 30
LHSV (h <sup>-1</sup> )	1.5 - 2.5
Volume of Catalyst (ml)	4
H <sub>2</sub> /feed molar ratio	10
Carrier gas	H <sub>2</sub>

### 3.5 Product Analysis

#### 3.5.1 Liquid Products Analysis

The liquid products were quantified by a gas chromatograph (Agilent 7890) equipped with FID detector. The liquid products from the hydrocracking of PFAD contain non-polar hydrocarbons. The non-polar hydrocarbons were determined by using DB-5 column (non-polar column).

The GC operating condition was summarized as follows:

Injector temperature:	50 °C
Detector temperature:	380 °C
Carrier gas:	He
Column type:	Capillary column (DB-5HT: diameter 0.32 mm length 30 m)

The following chromatographic temperature program in Table 3.3 was used for liquid product analysis:

**Table 3.3** The chromatographic temperature program for liquid product analysis

Step	Temperature (°C)	Rate (°C/min)	Holding time (min)
1	50	-	5
2	169	10	10
3	380	20	10

For the quantitative calculations of liquid product, the areas of each peak analyzed hourly by a GC/FID (Agilent 7890) were converted to gram unit by Equation 3.1 because the each peak of products detected by FID detector can be varied from area unit to gram unit directly.

$$\text{Weight of product } i \text{ (g)} = \frac{(\text{areas of product } i) \times (\text{grams of liquid product})}{\text{total area of liquid product}} \quad (3.1)$$

The conversion and products selectivity of each product were calculated by Equations 3.2 and 3.3:

$$\text{Conversion(\%)} = \frac{\text{moles of feed converted} \times 100}{\text{moles of feed input}} \quad (3.2)$$

$$\text{Selectivity to product i (\%)} = \frac{\text{moles of product i} \times 100}{\text{moles of overall products}} \quad (3.3)$$

### 3.5.2 Gas Products Analysis

The composition of gas product was analyzed hourly by GC/FID (Shimadzu GC-17A). The GC operating condition was summarized as follows:

Injection temperature:	150 °C
Detector temperature:	250 °C
Carrier gas:	He
Column type:	capillary HP-PLOT/Al <sub>2</sub> O <sub>3</sub> “S” deactivated column

The following chromatographic temperature program in Table 3.4 was used for gas product analysis:

**Table 3.4** The chromatographic temperature program for gas-phase product analysis

Step	Temperature (°C)	Rate (°C/min)	Holding time (min)
1	40	-	3
2	70	15	0
3	170	5	0
4	190	1	1

For the quantitative calculations of gas product, the areas of each peak analyzed hourly by GC/FID (Shimadzu GC-17A) were converted to gram unit by comparing with the area of methane from gas standard by mol% (equal to vol%), as shown in Equation 3.4.



$$\text{Weight of product i (g)} = \frac{(\text{areas of product i per 1 ml}) \times (\text{mol of methane per 1 ml}) \times (\text{overall gas product } (\frac{\text{ml}}{\text{h}}))}{(\text{mol of carbon atom}) \times (\text{reference area of methane per 1 ml}) \times (\text{molecular weight } (\frac{\text{g}}{\text{mol}}))} \quad (3.4)$$

The calculations of conversion, selectivity and yield of product are defined as shown in Equations 3.5, 3.6 and 3.7, respectively.

$$\text{Conversion (\%)} = \frac{(\text{weight of feed input} - \text{weight of feed remaining}) \times 100}{\text{weight of feed input}} \quad (3.5)$$

$$\text{Selectivity of product i (\%)} = \frac{\text{weight of product i} \times 100}{\text{weight of total products}} \quad (3.6)$$

$$\text{Yield of product i (\%)} = (\text{conversion}) \times (\text{selectivity of product i}) \quad (3.7)$$

## CHAPTER IV

### RESULTS AND DISCUSSION

In this research, the parent HZSM-12 catalyst with a SiO<sub>2</sub>/Al<sub>2</sub>O<sub>3</sub> molar ratio of 100 was successfully synthesized by hydrothermal synthesis. It can be confirmed by XRD and XRF techniques. The Ni metal was loaded on the zeolite support by incipient wetness impregnation method and also investigated the catalytic activity of Ni/HZSM-12 catalyst for production biojet fuel from PFAD.

#### 4.1 Characterization of Fresh Catalysts

##### 4.1.1 X-ray Diffraction (XRD)

In this work, Ni/HZSM-12 catalyst was synthesized and investigated. The XRD patterns of synthesized ZSM-12, HZSM-12, 5, 10 and 15 wt.% Ni/HZSM-12 are shown in Figure 4.1. The characteristic peaks of ZSM-12 zeolite illustrates the dominant peaks at  $2\theta = 7.55^\circ$ ,  $8.93^\circ$  and  $21.0^\circ$  which represent the (101), (201) and (310) planes of ZSM-12 zeolite, respectively. The positions and relative intensities of ZSM-12 zeolite agreed with data from previous studies (Meier *et al.*, 1996; Pedrosa *et al.*, 2006). All the peaks were indexed as a monoclinic unit cells. According to XRD patterns of ZSM-12 and HZSM-12, no significant changes occurred after doing acidic form. It indicates that the parent HZSM-12 also had high crystallinity. Moreover, the characteristic peaks of NiO species at  $2\theta = 37.24^\circ$  and  $43.34^\circ$  occurred after impregnation of nickel (5, 10 and 15 wt.% Ni/HZSM-12 catalyst) which are corresponding to the planes (111) and (200) of cubic NiO species, respectively.

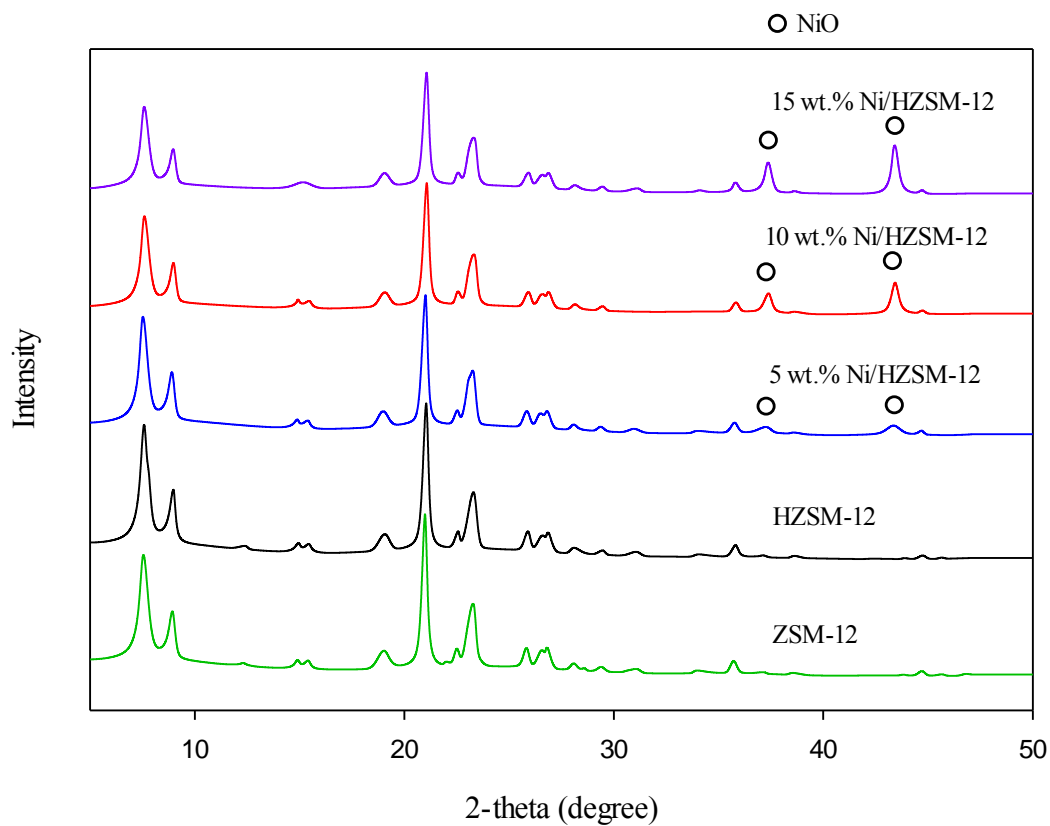


**Figure 4.1** XRD patterns of synthesized parent ZSM-12, HZSM-12 and 5, 10 and 15 wt.% Ni/HZSM-12 catalysts.

#### 4.1.2 X-ray Fluorescence (XRF)

The synthesized HZSM-12 catalyst synthesized by hydrothermal treatment with the following molar composition:  $1\text{Na}_2\text{O}:100\text{SiO}_2:1\text{Al}_2\text{O}_3:25\text{TEAOH}:1500\text{H}_2\text{O}$ . The XRF technique was used to characterize and identify the chemical composition as illustrated in Table 4.1. The results showed that the average of  $\text{SiO}_2/\text{Al}_2\text{O}_3$  molar ratio from XRF was 104.9 which was a little higher than the theoretical value and weight percent of Ni of each catalyst were slightly different from theoretical values.

**Table 4.1** Chemical composition of the synthesized HZSM-12 and 5, 10 and 15 wt.% Ni/HZSM-12 catalysts

Catalyst	SiO <sub>2</sub> /Al <sub>2</sub> O <sub>3</sub> molar ratio		%Ni (wt.%)	
	Theoretical	XRF	Theoretical	XRF
HZSM-12	100	102.9	-	-
5 wt.% Ni/HZSM-12	100	105.8	5	5.1
10 wt.% Ni/HZSM-12	100	96.9	10	8.7
15 wt.% Ni/HZSM-12	100	113.9	15	12.9

#### 4.1.3 Transmission Electron Microscope (TEM)

The average crystallite size of prepared HZSM-12 zeolite and dispersion of nickel over HZSM-12 support was observed by transmission electron microscope as shown in Figures 4.2 - 4.5. In Figure 4.2, the prepared HZSM-12 zeolite was in cubic shaped agglomerates with cubic size around 55 nm and agglomerated size of the cubic particles about 0.6  $\mu\text{m}$  that was similar to previous study (Parmar *et al.*, 2014; Sanhoob *et al.*, 2014). TEM images of 5, 10 and 15 wt.% Ni/HZSM-12 catalysts are shown in Figures 4.3 – 4.5, respectively. The dark spots were nickel particles which were dispersed on HZSM-12 zeolite. The dark spots of nickel particles in Figures 4.3 and 4.4 were highly dispersed, indicating that 5 and 10 wt.% Ni/HZSM-12 catalysts had good dispersion of nickel particles on zeolite support while 15 wt.% Ni/HZSM-12 catalyst had some particles seem to be agglomerated as shown in Figure 4.5.

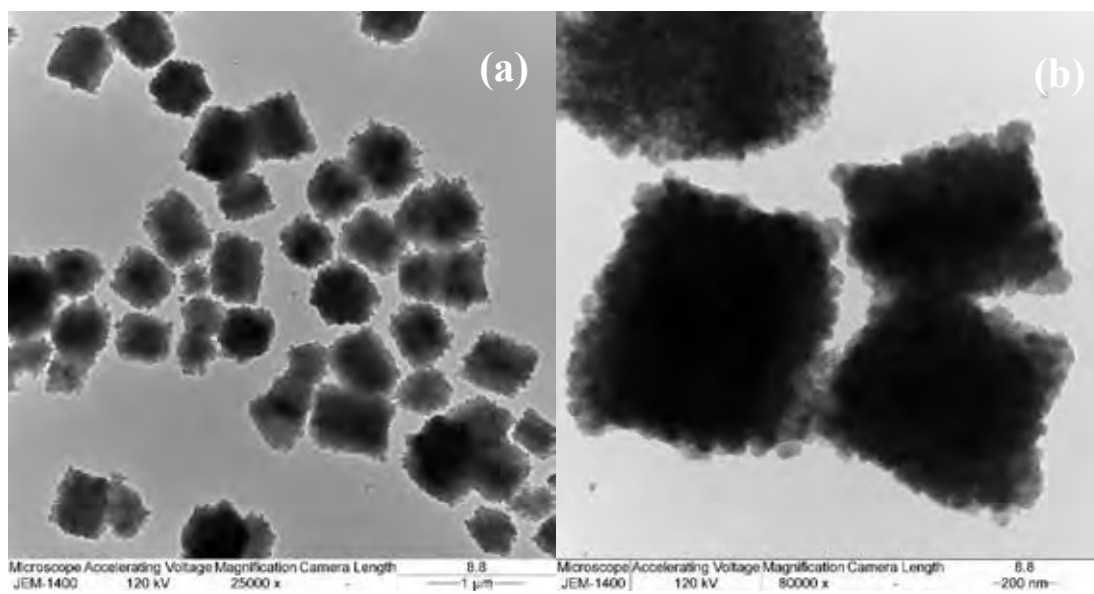


**Figure 4.2** (a), (b) TEM images of calcined parent HZSM-12 zeolite.

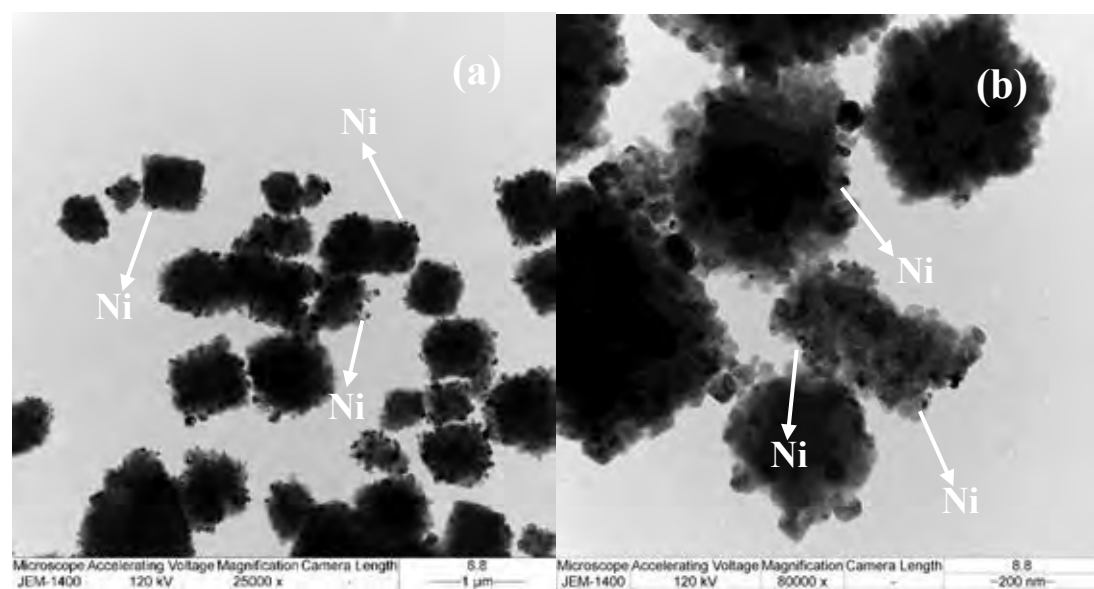


**Figure 4.3** (a), (b) TEM images of calcined 5 wt.% Ni/HZSM-12 catalyst.

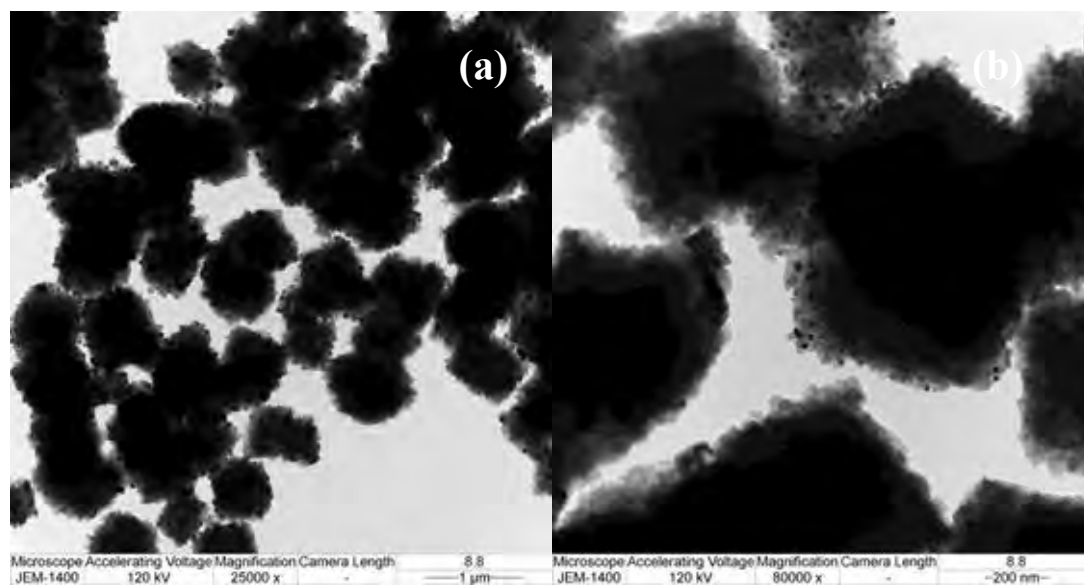


**Figure 4.4** (a), (b) TEM images of calcined 10 wt.% Ni/HZSM-12 catalyst.

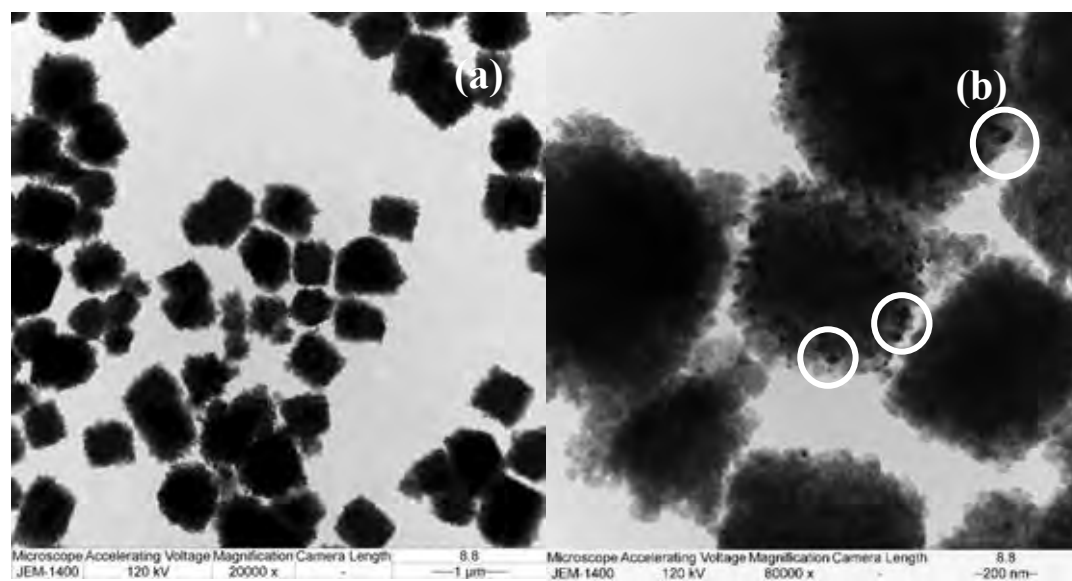


**Figure 4.5** (a), (b) TEM images of calcined 15 wt.% Ni/HZSM-12 catalyst.

#### 4.1.4 Brunauer-Emmett-Teller (BET)

The textural properties of the parent HZSM-12, 5, 10 and 15 wt.% Ni/HZSM-12 catalysts are summarized in Table 4.2. The total surface area was calculated by the Brunauer-Emmett-Teller (BET) equation, the external surface area and the micropore volume was obtained by the t-plot method and the total pore volume was obtained by Barrett-Jayner-Halenda (BJH) analysis of the adsorption branch of the isotherm. The BET surface area, external surface area, micropore volume and total pore volume of 5 wt.% Ni/HZSM-12 catalyst was similar to the parent HZSM-12, indicating that 5 wt.% Ni/HZSM-12 catalyst had highly dispersion of nickel particles on zeolite support corresponded to the TEM results. After loading more nickel to 10 and 15 wt.%, the BET surface area, external surface area, micropore volume and total pore volume of samples were decreased in 10 wt.% Ni/HZSM-12 catalyst and much decreased in 15 wt.% Ni/HZSM-12 catalyst. These results indicated that nickel particles blocked micropores to some extent in 10 wt.% Ni/HZSM-12 catalyst and highly blocked micropores in 15 wt.% Ni/HZSM-12 catalyst.

**Table 4.2** Physical characteristics of the prepared catalysts

<b>Zeolite</b>	<b>S<sub>BET</sub> (m<sup>2</sup>/g)</b>	<b>S<sub>Ext</sub> (m<sup>2</sup>/g)</b>	<b>V<sub>micro</sub> (ml/g)</b>	<b>V<sub>total</sub> (ml/g)</b>
HZSM-12	274	80	0.102	0.192
5 wt.% Ni/HZSM-12	268	80	0.099	0.194
10 wt.% Ni/HZSM-12	262	74	0.099	0.177
15 wt.% Ni/HZSM-12	238	67	0.090	0.186

#### 4.1.5 Temperature Programmed Reduction (TPR)

Temperature programmed reduction was used to evaluate the reduction temperature of the prepared catalysts. The reduction of particles is depended on the location of the metal on the support and of its interaction with the support, as also with the structure of the oxide formed. The interaction between NiO with the support was decreased its reducibility. In Figure 4.6, two dominant peak regions were found at approximately 330-550 °C corresponding to the reduction of Ni<sup>2+</sup> from the NiO formed and NiO from the different crystal sizes (Pedrosa *et al.*, 2006) and at 550-620 °C corresponding to the reduction of the NiO and supports with strong interaction (Cao *et al.*, 2017). These results can be explained that the content of bulk NiO greatly increased with increasing content on nickel loading more than the increasing of NiO strongly interacted with support content.

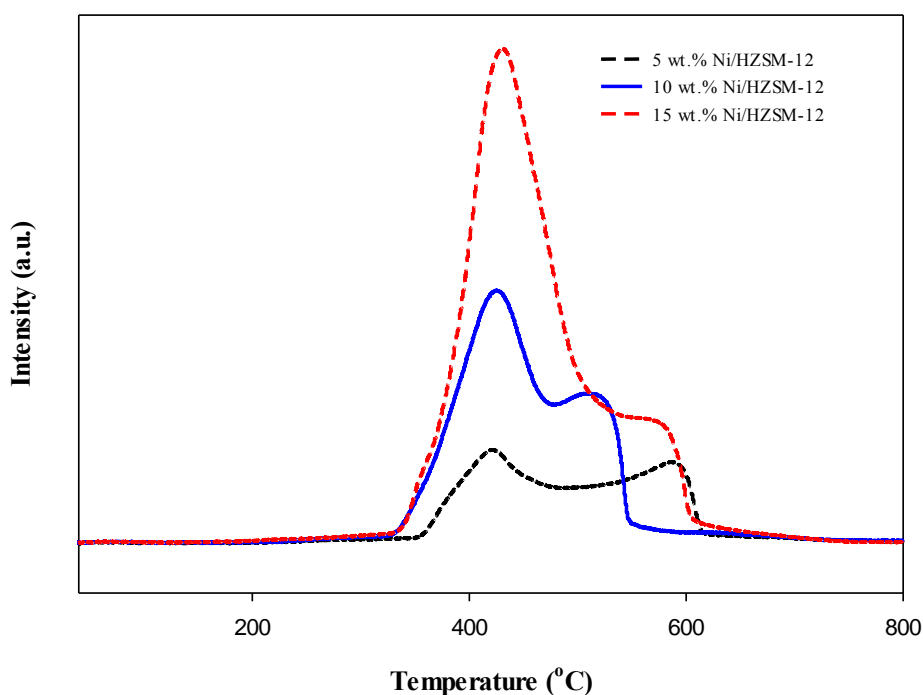


**Figure 4.6** Temperature programmed reduction (TPR) profiles of the 5, 10 and 15 wt.% Ni/HZSM-12 catalysts.



#### 4.1.6 Temperature Programmed Desorption of Isopropylamine (IPA-TPD)

The Brønsted acid sites of prepared catalysts were calculated based on the results from the temperature programmed desorption (TPD) of isopropylamine. The acid sites catalyzed the conversion of isopropylamine into propylene and ammonia (Pereira and Gorte, 1992). The Brønsted acidities of the parent HZSM-12 and 5, 10, 15 wt.% Ni/HZSM-12 and 10 wt.% Ni/HY catalysts are shown in Figure 4.7 and summarized in Table 4.3. The results showed that the bifunctional Ni on zeolite catalysts had lower amount of Brønsted acid sites than the parent zeolite catalysts. Furthermore, the higher content of nickel loaded gave lower Brønsted acid sites. In addition, the 10 wt.% Ni/HY catalyst provided slightly lower amount of Brønsted acid sites than the 10 wt.% Ni/HZSM-12 catalyst.

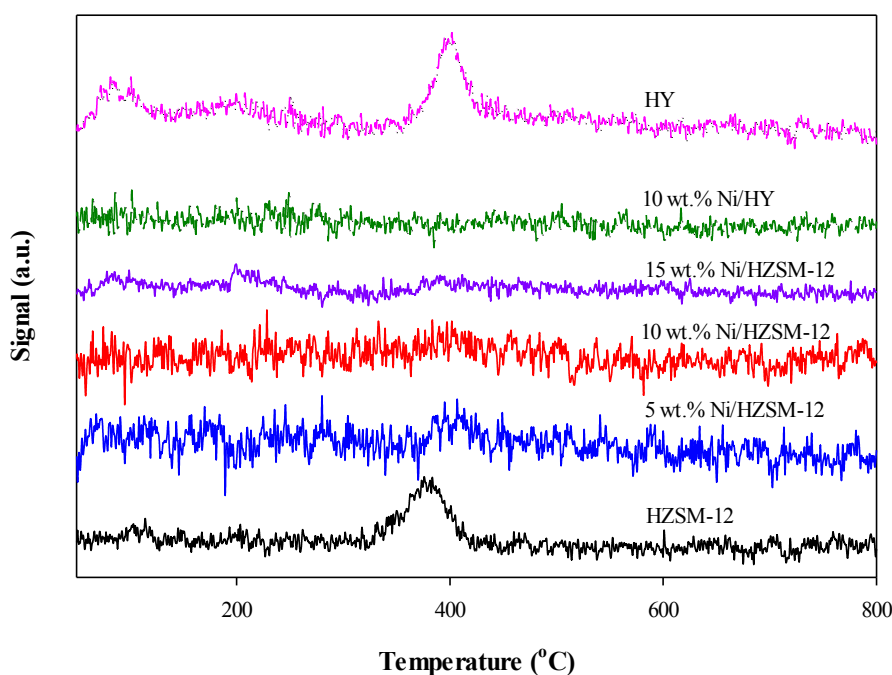


**Figure 4.7** Temperature programmed desorption of isopropylamine (IPA-TPD) profiles of the parent HZSM-12 and 5, 10, 15 wt.% Ni/HZSM-12, 10 wt.% Ni/HY and the parent HY catalysts.

**Table 4.3** Brønsted acidity of the parent HZSM-12 and 5,10, 15 wt.% Ni/HZSM-12, 10 wt.% Ni/HY and the parent HY catalysts from IPA-TPD

Catalysts	Brønsted Acidity (mmol/g)
HZSM-12	0.47
5 wt.% Ni/HZSM-12	0.21
10 wt.% Ni/HZSM-12	0.15
15 wt.% Ni/HZSM-12	0.11
10 wt.% Ni/HY	0.08
HY	0.54

## 4.2 Gas Chromatography of Feed and Standard Analysis

### 4.2.1 Feed Analysis

The chromatogram and compositions of PFAD feedstock analyzed by a GC/FID (Agilent 7890A) are shown in Figure 4.8 and Table 4.4, respectively. In Figure 4.8, the main peaks are hexadecane, octadecane, palmitic acid, oleic acid, stearic acid, mono-glycerides, di-glycerides and tri-glycerides that the retention times are at 14.8, 17.0, 19.9, 24.1, 24.9, 29-33, 33-38 and 38-43, respectively. Besides, the composition of PFAD as shown in Table 4.4, it can be revealed that PFAD contains palmitic acid and oleic acid as main components and also trace amount of hexadecane, octadecane, stearic acid, mono-, di- and tri-glycerides.

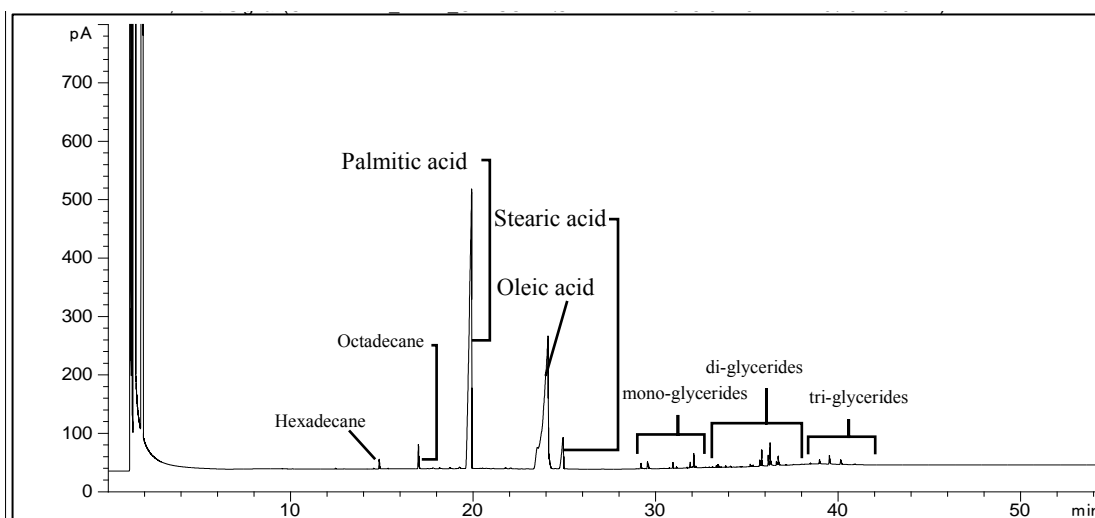


**Figure 4.8** The chromatogram of various components in PFAD range analyzed by a GC/FID.

**Table 4.4** Composition of PFAD feedstock

Feed components	Amount (wt. %)
Palmitic acid	46.48
Oleic acid	43.41
Stearic acid	4.00
di-glycerides	2.28
mono-glycerides	1.45
Octadecane	1.14
tri-glycerides	0.86
Hexadecane	0.38

#### 4.2.2 Standard Analysis

The chromatograms of liquid standard were analyzed by gas chromatograph equipped with an FID detector (Agilent 7890) to identify peaks of the compositions in PFAD feedstock are shown in Figure 4.9 which are polarity liquid standard (oxygenated compounds) and Figure 4.10 which are non-polarity liquid standard (*n*-alkanes).

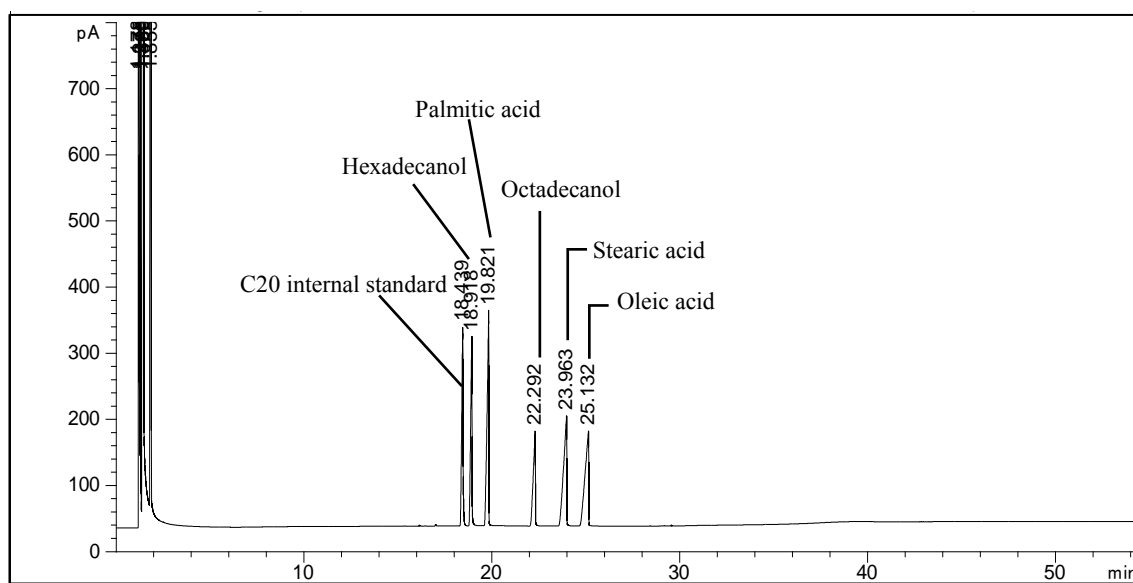


**Figure 4.9** Chromatograms of standard oxygenated compounds.

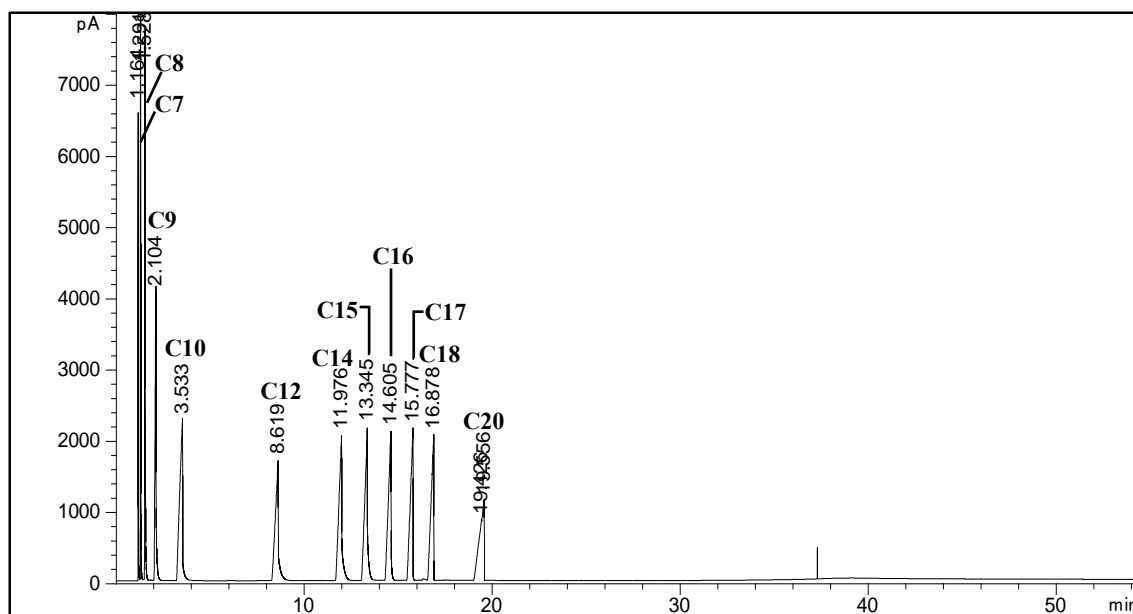


**Figure 4.10** Chromatograms of standard *n*-alkanes.

Figure 4.9 shows the chromatograms of standard oxygenated compounds in types of fatty acid and alcohol which are feed and intermediates in catalytic activity testing. Moreover, the chromatograms of standard *n*-alkanes from catalytic activity testing such as heptane (C7), octane (C8), nonane (C9), decane (C10), undecane (C11), dodecane (C12), tetradecane (C14), pentadecane (C15), hexadecane (C16), heptadecane (C17), and octadecane (C18) were also shown in Figure 4.10.

### 4.3 Catalytic Activity Testing

In this part, the PFAD conversion, product yield and selectivity of from PFAD over 5-15 wt.% Ni/HZSM-12 catalysts were investigated. The reaction conditions were at temperature of 350-400 °C, pressure of 10-30 bar, liquid hourly space velocity (LHSV) of 1.5 - 2.5 h<sup>-1</sup>, and H<sub>2</sub>/feed molar ratio of 10.

#### 4.3.1 Effect of Reaction Temperature

In order to study the effect of reaction temperature on product selectivity, the biojet production from PFAD over 10 wt.% Ni/HZSM-12 was conducted at 30 bar, LHSV of 1.5 h<sup>-1</sup>, and H<sub>2</sub>/feed molar ratio of 10. The reaction temperature was varied from 350 to 400 °C. In Figure 4.11, the results demonstrate that the reaction at temperature between 350-400 °C provided almost complete conversions. In addition, the selectivity of light product, gasoline and biojet increased with increasing reaction temperature, whereas the selectivity of diesel and intermediate decreased. This indicated that the hydrocracking of diesel to biojet and lighter hydrocarbon products was favor at high reaction temperature which is correspond to previous study (Jadpon, 2014). Jadpon explained that the increase in cracking yield related to the increase in a catalytic activity and reaction rate according to the Arrhenius equation ( $k = k_0e^{-E/RT}$ ). However, the highest selectivity of biojet which is hydrocarbons in the range of C9-C14 was found at 375 °C as shown in Figure 4.12. Therefore, the reaction temperature at 375 °C was selected as the optimal reaction temperature for further study the effect of reaction pressure of the biojet production due to lowering diesel and intermediates and moderate amount in lighter gas (C1-C4) production.

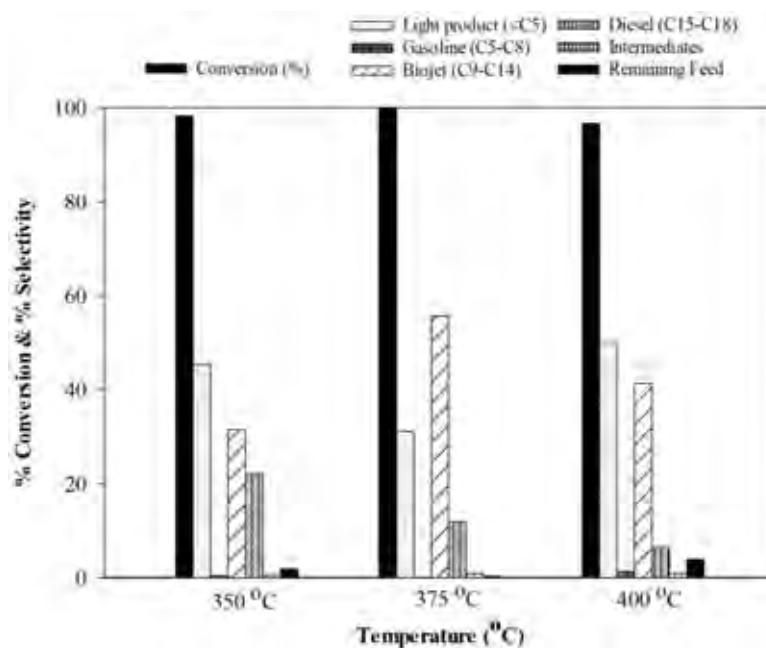


**Figure 4.11** The conversion and selectivity of products that obtained over 10 wt.% Ni/HZSM-12 catalyst at different temperatures (Reaction condition: 30 bar,  $H_2$ /feed molar ratio of 10, LHSV of  $1.5 h^{-1}$ , and TOS at 5 h).

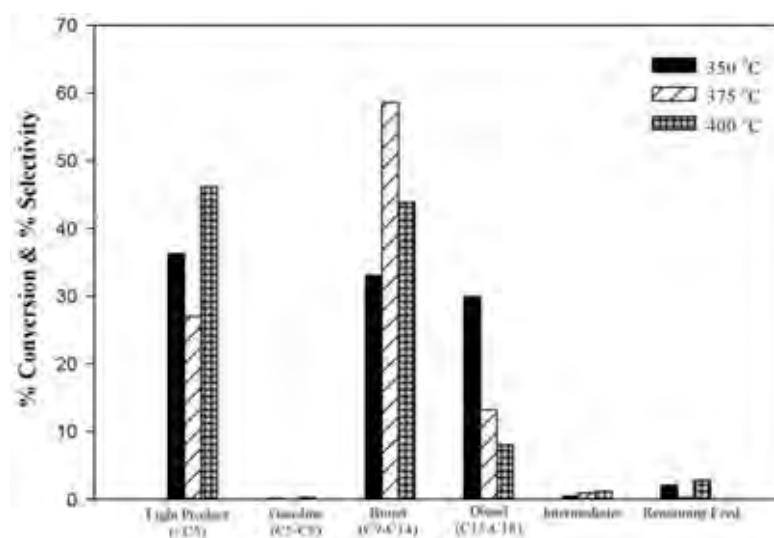


**Figure 4.12** The product distribution over 10 wt.% Ni/HZSM-12 catalyst at different temperatures (Reaction condition: 30 bar,  $H_2$ /feed molar ratio of 10, LHSV of  $1.5 h^{-1}$ , and TOS at 5 h).

### 4.3.2 Effect of Reaction Pressure

In order to study the effect of reaction temperature on product selectivity, the biojet production from PFAD over 10 wt.% Ni/HZSM-12 was conducted at 375 °C, LHSV of 1.5 h<sup>-1</sup>, and H<sub>2</sub>/feed molar ratio of 10. Figure 4.13 illustrates that the PFAD conversion increased with increasing reaction pressure (from 85.58 to 99.79%). Moreover, it can be observed that the selectivity of diesel and intermediates were decreased at high pressure level because diesel and intermediates (such as fatty aldehyde, fatty alcohol, and ester) can be more converted to biojet fuel and lighter products. Therefore, the reaction at 30 bar provided the highest selectivity to biojet fuel about 55.79%.

From the results obtained from varying reaction temperatures and pressures, the condition at 375 °C and 30 bar was selected as the optimal reaction condition for further study the effect of percent nickel loading of the biojet production due to giving the highest biojet product.

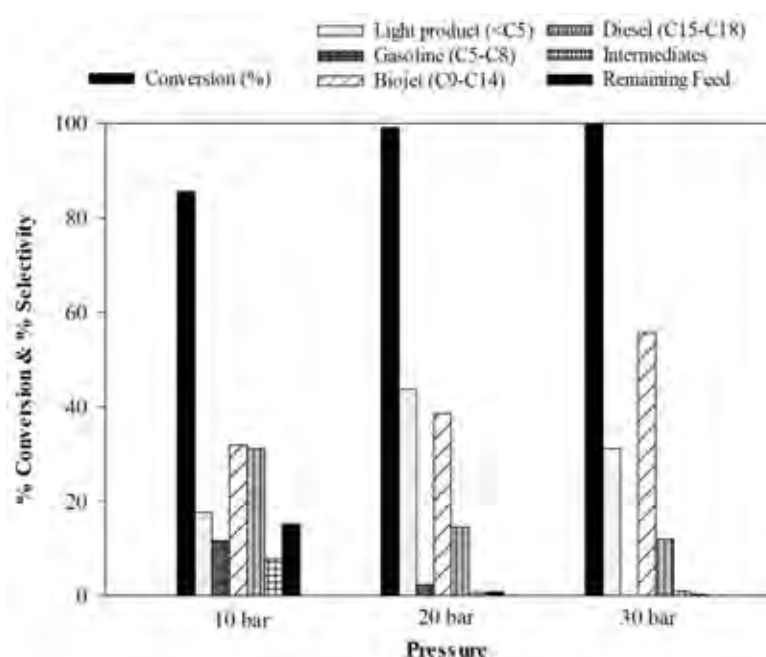


**Figure 4.13** The conversion and selectivity of products that obtained over 10 wt.% Ni/HZSM-12 catalyst at different pressures (Reaction condition: 375 °C, H<sub>2</sub>/feed molar ratio of 10, LHSV of 1.5 h<sup>-1</sup>, and TOS at 5 h).



### 4.3.3 Effect of Ni Loading

In order to study the effect of nickel loading on product selectivity, the biojet production from PFAD was conducted at 375 °C, 30 bar, LHSV of 1.5 h<sup>-1</sup>, and H<sub>2</sub>/feed molar ratio of 10. The percent nickel loading was varied from 5 to 15 wt.% on parent HZSM-12 support. Figure 4.14 demonstrates that 5 and 10 wt.% Ni/HZSM-12 catalysts provided the complete conversion, whereas 15 wt.% Ni/HZSM-12 catalyst provided only 80.46 % PFAD conversion. According to TEM images and BET results, the 15 wt.% Ni/HZSM-12 catalyst had some nickel particles agglomerated while the nickel particles of 5 and 10 wt.% Ni/HZSM-12 catalysts had more complete dispersion on parent HZSM-12 support. Furthermore, the selectivity of these both catalysts seem to be similar. However, the 5 wt.% Ni/HZSM-12 catalyst gave higher selectivity to light product that can be explained by TPD-IPA results (5 wt.% Ni/HZSM-12 catalyst had higher Brønsted acid sites more than 10 wt.% Ni/HZSM-12 catalyst) so the 10 wt.% Ni/HZSM-12 catalyst gave the highest selectivity to biojet product about 55.79%.

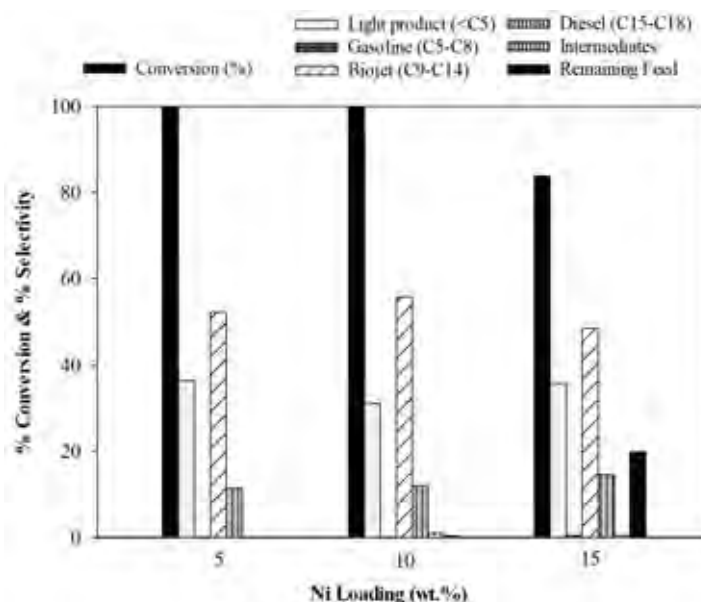


**Figure 4.14** The conversion and selectivity of products that obtained over different percent nickel loading over parent HZSM-12 support (Reaction condition: 375 °C, 30 bar, H<sub>2</sub>/feed molar ratio of 10, LHSV of 1.5 h<sup>-1</sup>, and TOS at 5 h).

#### 4.3.4 Effect of LHSV

In order to study the effect of reaction temperature on product selectivity, the biojet production from PFAD over 10 wt.% Ni/HZSM-12 was conducted at 375 °C, 30 bar and H<sub>2</sub>/feed molar ratio of 10. The LHSV was varied from 1.5-2.5 h<sup>-1</sup>. Figure 4.15 and 4.16 exhibit that the PFAD conversion and the selectivity to biojet, gasoline and light product decreased with increasing LHSV which were opposed to the selectivity to diesel and intermediates. These results indicated that the longer residence time by decreasing LHSV, the existing fatty acids and intermediates were highly converted to hydrocarbons in a range of diesel then further cracked to produce biojet, gasoline and light products.

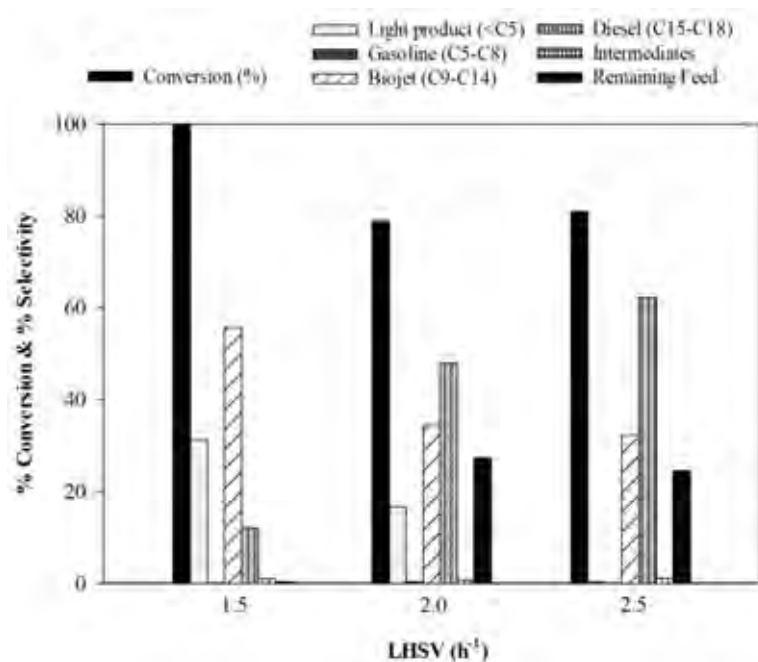


**Figure 4.15** The conversion and selectivity of products that obtained over 10 wt.% Ni/HZSM-12 catalyst at different LHSV (Reaction condition: 375 °C, 30 bar, H<sub>2</sub>/feed molar ratio of 10, and TOS at 5 h).

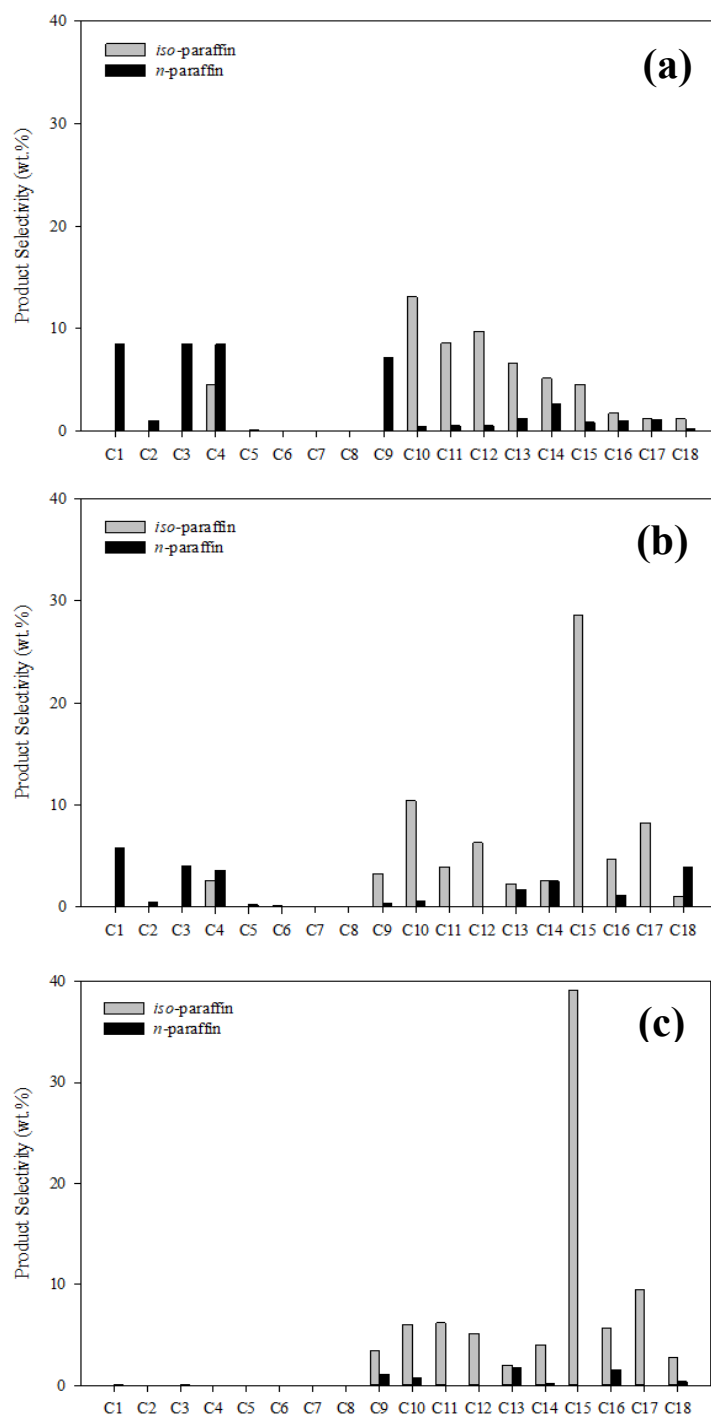


**Figure 4.16** Product distribution of products that obtained over 10 wt.% Ni/HZSM-12 catalyst at different LHSV (a) LHSV 1.5 h<sup>-1</sup> (b) LHSV 2.0 h<sup>-1</sup> (c) LHSV 2.5 h<sup>-1</sup> (Reaction condition: 375 °C, 30 bar, H<sub>2</sub>/feed molar ratio of 10, and TOS at 5 h).

#### 4.3.5 Effect of Supported Catalyst (Ni/HZSM-12 and Ni/HY)

In order to study the effect of catalyst supports on product selectivity, the biojet production from PFAD over 10 wt.% Ni on HZSM-12 and HY zeolite supports were conducted at 375 °C, 30 bar, LHSV of 1.5 h<sup>-1</sup>, and H<sub>2</sub>/feed molar ratio of 10. The liquid products obtained over Ni on HZSM-12 and HY zeolites are shown in Figure 4.17.

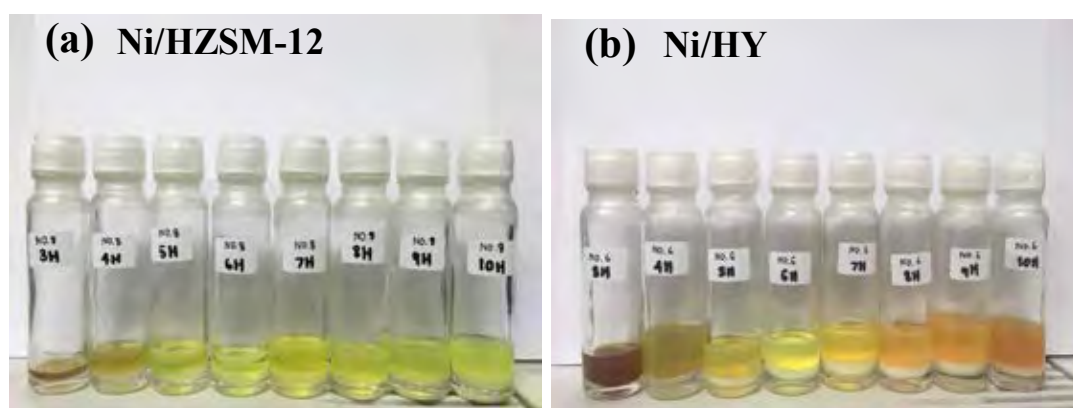


**Figure 4.17** Liquid products obtained over (a) 10 wt.% Ni/HZSM-12 and (b) 10 wt.% Ni/HY catalysts (Reaction condition: 375 °C, 30 bar, LHSV 1.5 h<sup>-1</sup>, H<sub>2</sub>/feed molar ratio of 10).

The catalytic activity of Ni/HZSM-12 and Ni/HY catalysts can be seen in Figures 4.18 (a) and (b), respectively. The fatty acid in PFAD feedstock was deoxygenated to long chain hydrocarbon in the range of diesel (C15–C18). At the first period, the light product (C1-C4) was observed as a main product and then decreased slightly with time. In the contrary, diesel was increased sharply with time. It can be described that diesel was converted very rapidly into smaller molecules as light product, gasoline and biojet because it was a severe condition with high temperature and pressure. Furthermore, the selectivity to biojet of Ni/HZSM-12 catalyst was higher than Ni/HY catalyst that diesel had more converting to lighter products.

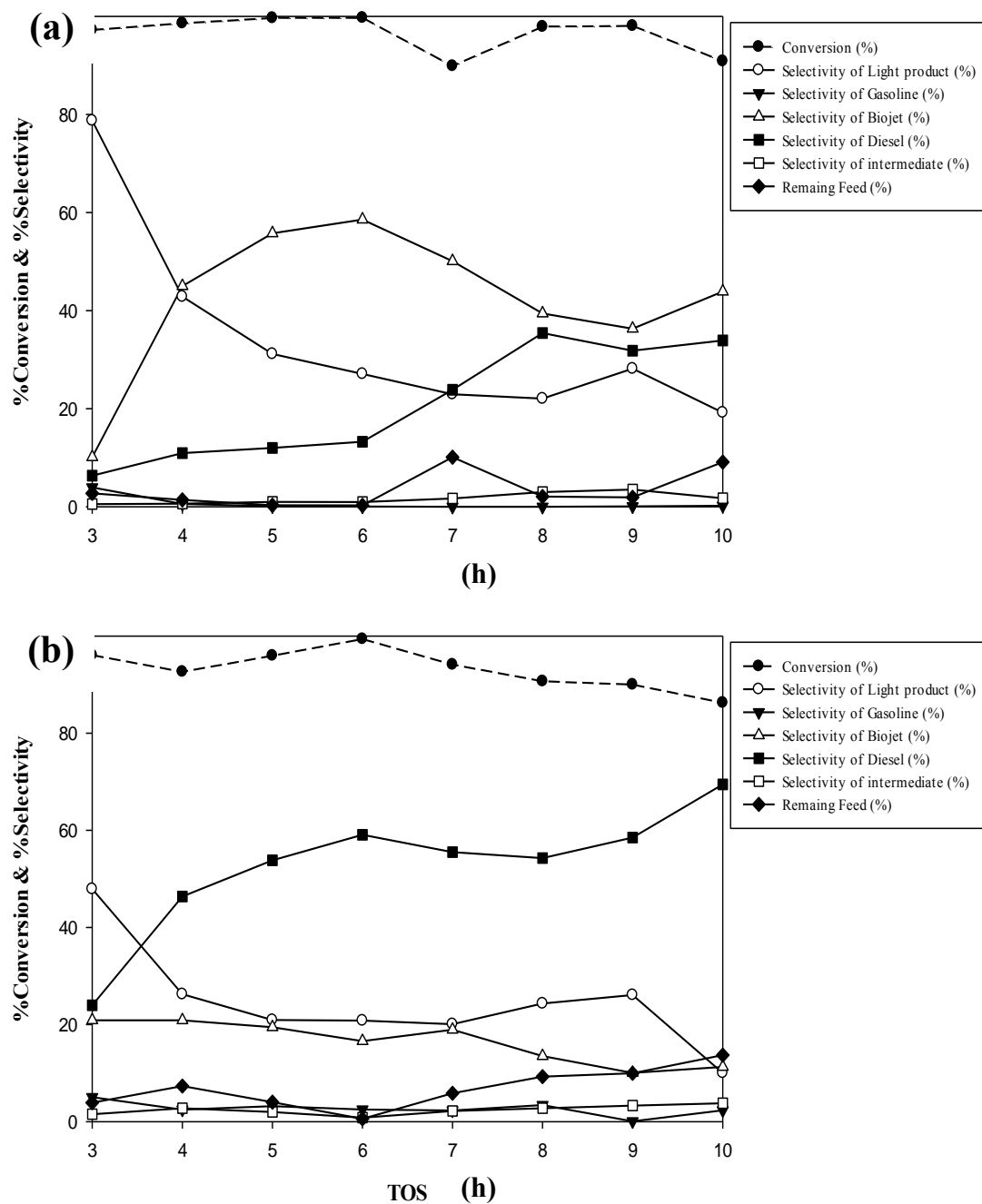


**Figure 4.18** The conversion and selectivity of products that obtained over (a) 10 wt.% Ni/HZSM-12 and (b) 10 wt.% Ni/HY catalysts (Reaction condition: 375 °C, 30 bar, LHSV 1.5 h<sup>-1</sup>, H<sub>2</sub>/feed molar ratio of 10).

Figure 4.19 demonstrates that both catalysts provided almost complete conversion. Ni/HZSM-12 catalyst favored to produce biojet, gasoline and light products more than Ni/HY catalyst. Moreover, Ni/HZSM-12 had higher selectivity to *iso*-paraffin products more than Ni/HY catalyst that is shown in Figure 4.20. This results can be explained by pore mouth catalysis that each catalyst favor different – scission modes. The Ni/HZSM-12 catalyst predominately produced the lighter cracked products whereas Ni/HY catalyst predominate in each carbon number fraction (Souverijns *et al.*, 1998).

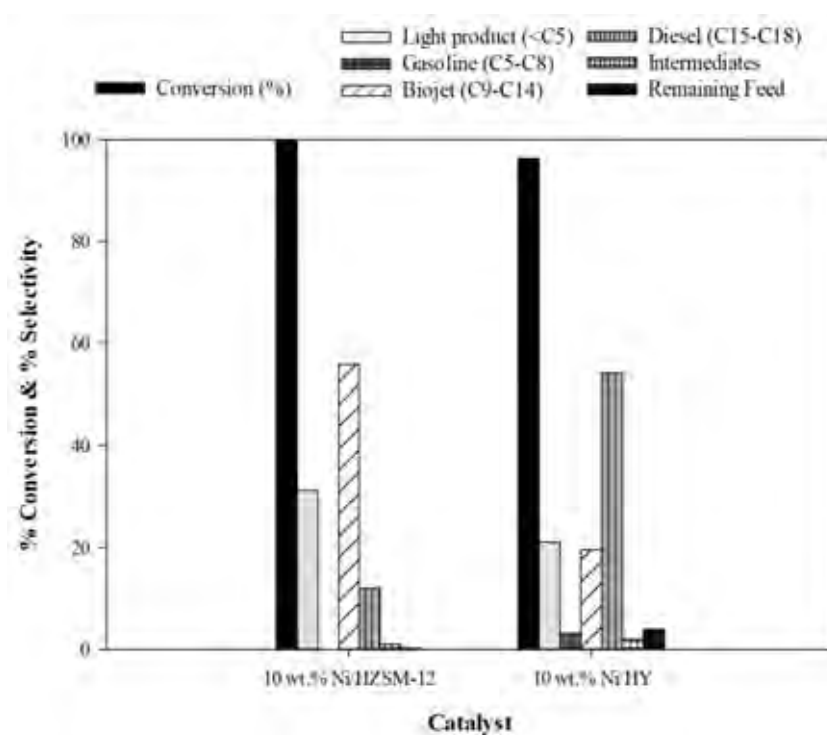


**Figure 4.19** The conversion and selectivity of products that obtained over 10 wt.% Ni/HZSM-12 and 10 wt.% Ni/HY catalysts (Reaction condition: 375 °C, 30 bar, LHSV 1.5 h<sup>-1</sup>, H<sub>2</sub>/feed molar ratio of 10 and TOS at 5 h).

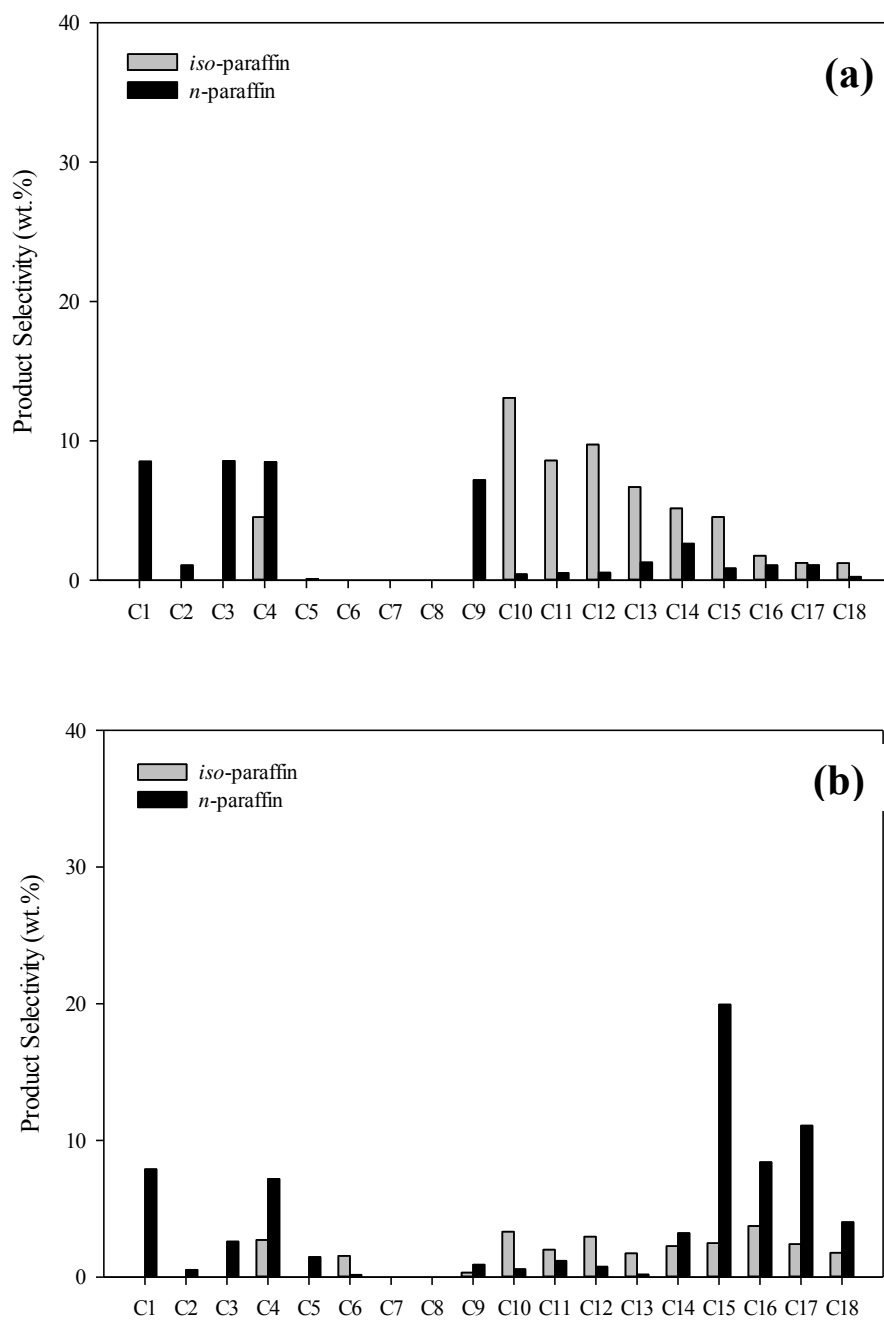


**Figure 4.20** Product distribution of products that obtained over (a) 10 wt.% Ni/HZSM-12 and (b) 10 wt.% Ni/HY catalysts (Reaction condition: 375 °C, 30 bar, LHSV 1.5 h<sup>-1</sup>, H<sub>2</sub>/feed molar ratio of 10, and TOS at 5 h).

The chromatogram of liquid and gas products obtained over Ni/HZSM-12 and Ni/HY catalysts operated at operating conditions: 375 °C, 30 bar, LHSV of 1.5 h<sup>-1</sup>, H<sub>2</sub>/feed molar ratio of 10, and TOS of 5 h are shown in Figures 4.21 and 4.22, respectively. In Figures 4.21 (a) and 4.22 (a), the chromatogram of liquid product can be divided into five main parts which are gasoline (C5-C8), biojet (C9-C14), diesel (C15-C18), intermediates and remaining feed at the retention times of (1.16-1.53), (2.10-11.98), (13.34-16.88), (18.92, 22.29) and (19.82, 23.96-42), respectively. Figures 4.21 (b) and 4.22 (b) illustrate the chromatogram of gas product, consisting of three main part which are light product (C1-C4), gasoline (C5-C8) and biojet (C9) at the retention times of (1.17-7.31), (12.92-27.0) and 30.8, respectively. The Ni/HY catalyst provided diesel as the main product while the Ni/HZSM-12 produced biojet as the main product.



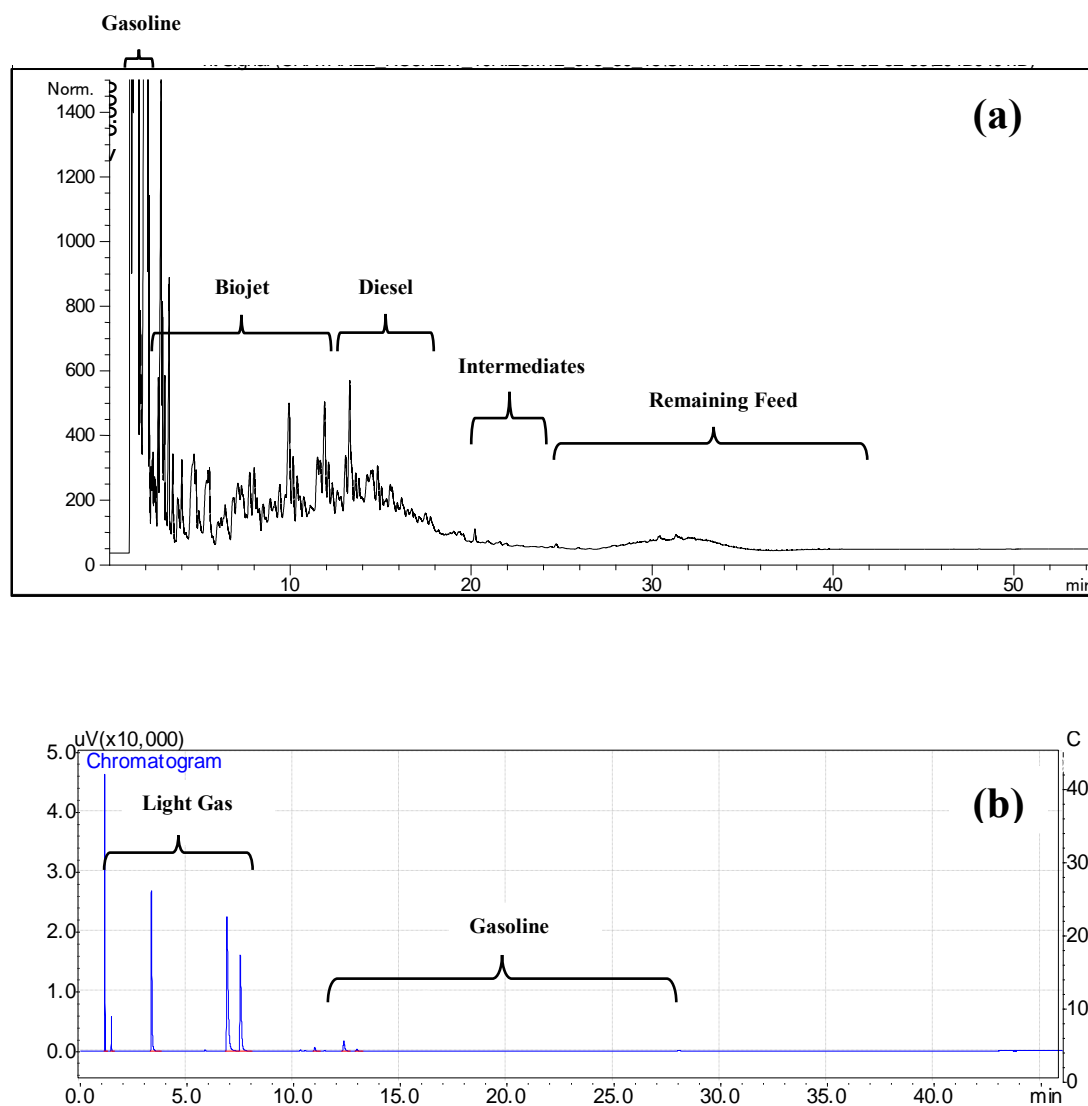


**Figure 4.21** (a) liquid products chromatogram, and (b) gas products chromatogram over Ni/HZSM-12 catalyst operated at operating conditions: 375 °C, 30 bar, LHSV of 1.5 h<sup>-1</sup>, H<sub>2</sub>/feed molar ratio of 10, and TOS of 5 h.

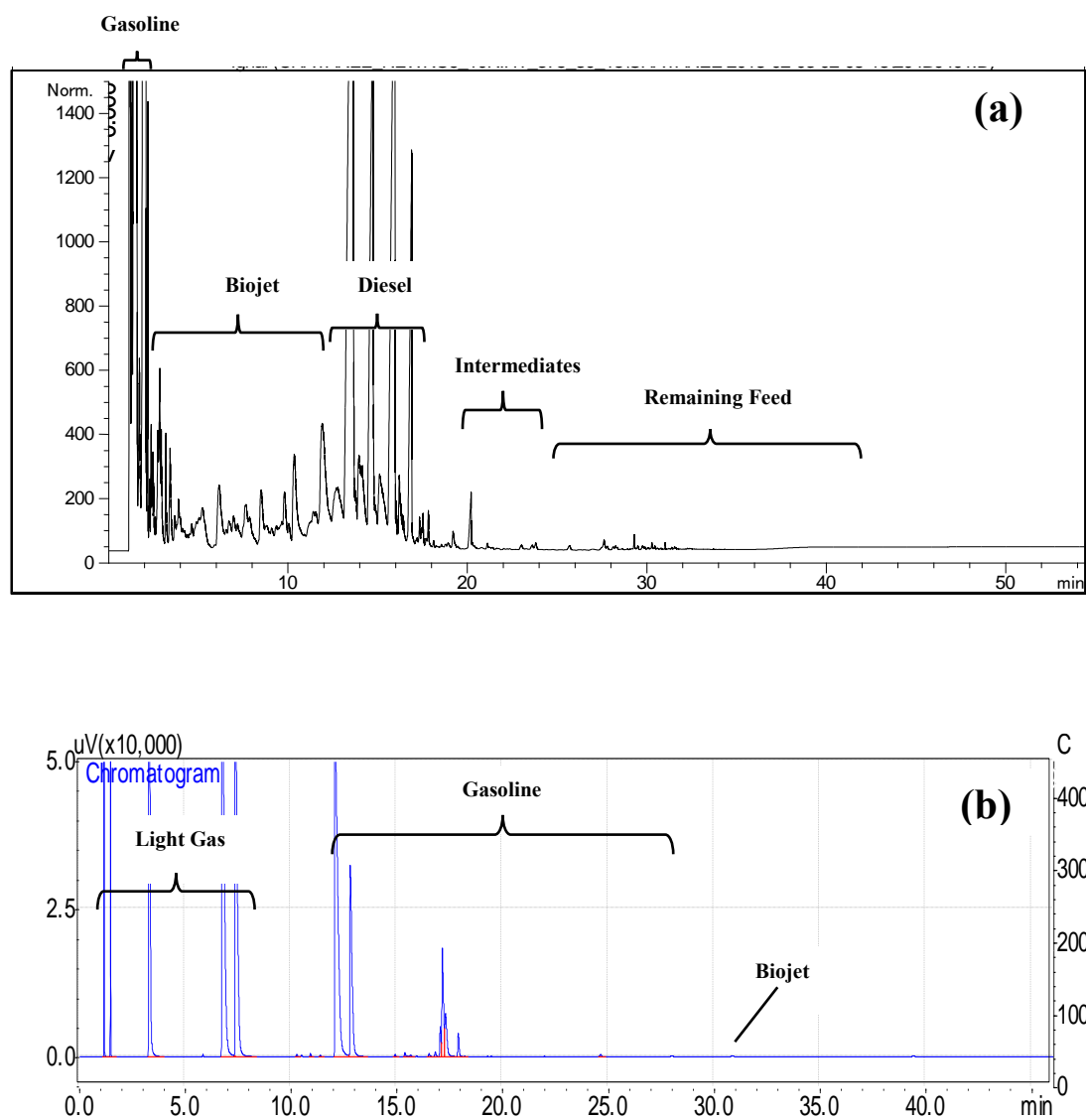


**Figure 4.22** (a) liquid products chromatogram, and (b) gas products chromatogram over Ni/HY catalyst operated at operating conditions: 375 °C, 30 bar, LHSV of 1.5  $\text{h}^{-1}$ ,  $\text{H}_2/\text{feed}$  molar ratio of 10, and TOS of 5 h.

#### 4.4 Proposed Reaction Pathway

The proposed reaction pathway is shown in Figure 4.23. The pathway of biojet production from palmitic acid (main component in PFAD) was deoxygenation of fatty acid to long chain hydrocarbon in the range of diesel (C15–C18) then further hydrocracking/ hydroisomerization into bio-jet range (C9–C14). There are three major reaction pathways deoxygenation to convert fatty acid to long chain hydrocarbon by (i) Hydrodeoxygenation (HDO) pathway which consumed large quantity of H<sub>2</sub> and consequence produced H<sub>2</sub>O, separation of oxygen in fatty acid takes place via C=O bond hydrogenation, C–O bond rupture and further C–C bond cleavage by aldehyde and alcohol as intermediates, (ii) Decarbonylation (DCN) pathway which consumed H<sub>2</sub> for forming aldehyde as an intermediate and producing H<sub>2</sub>O and CO (carbon monoxide) by C–O bond cleavage and C–C bond rupture, respectively, (iii) Decarboxylation (DCX) pathway, occur by elimination –COOH as CO<sub>2</sub> which consumed no H<sub>2</sub> and favor increasing reaction temperature, oxygen in fatty acid is removed in the form of CO<sub>2</sub> (carbon dioxide) by the direct attack at C–C bond (Hermida *et al.*, 2015).

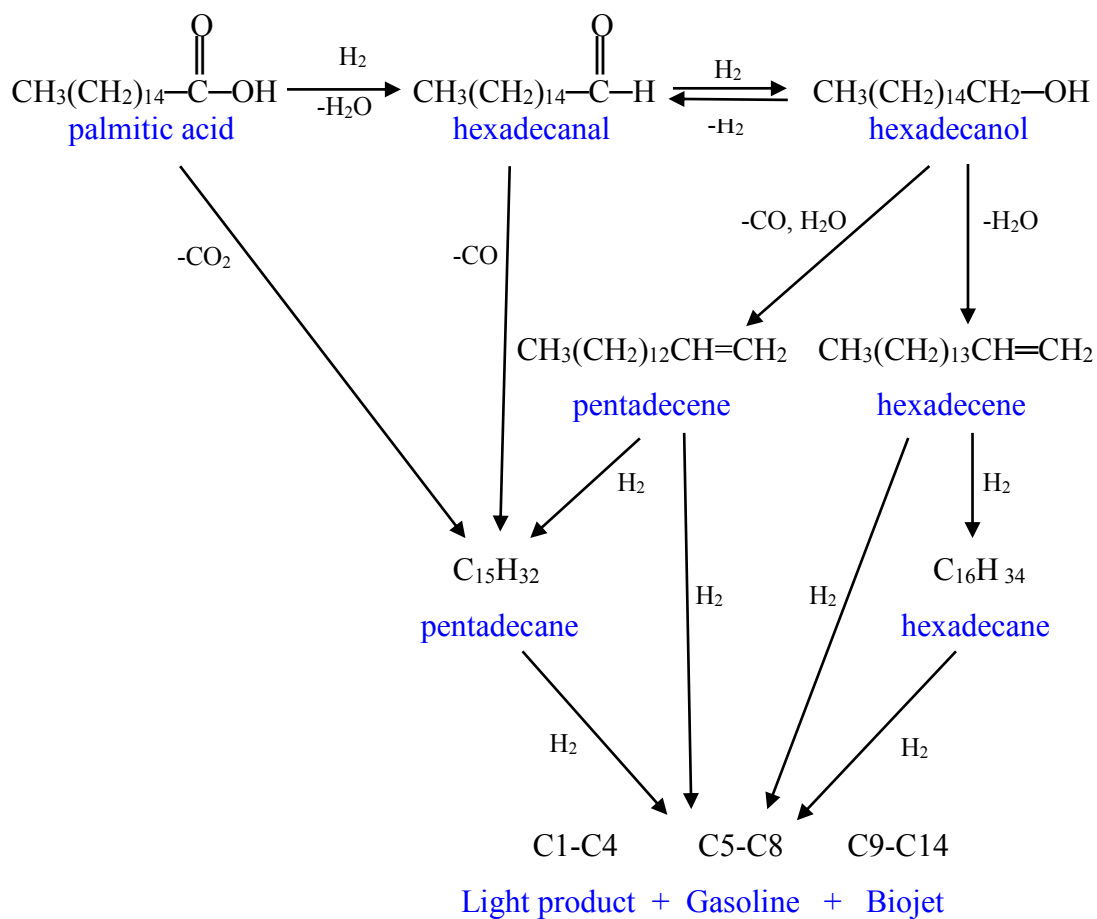


**Figure 4.23** Proposed reaction pathway of biojet fuel production from palmitic acid.

## 4.5 Characterization of Spent Catalysts

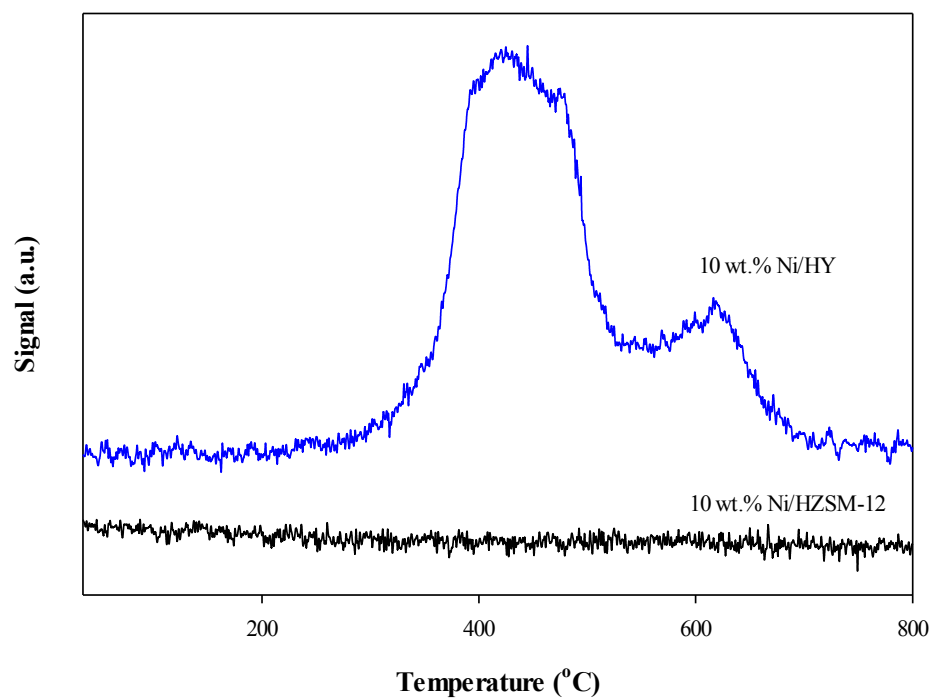
### 4.5.1 Temperature Programmed Oxidation (TPO)

Table 4.5 and Figure 4.24 illustrate the amounts of coke deposit on spent catalysts and TPO profiles after 10 h on stream, respectively. The results showed that 10 wt.% Ni/HZSM-12 catalyst exhibit lower coke formation at 4.66 wt.% while 10 wt.% Ni/HY catalyst exhibit coke formation at 39.81 wt.%. The peaks observed at temperatures below 450 °C represented the weakly coke deposit on the support. The Ni/HZSM-12 catalyst showed amount of coke contained lower oxidation temperature than Ni/HY catalyst. It was because HZSM-12 catalyst has one-dimensional non-interpenetrating puckered channels, act as perfect tubes which do not trap coke precursors (Zhang *et al.*, 1999).

**Table 4.5** Amount of carbon deposits on prepared catalyst after reaction

Spent Catalysts	Coke (wt.%)
10 wt.% Ni/HZSM-12	4.66
10 wt.% Ni/HY	39.81

2D Graph 1



**Figure 4.24** Temperature programmed oxidation (TPO) profiles of 10 wt.% Ni/HZSM-12 and 10 wt.% Ni/HY catalysts.

## CHAPTER V

### CONCLUSIONS AND RECOMMENDATIONS

#### 5.1 Conclusions

The synthesized HZSM-12 catalyst can be confirmed the containing parent catalyst structures by XRD, XRF results and TEM images. The 5 and 10 wt.% Ni/HZSM-12 catalysts had highly dispersion of nickel particles on zeolite support while 15 wt.% Ni/HZSM-12 catalyst had some Ni particles seem to be agglomerated to some extent corresponded to the TEM images and BET results. The 10 wt.% Ni/HZSM-12 catalyst exhibited 99.74% conversion and provided highest selectivity (55.8 %) toward biojet fuel at 375 °C, 30 bar, LHSV of 1.5 h<sup>-1</sup> and H<sub>2</sub>/feed molar ratio of 10. The effect of increasing temperature from 350 to 400 °C gave high selectivity of light product, gasoline and biojet while the appropriate temperature for giving highest biojet fuel selectivity was 375 °C. In addition, the effect of increasing pressure was influenced higher conversion and selective biojet fuel production due to diesel and intermediates were more converted to biojet fuel. For the effect of increasing percent Ni loading, the 5 and 10 wt.% Ni/HZSM-12 catalysts provided almost complete conversions, whereas 15 wt.% Ni/HZSM-12 catalyst provided only 80.46 % due to agglomerated of some Ni particles of 15 wt.% Ni/HZSM-12 catalyst. In addition, Ni/HZSM-12 catalyst favored to produce biojet, gasoline and light products and provided selectivity to produce *iso*-paraffin products more than Ni/HY catalyst because HZSM-12 had narrower pore size so it predominately produced the lighter cracked products and provided *iso*-products. Moreover, Ni/HZSM-12 had low tendency for coke formation, corresponding to the high stability of HZSM-12 catalyst. The formation of hydrocarbons from fatty acid over bi-functional catalyst occurs through an aldehyde and alcohol intermediates further transform to heavier hydrocarbon then subsequently hydroisomerization/ hydrocracking to biojet fuel.

## **5.2 Recommendations**

The percent weight of Ni loading can be decreased to lower 5 wt.% because there is no significant between 5 wt.% and 10 wt.% Ni loading for converting PFAD to products.

In order to improve biojet fuel production from PFAD, the particle size of catalyst should be reduced for increasing external surface area which can provide greater metal dispersion over support to exhibit higher catalytic activity.



## REFERENCES

- Bartholomew, C.H. and Farrauto R.J. (2005) Fundamentals of Industrial Catalytic Processes. New Jersey: Wiley and Sons.
- Borghet, K.V.d. (2010) Experimental Study and Kinetic Modeling of the Synergy in Hydro-isomerisation under Industrial Conditions. Universiteit Gent.
- Brouwer, D.H. (2008) A structure refinement strategy for NMR crystallography: an improved crystal structure of silica-ZSM-12 zeolite from <sup>29</sup>Si chemical shift tensors. Journal of Magnetic Resonance 194(1), 136-146.
- Cao, Y., Shi, Y., Liang, J., Wu, Y., Huang, S., Wang, J., Yang, M. and Hu, H. (2017) High iso-alkanes production from palmitic acid over bi-functional Ni/H-ZSM-22 catalysts. Chemical Engineering Science 158, 188-195.
- Cheng, J., Li, T., Huang, R., Zhou, J., and Cen, K (2014) Optimizing catalysis conditions to decrease aromatic hydrocarbons and increase alkanes for improving jet biofuel quality. Bioresource Technology 158, 378-382.
- Choi, I.H., Hwang, K.R., Han, J.-S., Lee, K.H., Yun, J.S. and Lee, J.S. (2015) The direct production of jet-fuel from non-edible oil in a single-step process. Fuel 158, 98-104.
- Chu, P. and Kuehl, G.H. (1984) Method of preparing crystalline zeolite. United States Patent 4 452 769.
- connor', H.A. (1932) Hydrogenolysis of oxygenated organic compounds The Department of Chemistry of Standford University 54, 4678-4690.
- De Lucas, A., Sánchez, P., Fúnez, A., Ramos, M.J. and Valverde, J.L. (2006) Influence of clay binder on the liquid phase hydroisomerization of n-octane over palladium-containing zeolite catalysts. Journal of Molecular Catalysis A: Chemical 259(1-2), 259-266.
- de Sousa, F.P., Cardoso, C.C. and Pasa, V.M.D. (2016) Producing hydrocarbons for green diesel and jet fuel formulation from palm kernel fat over Pd/C. Fuel Processing Technology 143, 35-42.
- Deldari, H. (2005) Suitable catalysts for hydroisomerization of long-chain normal paraffins. Applied Catalysis A: General 293, 1-10.

- Galadima, A. and Muraza, O. (2015) Catalytic upgrading of vegetable oils into jet fuels range hydrocarbons using heterogeneous catalysts: A review. Journal of Industrial and Engineering Chemistry 29, 12-23.
- Gopal, S. and Smirniotis, P.G. (2002) Deactivation Behavior of Bifunctional Pt/H-Zeolite Catalysts during Cyclopentane Hydroconversion. Journal of Catalysis 205(2), 231-243.
- Gopal, S. and Smirniotis, P.G. (2003) Pt/H-ZSM-12 as a catalyst for the hydroisomerization of C5–C7 n-alkanes and simultaneous saturation of benzene. Applied Catalysis A: General 247(1), 113-123.
- Hagen, J. (2015) Industrial Catalysis: A Practical Approach. Wiley-VCH.
- Hermida, L., Abdullah, A.Z. and Mohamed, A.R. (2015) Deoxygenation of fatty acid to produce diesel-like hydrocarbons: A review of process conditions, reaction kinetics and mechanism. Renewable and Sustainable Energy Reviews 42, 1223-1233.
- Ju, C., Zhou, Y., He, M., Wu, Q. and Fang, Y. (2016) Improvement of selectivity from lipid to jet fuel by rational integration of feedstock properties and catalytic strategy. Renewable Energy 97, 1-7.
- Kapor, N.Z., Maniam, G.P., Rahim, M.H.A. and Yusoff, M.M. (2017) Palm fatty acid distillate as a potential source for biodiesel production-a review. Journal of Cleaner Production 143, 1-9.
- Kiatkittipong, W., Phimsen, S., Kiatkittipong, K., Wongsakulphasatch, S., Laosiripojana, N. and Assabumrungrat, S. (2013) Diesel-like hydrocarbon production from hydroprocessing of relevant refining palm oil. Fuel Processing Technology 116, 16-26.
- Lee, H.W., Jeon, J.-K., Jeong, K.-E., Kim, C.-U., Jeong, S.-Y., Han, J. and Park, Y.-K. (2013) Hydroisomerization of n-dodecane over Pt/Y zeolites with different acid characteristics. Chemical Engineering Journal 232, 111-117.
- Li, T., Cheng, J., Huang, R., Yang, W., Zhou, J. and Cen, K. (2016) Hydrocracking of palm oil to jet biofuel over different zeolites. International Journal of Hydrogen Energy 41(47), 21883-21887.

- Liu, G., Yan, B. and Chen, G. (2013) Technical review on jet fuel production. Renewable and Sustainable Energy Reviews 25, 59-70.
- Liu, S., Zhu, Q., Guan, Q., He, L. and Li, W. (2015) Bio-aviation fuel production from hydroprocessing castor oil promoted by the nickel-based bifunctional catalysts. Bioresource Technology 183, 93-100.
- Liu, Y., Yao, L., Xin, H., Wang, G., Li, D. and Hu, C. (2015) The production of diesel-like hydrocarbons from palmitic acid over HZSM-22 supported nickel phosphide catalysts. Applied Catalysis B: Environmental 174-175, 504-514.
- Lokman, I.M., Rashid, U. and Taufiq-Yap, Y.H. (2015) Production of biodiesel from palm fatty acid distillate using sulfonated-glucose solid acid catalyst: Characterization and optimization. Chinese Journal of Chemical Engineering 23(11), 1857-1864.
- Mante, O.D., Agblevor, F.A., Oyama, S.T. and McClung, R. (2012) The effect of hydrothermal treatment of FCC catalysts and ZSM-5 additives in catalytic conversion of biomass. Applied Catalysis A: General 445-446, 312-320.
- Martens, G. Vanbutsele, P.A. Jacobs, J. Denayer, R. Ocaño, G. Baron, J.A. Muñoz Arroyo, J. Thybaut, G.B. Marin (2001) Evidences for pore mouth and key-lock catalysis in hydroisomerization of long n-alkanes over 10-ring tubular pore bifunctional zeolites Catalysis Today 65, 111-116.
- Mehla, S., Krishnamurthy, K.R., Viswanathan, B., John, M., Niwate, Y., Kishore Kumar, S.A., Pai, S.M. and Newalkar, B.L. (2013) n-Hexadecane hydroisomerization over BTMABr/TEABr/MTEABr templated ZSM-12. Microporous and Mesoporous Materials 177, 120-126.
- Meier, W.M., Olson, D.H. and Baerlocher, Ch. (1996) Atlas of Zeolite Structure Types: Elsevier.
- Ong, H.C., Mahlia, T.M.I., Masjuki, H.H. and Norhasyima, R.S. (2011) Comparison of palm oil, *Jatropha curcas* and *Calophyllum inophyllum* for biodiesel: A review. Renewable and Sustainable Energy Reviews 15(8), 3501-3515.
- Parmar, S., Pant, K.K., John, M., Kumar, K., Pai, S.M., Gupta, S. and Newalkar, B.L. (2014) Hydroisomerization of n-hexadecane over Brønsted acid site tailored Pt/ZSM-12. Journal of Porous Materials 21(5), 849-857.

- Pattanaik, B.P. and Misra, R.D. (2017) Effect of reaction pathway and operating parameters on the deoxygenation of vegetable oils to produce diesel range hydrocarbon fuels: A review. Renewable and Sustainable Energy Reviews 73, 545-557.
- Pedrosa, A.M.G., Souza, M.J.B., Silva, A.O.S., Melo, D.M.A. and Araujo, A.S. (2006) Synthesis, characterization and catalytic properties of the cobalt and nickel supported on HZSM-12 zeolite. Catalysis Communications 7(10), 791-796.
- Peng, B., Yao, Y., Zhao, C. and Lercher, J.A. (2012) Towards Quantitative Conversion of Microalgae Oil to Diesel-Range Alkanes with Bifunctional Catalysts. Angewandte Chemie. 124, 2114-2117.
- Pereira, C. and Gorte, R.J. (1992) Method for distinguishing Brønsted-acid sites in mixtures of H-ZSM-5, H-Y and silica-alumina Applied Catalysis 90, 145-157.
- Ping, B.T.Y. and Yusof, M. (2009) Characteristics and properties of fatty acid distillates from palm oil. Oil Palm Bull. 59, 5-11.
- Rabaev, M., Landau, M.V., Vidruk-Nehemya, R., Koukouliev, V., Zarchin, R. and Herskowitz, M. (2015) Conversion of vegetable oils on Pt/Al<sub>2</sub>O<sub>3</sub> /SAPO-11 to diesel and jet fuels containing aromatics. Fuel 161, 287-294.
- Rosinski, E. (1974) United States Patent 3 855 388.
- Rubin, M.K. (1986) Synthesis of crystalline silicate ZSM-12 United States Patent 4 585 637.
- Sanhoob, M., Muraza, O., Yamani, Z.H., Al-Mutairi, E.M., Tago, T., Merzougui, B. and Masuda, T. (2014) Synthesis of ZSM-12 (MTW) with different Al-source: Towards understanding the effects of crystallization parameters. Microporous and Mesoporous Materials 194, 31-37.
- Santos, R.C.R., Valentini, A., Lima, C.L., Filho, J.M. and Oliveira, A.C. (2011) Modifications of an HY zeolite for n-octane hydroconversion. Applied Catalysis A: General 403(1-2), 65-74.
- Scherzer, J. and Gruia, A.J. (1996) Hydrocracking Science and Technology. New York: Marcel Dekker.

- Shahinuzzaman, M., Yaakob, Z. and Ahmed, Y. (2017) Non-sulphide zeolite catalyst for bio-jet-fuel conversion. Renewable and Sustainable Energy Reviews 77, 1375-1384.
- Snåre, M., Kubičková, I., Mäki-Arvela, P., Eränen, K. and Murzin, D.Y. (2006) Heterogeneous Catalytic Deoxygenation of Stearic Acid for Production of Biodiesel. Industrial & Engineering Chemistry Research, 45, 5708-5715.
- Souverijns, W., Martens J.A., Froment, G.F., and Jacobs, P.A. (1998) Hydrocracking of Isoheptadecanes on Pt/H-ZSM-22: An Example of Pore Mouth Catalysis. Journal of Catalysis 174, 177-184.
- Talebian-Kiakalaieh, A., Amin, N.A.S. and Mazaheri, H. (2013) A review on novel processes of biodiesel production from waste cooking oil. Applied Energy 104, 683-710.
- Tamiyakul, S., Anutamjarikun, S. and Jongpatiwut, S. (2016) The effect of Ga and Zn over HZSM-5 on the transformation of palm fatty acid distillate (PFAD) to aromatics. Catalysis Communications 74, 49-54.
- Twaiq, F.A., Zabidi, N.A.M., and Bhatia, S. (1999) Catalytic Conversion of Palm Oil to Hydrocarbons: Performance of Various Zeolite Catalyst Industrial & Engineering Chemistry Research 38, 3230-3237.
- Verma, D., Rana, B.S., Kumar, R., Sibi, M.G. and Sinha, A.K. (2015) Diesel and aviation kerosene with desired aromatics from hydroprocessing of jatropha oil over hydrogenation catalysts supported on hierarchical mesoporous SAPO-11. Applied Catalysis A: General 490, 108-116.
- Wang, W.C. and Tao, L. (2016) Bio-jet fuel conversion technologies. Renewable and Sustainable Energy Reviews 53, 801-822.
- Yoo, K., Kashfi, R., Gopal, S., Smirniotis, P.G., Gangoda, M. and Bose, R.N. (2003) TEABr directed synthesis of ZSM-12 and its NMR characterization. Microporous and Mesoporous Materials 60(1-3), 57-68.
- Zhang, C., Hui, X., Lin, Y. and Sung, C.J. (2016) Recent development in studies of alternative jet fuel combustion: Progress, challenges, and opportunities. Renewable and Sustainable Energy Reviews 54, 120-138.

- Basiron, Y. "Industry Performance Report 2014" Palm Oil Today. 21 May 2015. 1 July 2017 <<http://palmoiltoday.net/industry-performance-report-2014/>>
- Eia. "Hydrocracking is an important source of diesel and jet fuel." eia. 13 Jan 2013. 1 July 2017 <<https://www.eia.gov/todayinenergy/detail.php?id=9650>>
- May, C.Y. "Overview of the Malaysian Oil Palm Industry 2015." PalmOilis. Feb 2016. 1 July 2017. <<http://palmoilis.mpob.gov.my/index.php/overview-of-industry/408-overview-of-industry-2015>>

## APPENDIX

### APPENDIX A1 Overall Mass Balance of Deoxygenation-hydroprocessing at Different in Temperature (350, 375 and 400 °C)

**Table A1** Overall mass balance of deoxygenation-hydroprocessing one-pot reaction over 10 wt.% Ni/HZSM-12 catalyst at different in temperature. (Reaction condition: 30 bar, H<sub>2</sub>/feed molar ratio of 10, LHSV of 1.5 h<sup>-1</sup> and TOS at 5 h)

Temperature		350 °C	375 °C	400 °C
Selectivity of product (wt.%)	C1	0.072500	0.085193	0.219004
	C2	0.084195	0.010637	0.021508
	C3	0.092940	0.085556	0.115113
	<i>iso</i> -C4	0.077045	0.045190	0.060678
	<i>n</i> -C4	0.126498	0.084879	0.081783
	<i>iso</i> -C5	0.000000	0.000000	0.000000
	<i>n</i> -C5	0.004435	0.000966	0.012050
	<i>iso</i> -C6	0.000000	0.000000	0.001944
	<i>n</i> -C6	0.000000	0.000000	0.000000
	<i>iso</i> -C7	0.000000	0.000000	0.000000
	<i>n</i> -C7	0.000000	0.000000	0.000000
	<i>iso</i> -C8	0.000000	0.000000	0.000498
	<i>n</i> -C8	0.000000	0.000000	0.000000
	<i>iso</i> -C9	0.000000	0.000000	0.000000
	<i>n</i> -C9	0.020134	0.071785	0.072564
	<i>iso</i> -C10	0.112443	0.130759	0.093991
<i>n</i> -C10	0.006730	0.004263	0.004741	

**Table A1 (Cont.)** Overall mass balance of deoxygenation-hydroprocessing one-pot reaction over 10 wt.% Ni/HZSM-12 catalyst at different in temperature. (Reaction condition: 30 bar, H<sub>2</sub>/feed molar ratio of 10, LHSV of 1.5 h<sup>-1</sup> and TOS at 5 h)

<b>Temperature</b>		<b>350 °C</b>	<b>375 °C</b>	<b>400 °C</b>
Selectivity of product (wt.%)	<i>iso</i> -C11	0.045897	0.085907	0.064416
	<i>n</i> -C11	0.002889	0.005235	0.005339
	<i>iso</i> -C12	0.045642	0.097354	0.067870
	<i>n</i> -C12	0.004931	0.005395	0.003786
	<i>iso</i> -C13	0.031497	0.066802	0.015377
	<i>n</i> -C13	0.003635	0.012734	0.029264
	<i>iso</i> -C14	0.027392	0.051485	0.034937
	<i>n</i> -C14	0.014115	0.026225	0.021345
	<i>iso</i> -C15	0.032062	0.045371	0.018423
	<i>n</i> -C15	0.070103	0.008522	0.016014
	<i>iso</i> -C16	0.030104	0.017562	0.010582
	<i>n</i> -C16	0.024413	0.010632	0.004243
	<i>iso</i> -C17	0.029927	0.012352	0.005143
	<i>n</i> -C17	0.021312	0.010785	0.005551
	<i>iso</i> -C18	0.012216	0.012186	0.002913
	<i>n</i> -C18	0.001024	0.002421	0.000947
<b>Intermediates</b>		0.005922	0.009805	0.009976
<b>Feed Remaining</b>		1.758658	0.211106	3.305591
<b>%Conversion</b>		98.24134	99.78889	96.69441



**Appendix A2 Overall Mass Balance of Deoxygenation-hydroprocessing at Different in Pressure (10, 20 and 30 bar)**

**Table A2** Overall mass balance of deoxygenation-hydroprocessing one-pot reaction over 10 wt.% Ni/HZSM-12 catalyst at different in pressure. (Reaction condition: 375 °C, H<sub>2</sub>/feed molar ratio of 10, LHSV of 1.5 h<sup>-1</sup> and TOS at 5 h)

Pressure		10 bar	20 bar	30 bar
Selectivity of product (wt.%)	C1	0.088062	0.098564	0.085193
	C2	0.007321	0.015202	0.010637
	C3	0.032528	0.125540	0.085556
	<i>iso</i> -C4	0.020721	0.077578	0.045190
	<i>n</i> -C4	0.027158	0.121078	0.084879
	<i>iso</i> -C5	0.000000	0.000000	0.000000
	<i>n</i> -C5	0.012620	0.014957	0.000966
	<i>iso</i> -C6	0.065147	0.008790	0.000000
	<i>n</i> -C6	0.005636	0.000000	0.000000
	<i>iso</i> -C7	0.031046	0.000000	0.000000
	<i>n</i> -C7	0.000622	0.000000	0.000000
	<i>iso</i> -C8	0.001419	0.000000	0.000000
	<i>n</i> -C8	0.000000	0.000000	0.000000
	<i>iso</i> -C9	0.025464	0.000000	0.000000
	<i>n</i> -C9	0.074776	0.022249	0.071785
	<i>iso</i> -C10	0.085141	0.123261	0.130759
	<i>n</i> -C10	0.000000	0.009845	0.004263
<i>iso</i> -C11	0.019454	0.047694	0.085907	
<i>n</i> -C11	0.017281	0.004450	0.005235	

**Table A2 (Cont.)** Overall mass balance of deoxygenation-hydroprocessing one-pot reaction over 10 wt.% Ni/HZSM-12 catalyst at different in pressure. (Reaction condition: 375 °C, H<sub>2</sub>/feed molar ratio of 10, LHSV of 1.5 h<sup>-1</sup> and TOS at 5 h)

<b>Pressure</b>		<b>10 bar</b>	<b>20 bar</b>	<b>30 bar</b>
Selectivity of product (wt.%)	<i>iso</i> -C12	0.039597	0.066133	0.097354
	<i>n</i> -C12	0.000000	0.005591	0.005395
	<i>iso</i> -C13	0.020095	0.044107	0.066802
	<i>n</i> -C13	0.000000	0.004923	0.012734
	<i>iso</i> -C14	0.018460	0.042980	0.051485
	<i>n</i> -C14	0.019291	0.014795	0.026225
	<i>iso</i> -C15	0.013151	0.029528	0.045371
	<i>n</i> -C15	0.208163	0.051063	0.008522
	<i>iso</i> -C16	0.006835	0.016437	0.017562
	<i>n</i> -C16	0.012980	0.012805	0.010632
	<i>iso</i> -C17	0.019555	0.017495	0.012352
	<i>n</i> -C17	0.035982	0.007407	0.010785
	<i>iso</i> -C18	0.000798	0.009024	0.012186
	<i>n</i> -C18	0.013581	0.001682	0.002421
<b>Intermediates</b>		0.077116	0.006825	0.009805
<b>Feed Remaining</b>		14.42264	0.803579	0.211106
<b>%Conversion</b>		85.57736	99.19642	99.78889

**Appendix A3 Overall Mass Balance of Deoxygenation-hydroprocessing at Different in Percent Ni Loading (5, 10 and 15 wt.%)**

**Table A3** Overall mass balance of deoxygenation-hydroprocessing one-pot reaction over Ni/HZSM-12 catalyst at different in percent Ni loading. (Reaction condition: 375 °C, 30 bar, H<sub>2</sub>/feed molar ratio of 10, LHSV of 1.5 h<sup>-1</sup> and TOS at 5 h)

Percent Ni Loading		5 wt.%	10 wt.%	15 wt.%
Selectivity of product (wt.%)	C1	0.075835	0.085193	0.084738
	C2	0.011447	0.010637	0.010515
	C3	0.106075	0.085556	0.100353
	<i>iso</i> -C4	0.066823	0.045190	0.064095
	<i>n</i> -C4	0.104419	0.084879	0.098859
	<i>iso</i> -C5	0.000000	0.000000	0.000000
	<i>n</i> -C5	0.000000	0.000966	0.004016
	<i>iso</i> -C6	0.000000	0.000000	0.000000
	<i>n</i> -C6	0.000000	0.000000	0.000000
	<i>iso</i> -C7	0.000000	0.000000	0.000000
	<i>n</i> -C7	0.000000	0.000000	0.000000
	<i>iso</i> -C8	0.000000	0.000000	0.000000
	<i>n</i> -C8	0.000000	0.000000	0.000000
	<i>iso</i> -C9	0.015320	0.000000	0.016797
	<i>n</i> -C9	0.002066	0.071785	0.002329
	<i>iso</i> -C10	0.131505	0.130759	0.116927
	<i>n</i> -C10	0.007218	0.004263	0.006762
<i>iso</i> -C11	0.079408	0.085907	0.079594	
<i>n</i> -C11	0.000000	0.005235	0.000000	

**Table A3 (Cont.)** Overall mass balance of deoxygenation-hydroprocessing one-pot reaction over Ni/HZSM-12 catalyst at different in percent Ni loading. (Reaction condition: 375 °C, 30 bar, H<sub>2</sub>/feed molar ratio of 10, LHSV of 1.5 h<sup>-1</sup> and TOS at 5 h)

<b>Percent Ni Loading</b>		<b>5 wt.%</b>	<b>10 wt.%</b>	<b>15 wt.%</b>
Selectivity of product (wt.%)	<i>iso</i> -C12	0.102028	0.097354	0.098113
	<i>n</i> -C12	0.002597	0.005395	0.002311
	<i>iso</i> -C13	0.073363	0.066802	0.068000
	<i>n</i> -C13	0.010344	0.012734	0.005960
	<i>iso</i> -C14	0.089412	0.051485	0.087149
	<i>n</i> -C14	0.008184	0.026225	0.002894
	<i>iso</i> -C15	0.048123	0.045371	0.047448
	<i>n</i> -C15	0.000858	0.008522	0.000000
	<i>iso</i> -C16	0.041666	0.017562	0.030185
	<i>n</i> -C16	0.000000	0.010632	0.003918
	<i>iso</i> -C17	0.018558	0.012352	0.022705
	<i>n</i> -C17	0.000000	0.010785	0.001145
	<i>iso</i> -C18	0.004751	0.012186	0.011228
	<i>n</i> -C18	0.000000	0.002421	0.029101
<b>Intermediates</b>		0.000000	0.009805	0.004859
<b>Feed Remaining</b>		0.082076	0.211106	16.13265
<b>%Conversion</b>		99.91792	99.78889	83.86735

**Appendix A4 Overall Mass Balance of Deoxygenation-hydroprocessing at Different in Liquid Hourly Space Velocity (1.5, 2.0, 2.5 h<sup>-1</sup>)**

**Table A4** Overall mass balance of deoxygenation-hydroprocessing one-pot reaction over 10 wt.% Ni/HZSM-12 catalyst at different in LHSV. (Reaction condition: 375 °C, 30 bar, H<sub>2</sub>/feed molar ratio of 10 and TOS at 5 h)

LHSV (h <sup>-1</sup> )		1.5	2.0	2.5
Selectivity of product (wt.%)	C1	0.085193	0.058091	0.001016
	C2	0.010637	0.005476	0.000000
	C3	0.085556	0.040852	0.000822
	<i>iso</i> -C4	0.045190	0.026036	0.000396
	<i>n</i> -C4	0.084879	0.036295	0.000566
	<i>iso</i> -C5	0.000000	0.000000	0.000000
	<i>n</i> -C5	0.000966	0.002491	0.000000
	<i>iso</i> -C6	0.000000	0.001504	0.000000
	<i>n</i> -C6	0.000000	0.000000	0.000000
	<i>iso</i> -C7	0.000000	0.000000	0.000000
	<i>n</i> -C7	0.000000	0.000000	0.000000
	<i>iso</i> -C8	0.000000	0.000000	0.000000
	<i>n</i> -C8	0.000000	0.000000	0.000000
	<i>iso</i> -C9	0.000000	0.033083	0.035964
	<i>n</i> -C9	0.071785	0.004207	0.011484
	<i>iso</i> -C10	0.130759	0.104860	0.063966
	<i>n</i> -C10	0.004263	0.006102	0.007738
<i>iso</i> -C11	0.085907	0.039585	0.065315	
<i>n</i> -C11	0.005235	0.000000	0.000000	

**Table A4 (Cont.)** Overall mass balance of deoxygenation-hydroprocessing one-pot reaction over 10 wt.% Ni/HZSM-12 catalyst at different in LHSV. (Reaction condition: 375 °C, 30 bar, H<sub>2</sub>/feed molar ratio of 10 and TOS at 5 h)

<b>LHSV (h<sup>-1</sup>)</b>		<b>1.5</b>	<b>2.0</b>	<b>2.5</b>
Selectivity of product (wt.%)	<i>iso</i> -C12	0.097354	0.063444	0.054105
	<i>n</i> -C12	0.005395	0.000000	0.000000
	<i>iso</i> -C13	0.066802	0.023086	0.021096
	<i>n</i> -C13	0.012734	0.017383	0.018164
	<i>iso</i> -C14	0.051485	0.025876	0.042593
	<i>n</i> -C14	0.026225	0.025735	0.001632
	<i>iso</i> -C15	0.045371	0.287406	0.412466
	<i>n</i> -C15	0.008522	0.000000	0.000000
	<i>iso</i> -C16	0.017562	0.047465	0.059924
	<i>n</i> -C16	0.010632	0.011748	0.016042
	<i>iso</i> -C17	0.012352	0.082829	0.100373
	<i>n</i> -C17	0.010785	0.000000	0.000000
	<i>iso</i> -C18	0.012186	0.010987	0.028928
	<i>n</i> -C18	0.002421	0.038877	0.004291
<b>Intermediates</b>		0.009805	0.006581	0.010411
<b>Feed Remaining</b>		0.211106	21.10640	19.09334
<b>%Conversion</b>		99.788894	78.89360	80.90666

**Appendix A5 Overall Mass Balance of Deoxygenation-hydroprocessing over Different Catalyst (10 wt.% Ni/HZSM-12 and 10 wt.% Ni/HY catalysts)**

**Table A5** Overall mass balance of deoxygenation-hydroprocessing one-pot reaction over different catalyst. (Reaction condition: 375 °C, 30 bar, H<sub>2</sub>/feed molar ratio of 10, LHSV of 1.5 h<sup>-1</sup> and TOS at 5 h)

Catalyst		10 wt.% Ni/HZSM-12	10 wt.% Ni/HY
Selectivity of product (wt.%)	C1	0.085193	0.079450
	C2	0.010637	0.005397
	C3	0.085556	0.026173
	<i>iso</i> -C4	0.045190	0.027284
	<i>n</i> -C4	0.084879	0.072256
	<i>iso</i> -C5	0.000000	0.000000
	<i>n</i> -C5	0.000966	0.014766
	<i>iso</i> -C6	0.000000	0.015551
	<i>n</i> -C6	0.000000	0.001639
	<i>iso</i> -C7	0.000000	0.000000
	<i>n</i> -C7	0.000000	0.000000
	<i>iso</i> -C8	0.000000	0.000000
	<i>n</i> -C8	0.000000	0.000000
	<i>iso</i> -C9	0.000000	0.003316
	<i>n</i> -C9	0.071785	0.009188
	<i>iso</i> -C10	0.130759	0.033455
	<i>n</i> -C10	0.004263	0.005855
	<i>iso</i> -C11	0.085907	0.020129
<i>n</i> -C11	0.005235	0.012030	

**Table A5 (Cont.)** Overall mass balance of deoxygenation-hydroprocessing one-pot reaction over different catalyst. (Reaction condition: 375 °C, 30 bar, H<sub>2</sub>/feed molar ratio of 10, LHSV of 1.5 h<sup>-1</sup> and TOS at 5 h)

<b>Catalyst</b>		<b>10 wt.% Ni/HZSM-12</b>	<b>10 wt.% Ni/HY</b>
Selectivity of product (wt.%)	<i>iso</i> -C12	0.097354	0.029749
	<i>n</i> -C12	0.005395	0.007618
	<i>iso</i> -C13	0.066802	0.017371
	<i>n</i> -C13	0.012734	0.001852
	<i>iso</i> -C14	0.051485	0.022661
	<i>n</i> -C14	0.026225	0.032352
	<i>iso</i> -C15	0.045371	0.024945
	<i>n</i> -C15	0.008522	0.200700
	<i>iso</i> -C16	0.017562	0.037582
	<i>n</i> -C16	0.010632	0.084609
	<i>iso</i> -C17	0.012352	0.024218
	<i>n</i> -C17	0.010785	0.111516
	<i>iso</i> -C18	0.012186	0.017851
	<i>n</i> -C18	0.002421	0.040401
<b>Intermediates</b>		0.009805	0.020085
<b>Feed Remaining</b>		0.211106	3.774429
<b>%Conversion</b>		99.78889	96.22557



## CURRICULUM VITAE

**Name:** Ms. Chayanee Hiranyasiri

**Date of Birth:** September 2, 1994

**Nationality:** Thai

**University Education:**

2012–2016 Bachelor Degree of Chemical Technology, Faculty of Science,  
Chulalongkorn University, Bangkok, Thailand

**Work Experience:**

2015	Position:	Student Internship in Product Development Support
	Company name:	SCG Chemicals Co., Ltd.

**Proceedings:**

1. Hiranyasiri, C., and Jongpatiwut, S. (2018, June 5) Conversion of palm fatty acid distillate to biojet fuel over Ni/HZSM-12 catalyst. Proceedings of The 24<sup>th</sup> PPC Symposium on Petroleum, Petrochemicals, and Polymers and The 9<sup>th</sup> Research Symposium on Petrochemical and Materials Technology, Mandarin Hotel, Bangkok, Thailand.